



Transcriptomic analysis of glycan-processing genes in the dorsal root ganglia of diabetic mice and functional characterization on Ca_v3.2 channels

Robin N. Stringer, Joanna Lazniewska & Norbert Weiss

To cite this article: Robin N. Stringer, Joanna Lazniewska & Norbert Weiss (2020) Transcriptomic analysis of glycan-processing genes in the dorsal root ganglia of diabetic mice and functional characterization on Ca_v3.2 channels, *Channels*, 14:1, 132-140, DOI: 10.1080/19336950.2020.1745406

To link to this article: <https://doi.org/10.1080/19336950.2020.1745406>



© 2020 The Author(s). Published by Informa UK Limited, trading as Taylor & Francis Group.



Published online: 31 Mar 2020.



Submit your article to this journal [↗](#)



Article views: 1476



View related articles [↗](#)



View Crossmark data [↗](#)



Citing articles: 3 View citing articles [↗](#)

Transcriptomic analysis of glycan-processing genes in the dorsal root ganglia of diabetic mice and functional characterization on Ca_v3.2 channels

Robin N. Stringer^{a,b}, Joanna Lazniewska^a, and Norbert Weiss ^a

^aInstitute of Organic Chemistry and Biochemistry, Czech Academy of Sciences, Prague, Czech Republic; ^bThird Faculty of Medicine, Charles University, Prague, Czech Republic

ABSTRACT

Ca_v3.2 T-type calcium channels play an essential role in the transmission of peripheral nociception in the dorsal root ganglia (DRG) and alteration of Ca_v3.2 expression is associated with the development of peripheral painful diabetic neuropathy (PDN). Several studies have previously documented the role of glycosylation in the expression and functioning of Ca_v3.2 and suggested that altered glycosylation of the channel may contribute to the aberrant expression of the channel in diabetic conditions. In this study, we aimed to analyze the expression of glycan-processing genes in DRG neurons from a leptin-deficient genetic mouse model of diabetes (*db/db*). Transcriptomic analysis revealed that several glycan-processing genes encoding for glycosyltransferases and sialic acid-modifying enzymes were upregulated in diabetic conditions. Functional analysis of these enzymes on recombinant Ca_v3.2 revealed an unexpected loss-of-function of the channel. Collectively, our data indicate that diabetes is associated with an alteration of the glycosylation machinery in DRG neurons. However, individual action of these enzymes when tested on recombinant Ca_v3.2 cannot explain the observed upregulation of T-type channels under diabetic conditions.

Abbreviations: Galnt16: Polypeptide N-acetylgalactosaminyltransferase 16; B3gnt8: UDP-GlcNAc: betaGal beta-1,3-N-acetylglucosaminyltransferase 8; B4galt1: Beta-1,4-galactosyltransferase 1; St6gal1: Beta-galactoside alpha-2,6-sialyltransferase 1; Neu3: Sialidase-3

ARTICLE HISTORY

Received 26 February 2020
Revised 27 February 2020
Accepted 2 March 2020

KEYWORDS

Glycosylation; transcriptome; DRG neurons; diabetes; calcium channel; Ca_v3.2 channel; T-type channel

Introduction

It is well established that increased expression of the low-voltage-activated Ca_v3.2 T-type calcium channel within neurons of the dorsal root ganglia contribute to the sensitization of nociceptive sensory fibers in response to hyperglycemia associated with diabetes, leading to painful symptoms of peripheral diabetic neuropathy [1–3]. This notion is further exemplified by the observation that pharmacological blockade of T-type channels alleviates diabetes-induced hyperalgesia in a leptin-deficient genetic mouse model of diabetes (*ob/ob*) [4]. Furthermore, it has been reported that removal of terminal sialic acid moieties from complex glycan structures can normalize T-type currents in DRG neurons isolated from *ob/ob* mice, and reverse neuropathic pain *in vivo* [5], suggesting that glycosylation of Ca_v3.2 could possibly represent an underlying mechanisms contributing to the enhanced expression of the channel during diabetes.

Protein glycosylation is a posttranslational modification that refers to the co-valent addition of a sugar

molecule oligosaccharide (glycan) to specific residues within the target protein. It is an essential chemical process that contributes to the proper maturation, sorting, and functioning of proteins including ion channels [6,7], and several studies have documented the importance of glycosylation for the expression of Ca_v3.2 channels [8,9]. However, the underlying cellular mechanisms by which Ca_v3.2 channel may undergo aberrant glycosylation during diabetes have remained unknown.

In this study, we aimed to specifically analyzed the transcriptomic profile of glycan-modifying enzymes in DRG neurons from diabetic *db/db* mice and assess the effect of these enzymes on the expression of recombinant Ca_v3.2 channels.

Materials and methods

Animals

8 weeks old male *db/db* mice and their control hibernates were purchased from Janvier Labs and were

kept under standard conditions for 3 weeks to allow sufficient adaptation. The mean glycemia values measured using a glucocard X-meter ARKAY from blood samples drawn from the tail were 8.2 ± 0.6 mmol/L for wild-type animals ($n = 6$) and 29.9 ± 0.7 mmol/L for *db/db* animals ($n = 7$).

Transcriptomic analysis

Transcriptomic analysis of glycan-modifying enzymes was performed on total RNA harvested from the dorsal root ganglia (lumbar L4/L6) of wild-type and *db/db* mice using the Glycosylation RT2 Profiler PCR Array (Qiagen) according to the manufacturer's instructions. The PCR array and qRT-PCR were performed on a LightCycler[®] 480 (Roche) with the following PCR conditions: 95°C for 5 min, 40 cycles at 95°C for 15 sec, 60°C for 15 sec, and 72°C for 20 sec. Each test was run three times and the mean values were taken to eradicate any discrepancies. 84 key genes encoding glycan-processing enzymes were analyzed and included glycosyltransferase and glycosidase for several important sugars (galactose, glucose, mannose, N-acetylgalactosamine, N-acetylglucosamine, fucose and sialic acid).

Plasmid cDNA constructs

The cDNA construct encoding for the human $Ca_v3.2$ wild-type in pcDNA3.1 was previously described [10]. The plasmid cDNAs encoding for the human glycan-modifying enzymes Galnt16, B3gnt8, B4galt1, St6gal1, and Neu3 in pCMV3 were purchased from Sino Biological.

Cell culture and heterologous expression

Human embryonic kidney tsA-201 cells were grown in high glucose DMEM medium supplemented with 10% fetal bovine serum and 1% penicillin/streptomycin (all media were purchased from Invitrogen) and maintained under standard conditions. Cells were transfected using the calcium/phosphate method using $2.5 \pm g$ of $Ca_v3.2$ plasmid and $2.5 \pm g$ of plasmid encoding for the glycan-modifying enzymes. For transfections using the channel alone, $2.5 \pm g$ of empty pcDNA3 vector was added to the mixture to maintained the total amount of cDNA.

Electrophysiology

Patch clamp recording of T-type currents in tsA-201 cells expressing $Ca_v3.2$ channels was performed 72 h after transfection in the whole-cell configuration at room temperature (22–24°C) as previously described [11]. The external solution contained (in millimolar): 5 BaCl₂, 5 KCl, 1 MgCl₂, 128 NaCl, 10 TEA-Cl, 10 D-glucose, 10 4-(2-hydroxyethyl)-1-piperazineethanesulfonic acid (HEPES) (pH 7.2 with NaOH). Patch pipettes were filled with an internal solution containing (in millimolar): 110 CsCl, 3 Mg-ATP, 0.5 Na-GTP, 2.5 MgCl₂, 5 D-glucose, 10 EGTA, and 10 HEPES (pH 7.4 with CsOH), and had a resistance of 2–4 MΩ. Recordings were performed using an Axopatch 200B amplifier (Axon Instruments) and acquisition and analysis were performed using pClamp 10 and Clampfit 10 software, respectively (Axon Instruments). The linear leak component of the current was corrected online and current traces were digitized at 10 kHz and filtered at 2 kHz. The voltage dependence of activation of $Ca_v3.2$ channels was determined by measuring the peak T-type current amplitude in response to 150 ms depolarizing steps to various potentials applied every 10 s from a holding membrane potential of –100 mV. The current-voltage relationship (*I/V*) curve was fitted with the following modified Boltzmann Equation (1):

$$I(V) = G_{max} \frac{(V - V_{rev})}{1 + \exp\left(\frac{V_{0.5} - V}{k}\right)} \quad (1)$$

with *I(V)* being the peak current amplitude at the command potential *V*, G_{max} the maximum conductance, V_{rev} the reversal potential, $V_{0.5}$ the half-activation potential, and *k* the slope factor. The voltage dependence of the whole-cell Ba²⁺ conductance was fitted with the following modified Boltzmann Equation (2):

$$G(V) = \frac{G_{max}}{1 + \exp\left(\frac{V_{0.5} - V}{k}\right)} \quad (2)$$

with *G(V)* being the Ba²⁺ conductance at the command potential *V*.

The voltage dependence of the steady-state inactivation of $Ca_v3.2$ channels was ascertained by measuring the peak T-type current amplitude in response to a 150 ms depolarizing step to –20 mV

applied after a 5 s-long conditioning prepulse ranging from -120 mV to -30 mV. The current amplitude obtained during each test pulse was normalized to the maximal current amplitude and plotted as a function of the prepulse potential. The voltage dependence of the steady-state inactivation was fitted with the following two-state Boltzmann function (3):

$$I(V) = \frac{I_{max}}{1 + \exp\left(\frac{V-V_{0.5}}{k}\right)} \quad (3)$$

with I_{max} as the maximal peak current amplitude and $V_{0.5}$ as half-inactivation voltage.

The recovery from inactivation was determined using a double-pulse protocol from a holding potential of -100 mV. The cell membrane was depolarized for 2 s at 0 mV (inactivating prepulse) to ensure complete inactivation of the channel, and then to -20 mV for 150 ms (test pulse) after an increasing time period (interpulse) ranging between 0.1 ms and 2 s at -100 mV. The peak current from the test pulse was plotted as a ratio of the maximum prepulse current versus interpulse interval. The data were fitted with the following single-exponential function (4):

$$\frac{I}{I_{max}} = A \times \left(1 - \exp\left(\frac{-t}{\tau}\right)\right) \quad (4)$$

where τ denotes the time constant of channel recovery from inactivation.

Statistical analysis

Data values are presented as mean \pm S.E.M. for n measurements. Statistical analysis was performed using GraphPad Prism 7. Statistical significance was determined using a one-way ANOVA test and datasets were considered significantly different for $p \leq 0.05$.

Results

Expression of glycan-processing enzymes in the dorsal root ganglia of diabetic mice

In order to assess the expression of glycan-processing enzymes in diabetic conditions, we performed a differential transcriptomic analysis on the dorsal root ganglia isolated from a transgenic mouse

model of diabetes (*db/db*) versus wild-type animals (Figure 1). 19 out of 84 enzymes analyzed were found significantly upregulated ($p < 0.05$) in diabetic conditions (Figure 2am). The majority of these enzymes (53%) belonged to the family of glycosyltransferases (Galnt1, Galnt4, Galnt12, Galnt16, B3gnt8, Gcnt1, Mgat4 c, Ugg2, B3glct, and B4galt1) that catalyze the transfer of saccharide moieties from an activated nucleotide sugar to a nucleophilic glycosyl acceptor molecule. In addition, 16% belonged to the family of mannosidases (Man1a, Man2a1, and Man2b1) that hydrolyze mannose moieties; 16% to the family of fucosidases/fucosyltransferases (Fuca1, Fut8, and Pofut2); 5% to the family of galactosides/glucosidases/hexosaminidases (Ganab); and 10% to the family of sialidases/sialyltransferases (St6gal1, and Neu3) involved in the processing of sialic acid moieties from complex glycan structures (Figure 2m). In contrast, we did not observe any enzymes that were significantly down-regulated.

Functional effect of glycan-processing enzymes on the expression of recombinant $Ca_v3.2$ channels

Next, we aimed to assess the functional impact of up-regulated glycan-modifying enzymes on recombinant $Ca_v3.2$ channels expressed in tsA-201 cells. Six enzymes responsible for the processing of the glycan structure at different stages were assessed: Galnt16 (*N*-acetylgalactosaminyltransferase) responsible for catalyzing the initial addition of *N*-acetylgalactosamine to a serine or threonine residue on early protein precursors [12]; B3gnt8 (*N*-acetylglucosaminyltransferase) responsible for the elongation of the polylactosamine chains on tetraantennary *N*-glycans [13]; B4galt1 (Galactosyltransferase) which catalyzes the addition of galactose moieties to *N*-acetylglucosamine of complex *N*-glycans in the Golgi apparatus [14]; St6gal1 (Sialyltransferase) responsible for catalyzing the final transfer of sialic acid moieties from CMP-sialic acid to galactose acceptor substrates [15]; and Neu3 (sialidase) expressed in the plasma membrane and responsible for removing sialic acid moieties from glycoproteins and glycolipids, acting in the opposite way of St6gal1 [16]. Representative T-type current traces recorded

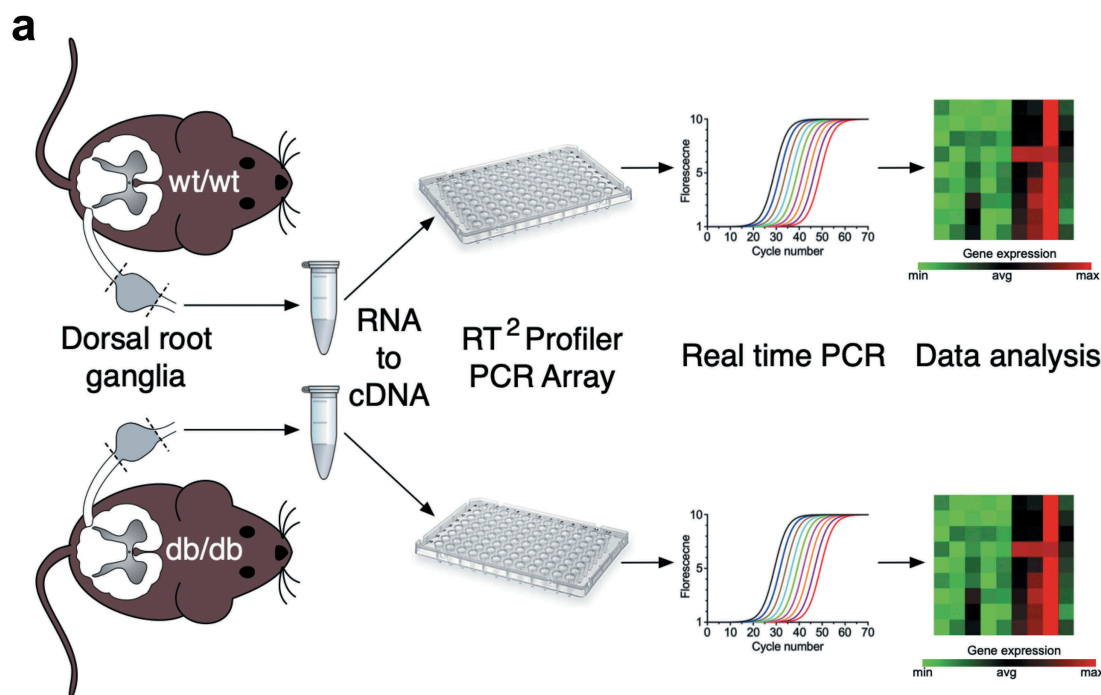


Figure 1. Schematic representation of the transcriptomic analysis process. (a) Total RNA harvested from the dorsal root ganglia (lumbar L4/L6) of wild-type and *db/db* mice and subjected to the Glycosylation RT² Profiler PCR Array to analyze the expression level of 84 genes encoding for glycan-processing enzymes.

from cells co-expressing Ca_v3.2 with glycosyltransferases (Galnt16, B3gnt8, or B4galt1) and sialic acid-modifying enzymes (St6gal1 or Neu3) are shown in Figure 3a in response to 150 ms depolarizing steps ranging between -90 mV and 30 mV from a holding potential of -100 mV. Unexpectedly, co-expression of glycosyltransferases with Ca_v3.2 nearly abolished T-type currents. For instance, the maximal T-type conductance (G_{\max}) in cells expressing Ca_v3.2 with Galnt16, B3gnt8, and B4galt1 was reduced by 98% ($p = 0.0001$) (20 ± 20 pS/pF, $n = 14$), 92% ($p = 0.0003$) (67 ± 28 pS/pF, $n = 5$), and 80% ($p = 0.0002$) (165 ± 21 pS/pF, $n = 7$), respectively, compared to cells expressing Ca_v3.2 alone (821 ± 68 pS/pF, $n = 37$) (Figure 3b,c). We also observed a significant decrease of G_{\max} in cells co-expressing the sialyltransferase St6gal1 by 52% ($p = 0.0028$) (395 ± 74 pS/pF, $n = 13$) (Figure 3ac and Table 1). In contrast, we did not observe a significant alteration ($p = 0.7542$) of G_{\max} in cells co-expressing the sialidase Neu3 (921 ± 104 pS/pF, $n = 24$) (Figure 3ac and Table 1). Altogether, these data indicate that some of the glycan-processing enzymes tested here can have a potent influence

on the expression of Ca_v3.2 that is consistent with a loss-of-channel function.

Electrophysiological properties of Ca_v3.2 channels in the presence of sialic acid-processing enzymes

Previous studies have shown that the terminal sialic acid moiety attached to complex glycan structures can affect the gating of voltage-gated ion channels [17]. Therefore, we further assessed the voltage-dependence of activation and inactivation of Ca_v3.2 channels in the presence of the sialyltransferase St6gal1 and sialidase Neu3. The mean half-activation potential in cells expressing St6gal1 was shifted by 4.9 mV ($p = 0.0001$) toward depolarized potentials (-38.7 ± 0.7 mV, $n = 13$) compared to cells expressing the channel alone (-43.6 ± 0.6 mV, $n = 37$) (Figure 4a,b and Table 1). In contrast, co-expression of Neu3 had no significant effect of the voltage-dependence of activation of Ca_v3.2. Furthermore, neither St6gal1 nor Neu3 altered the voltage-dependence of inactivation (Figure 4c,d and Table 1) or the recovery from inactivation of Ca_v3.2 channels (Figure 4e,f

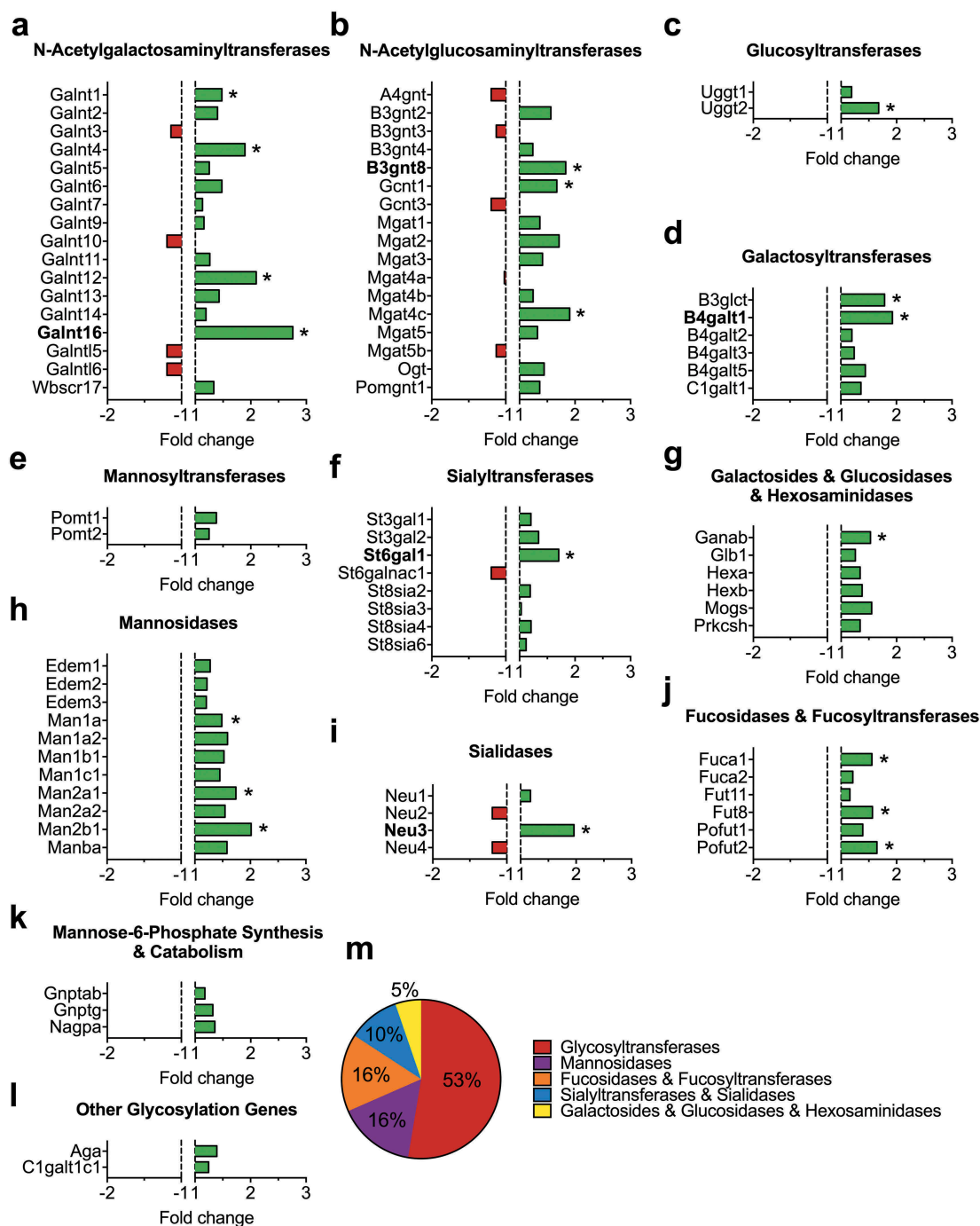


Figure 2. Summary of the transcriptomic profiling of glycan-modifying genes in the dorsal root ganglia of *db/db* mice. Data are presented as fold change compared to wild-type animals for (a) N-acetylgalactosaminyltransferases, (b) N-acetylglucosaminyltransferases, (c) Glucosyltransferases, (d) Galactosyltransferases, (e) Mannosyltransferases, (f) Sialyltransferases, (g) Galactosides/Glucosidases/Hexosaminidases, (h) Mannosidases, (i) Sialidases, (j) Fucosidases/Fucosyltransferases, (k) Mannose-6-Phosphate synthesis/catabolism, and (l) other glycosylation genes. Enzymes indicated in bold were functionally characterized on $Ca_v3.2$ channels. (m) Summary of up-regulated genes.

and Table 1). Altogether, these data indicate that increased sialylation activity tends to negatively modulate recombinant $Ca_v3.2$ channels when expressed in tsA-201 cells.

Discussion

Increased expression of $Ca_v3.2$ in primary afferent nociceptive fibers is causally linked to the

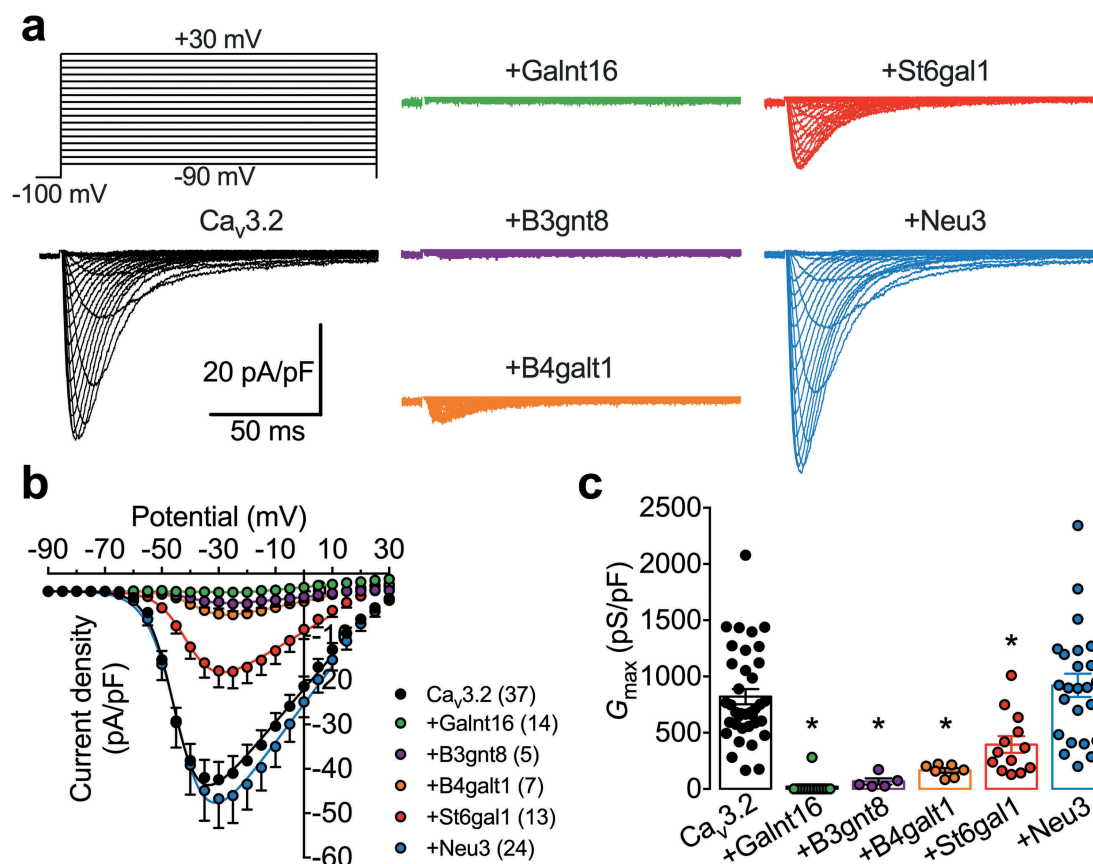


Figure 3. Influence of glycan-modifying enzymes on the functional expression of $\text{Ca}_v3.2$ channels. (a) Representative T-type current traces recorded from cells expressing $\text{Ca}_v3.2$ alone (black traces) and in combination with Galnt16 (green traces), B3gnt8 (purple traces), B4galt1 (orange traces), St6gal1 (red traces), Neu3 (blue traces) glycan-modifying enzymes in response to 150 ms depolarizing steps ranging between -90 mV and 30 mV from a holding potential of -100 mV. (b) Corresponding mean peak current density-voltage (I/V) relationship. (c) Corresponding mean maximal macroscopic conductance (G_{max}) values obtained from the fit of the I/V curves with the modified Boltzmann equation (1).

Table 1. Electrophysiological properties of human $\text{Ca}_v3.2$ channels expressed in tsA-201 cells in the presence of sialic acid-processing enzymes.

Channel	Activation				Inactivation				RFI	
	$V_{0.5}$ (mV)	k	(n)	G_{max} (pS/pF)	(n)	$V_{0.5}$ (mV)	k	(n)	τ (ms)	(n)
$\text{Ca}_v3.2$	-43.6 ± 0.6	4.5 ± 0.2	37	820 ± 68	37	-68.3 ± 0.9	2.9 ± 0.7	13	447 ± 34	11
+St6gal1	$-38.7 \pm 0.7^*$	5.5 ± 0.3	13	$395 \pm 74^*$	13	-70.7 ± 1.6	3.2 ± 0.3	8	550 ± 48	8
+Neu3	-41.8 ± 0.9	$5.3 \pm 0.2^*$	24	921 ± 104	24	-66.6 ± 1.3	3.7 ± 0.2	16	422 ± 39	7

development of peripheral painful neuropathy associated with nerve injury [18–20], antineoplastic drugs [21–23], inflammation [24,25], and diabetes [1,3]. Several studies have unraveled some of the mechanisms underlying the pathological expression of $\text{Ca}_v3.2$ and alteration of the posttranslational regulation of the channel including ubiquitinylation [26], SUMOylation [27] and phosphorylation [28,29]. Defects in these processes have emerged as some of the primary reasons leading to enhanced expression of the channel. Furthermore, altered

glycosylation of $\text{Ca}_v3.2$ was proposed to contribute to the sensitization of nociceptive fibers in response to hyperglycemia associated with diabetes [5]. In this study, we show using a differential transcriptomic approach that several glycan-modifying enzymes are upregulated in DRG neurons from *db/db* mice compared to wild-type animals. These results are consistent with previous studies reporting an alteration of glycan-processing enzymes in the kidney of diabetic mice [30]. Several of these enzymes contribute to the processing of important sugars including glucose,

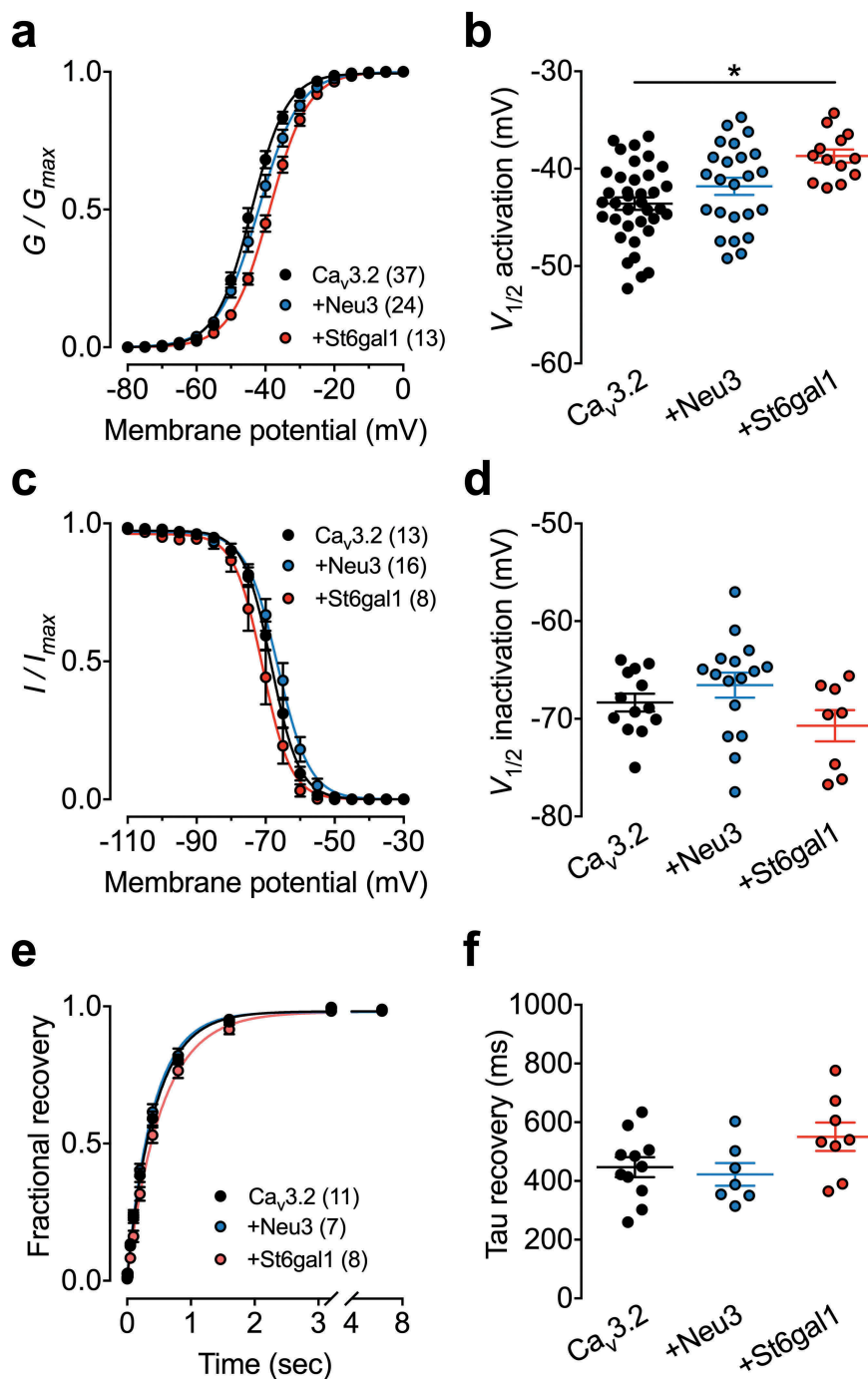


Figure 4. Influence of sialic acid-processing enzymes on the electrophysiological properties of $Ca_v3.2$ channels. (a) Mean normalized voltage-dependence of T-type current activation for cells expressing $Ca_v3.2$ alone (black circles) and in combination with Neu3 (blue circles) or St6gal1 (red circles). (b) Corresponding mean half-activation potential values obtained from the fit of the activation curves with the modified Boltzmann Equation (2). (c,d) Legend same as for (a,b) but for the voltage-dependence of steady state inactivation. Half-inactivation potential values was obtained from the fit of the inactivation curves with the two-state Boltzmann function (3). (e) Mean normalized recovery from inactivation kinetics. (f) Corresponding mean time constant values of recovery from inactivation obtained from the fit of the recovery curves with the single-exponential function (4).

galactose, mannose, and fucose, and therefore alteration of their expression level could potentially alter the processing and maturation of the glycan structures. Furthermore, we found that several enzymes

involved in the processing of the terminal sialic acid moieties found in complex glycan structures were upregulated in diabetic conditions. This aspect is particularly relevant in the context of PDN since

enzymatic removal of sialic acid moieties with neuraminidase was reported to normalize T-type currents in DRG neurons isolated from diabetic mice and to alleviate PDN *in vivo* [5]. Furthermore, sialylation was reported to contribute to the hyperexcitability of DRG neurons following peripheral nerve injury [31]. However, our functional analysis on recombinant Cav3.2 channels did not provide evidence in support of a role for these enzymes in the upregulation of Ca_v3.2 when co-expressed individually with the channel. For instance, co-expression of glycosyltransferases Galnt16, B3gnt8, and B4galt1 with Ca_v3.2 produced an almost complete loss of functional expression of the channel. However, several studies have previously shown that glycosyltransferases can form heterodimers that contribute to their subcellular expression, enzymatic activity, efficient biosynthesis of glycan chains, trafficking through intracellular vesicles, and substrate specificities [32]. For instance, binding of B3gnt8 appears to cause a conformational change in the catalytic site of B3gnt2 and increases its enzymatic activity [33]. Therefore, we cannot exclude that overexpression of individual enzymes with Ca_v3.2 in tsA-201 cells as performed in our study may not fully capture the more complex situation in DRG neurons where the expression several genes encoding for glycan-modifying enzymes is altered at the same time and there could be synergetic effects among the various players. Furthermore, tsA-201 cells were grown in high glucose medium which represents another variable that could have influenced the phenotypic effect of these enzymes on Ca_v3.2 channels. In contrast to glycosyltransferases, co-expression of the sialyltransferase St6gal1 produced a relatively mild decreased expression of the channel with a depolarized shift of the voltage-dependence of activation, indicating that sialylation contributes to the functioning of Ca_v3.2. However, co-expression of the neuraminidase Neu3 that removes sialic acid moieties did not altered expression of the channel, nor its gating properties. These results are consistent with previous studies showing that application of neuraminidase on tsA-201 cells expressing Ca_v3.2 channels did not alter channel function [8], which could suggest a low basal level of sialylation in these cells.

Altogether, this study identified several glycan-modifying genes whose expression is altered in DRG neurons under diabetic condition. However, we did

not find evidence for a role of these enzyme in the upregulation of Ca_v3.2 channels. At this stage, we cannot exclude that expression of glycan-modifying enzymes in DRG neurons may have produced a different phenotypic effect on Ca_v3.2 and this aspect would deserve further investigations in native conditions.

Acknowledgments

We thank IOCB Tech for financing the purchase of animals.

Disclosure statement

The authors report no conflict of interest.

Funding

N.W. is supported by a starting grant from the Institute of Organic Chemistry and Biochemistry.

ORCID

Norbert Weiss  <http://orcid.org/0000-0002-0040-1109>

References

- [1] Jagodic MM, Pathirathna S, Nelson MT, et al. Cell-specific alterations of T-type calcium current in painful diabetic neuropathy enhance excitability of sensory neurons. *J Neurosci.* 2007;27:3305–3316.
- [2] Obradovic AL, Hwang SM, Scarpa J, et al. CaV3.2 T-type calcium channels in peripheral sensory neurons are important for mibefradil-induced reversal of hyperalgesia and allodynia in rats with painful diabetic neuropathy. *PLoS One.* 2014;9:e91467.
- [3] Duzhyy DE, Viatchenko-Karpinski VY, Khomula EV, et al. Upregulation of T-type Ca²⁺ channels in long-term diabetes determines increased excitability of a specific type of capsaicin-insensitive DRG neurons. *Mol Pain.* 2015;11:29.
- [4] Latham JR, Pathirathna S, Jagodic MM, et al. Selective T-type calcium channel blockade alleviates hyperalgesia in ob/ob mice. *Diabetes.* 2009;58:2656–2665.
- [5] Orestes P, Osuru HP, McIntire WE, et al. Reversal of neuropathic pain in diabetes by targeting glycosylation of Ca(V)3.2 T-type calcium channels. *Diabetes.* 2013;62:3828–3838.
- [6] Lazniewska J, Weiss N. The “sweet” side of ion channels. *Rev Physiol Biochem Pharmacol.* 2014;167:67–114.
- [7] Lazniewska J, Weiss N. Glycosylation of voltage-gated calcium channels in health and disease. *Biochim Biophys Acta Biomembr.* 2017;1859:662–668.

- [8] Weiss N, Black SA, Bladen C, et al. Surface expression and function of Cav3.2 T-type calcium channels are controlled by asparagine-linked glycosylation. *Pflugers Arch*. 2013;465:1159–1170.
- [9] Lazniewska J, Rzhetsky Y, Zhang FX, et al. Cooperative roles of glucose and asparagine-linked glycosylation in T-type calcium channel expression. *Pflugers Arch*. 2016;468:1837–1851.
- [10] Dubel SJ, Altier C, Chaumont S, et al. Plasma membrane expression of T-type calcium channel alpha(1) subunits is modulated by high voltage-activated auxiliary subunits. *J Biol Chem*. 2004;279:29263–29269.
- [11] Carter MT, McMillan HJ, Tomin A, et al. Compound heterozygous CACNA1H mutations associated with severe congenital amyotrophy. *Channels (Austin)*. 2019;13:153–161.
- [12] Raman J, Guan Y, Perrine CL, et al. UDP-N-acetyl- α -D-galactosamine:polypeptideN-acetylgalactosaminyltransferases: completion of the family tree. *Glycobiology*. 2012;22:768–777.
- [13] Ishida H, Togayachi A, Sakai T, et al. A novel beta1,3-N-acetylglucosaminyltransferase (beta3Gn-T8), which synthesizes poly-N-acetyllactosamine, is dramatically upregulated in colon cancer. *FEBS Lett*. 2005;579:71–78.
- [14] Ramasamy V, Ramakrishnan B, Boeggeman E, et al. Oligosaccharide preferences of beta1,4-galactosyltransferase-I: crystal structures of Met340His mutant of human beta1,4-galactosyltransferase-I with a pentasaccharide and trisaccharides of the N-glycan moiety. *J Mol Biol*. 2005;353:53–67.
- [15] Kuhn B, Benz J, Greif M, et al. The structure of human α -2,6-sialyltransferase reveals the binding mode of complex glycans. *Acta Crystallogr D Biol Crystallogr*. 2013;69:1826–1838.
- [16] Monti E, Bassi MT, Papini N, et al. Identification and expression of NEU3, a novel human sialidase associated to the plasma membrane. *Biochem J*. 2000;349:343–351.
- [17] Ednie AR, Bennett ES. Modulation of voltage-gated ion channels by sialylation. *Compr Physiol*. 2012;2:1269–1301.
- [18] Jagodic MM, Pathirathna S, Joksovic PM, et al. Upregulation of the T-type calcium current in small rat sensory neurons after chronic constrictive injury of the sciatic nerve. *J Neurophysiol*. 2008;99:3151–3156.
- [19] Wen XJ, Xu SY, Chen ZX, et al. The roles of T-type calcium channel in the development of neuropathic pain following chronic compression of rat dorsal root ganglia. *Pharmacology*. 2010;85:295–300.
- [20] Yue J, Liu L, Liu Z, et al. Upregulation of T-type Ca²⁺ channels in primary sensory neurons in spinal nerve injury. *Spine (Phila Pa 1976)*. 1976;2013(38):463–470.
- [21] Flatters SJ, Bennett GJ. Ethosuximide reverses paclitaxel- and vincristine-induced painful peripheral neuropathy. *Pain*. 2004;109:150–161.
- [22] Okubo K, Takahashi T, Sekiguchi F, et al. Inhibition of T-type calcium channels and hydrogen sulfide-forming enzyme reverses paclitaxel-evoked neuropathic hyperalgesia in rats. *Neuroscience*. 2011;188:148–156.
- [23] Li Y, Tatsui CE, Rhines LD, et al. Dorsal root ganglion neurons become hyperexcitable and increase expression of voltage-gated T-type calcium channels (Cav3.2) in paclitaxel-induced peripheral neuropathy. *Pain*. 2017;158:417–429.
- [24] Watanabe M, Ueda T, Shibata Y, et al. Expression and regulation of Cav3.2 T-type calcium channels during inflammatory hyperalgesia in mouse dorsal root ganglion neurons. *PLoS One*. 2015;10:e0127572.
- [25] Sekiguchi F, Tsubota M, Kawabata A. Involvement of voltage-gated calcium channels in inflammation and inflammatory pain. *Biol Pharm Bull*. 2018;41:1127–1134.
- [26] García-Caballero A, Gadotti VM, Stenkowski P, et al. The deubiquitinating enzyme USP5 modulates neuropathic and inflammatory pain by enhancing Cav3.2 channel activity. *Neuron*. 2014;83:1144–1158.
- [27] Garcia-Caballero A, Zhang FX, Chen L, et al. SUMOylation regulates USP5-Cav3.2 calcium channel interactions. *Mol Brain*. 2019;12:73.
- [28] Gaifullina AS, Lazniewska J, Gerasimova EV, et al. A potential role for T-type calcium channels in homocysteinemia-induced peripheral neuropathy. *Pain*. 2019;160:2798–2810.
- [29] Gomez K, Calderón-Rivera A, Sandoval A, et al. Cdk5-dependent phosphorylation of Cav3.2 T-type channels: possible role in nerve ligation-induced neuropathic allodynia and the compound action potential in primary afferent C fibers. *J Neurosci*. 2020;40:283–296.
- [30] Qian X, Li X, Ilori TO, et al. RNA-seq analysis of glycosylation related gene expression in STZ-induced diabetic rat kidney inner medulla. *Front Physiol*. 2015;6:274.
- [31] Peng XQ, Zhang XL, Fang Y, et al. Sialic acid contributes to hyperexcitability of dorsal root ganglion neurons in rats with peripheral nerve injury. *Brain Res*. 2004;1026:185–193.
- [32] Seko A. Complex formation of glycosyltransferases and their biological significance. *Trends Glycosci Glycotechnol*. 2006;18: 209–230.
- [33] Seko A, Yamashita K. Activation of beta1,3-N-acetylglucosaminyltransferase-2 (beta3Gn-T2) by beta3Gn-T8. Possible involvement of beta3Gn-T8 in increasing poly-N-acetyllactosamine chains in differentiated HL-60 cells. *J Biol Chem*. 2008;283:33094–33100.

SHORT REPORT

Open Access



Electrophysiological and computational analysis of $Ca_v3.2$ channel variants associated with familial trigeminal neuralgia

Emilio R. Mustafá^{1†}, Eder Gambeta^{2†}, Robin N. Stringer^{1,3†}, Ivana A. Souza², Gerald W. Zamponi^{2*} and Norbert Weiss^{1*}

Abstract

Trigeminal neuralgia (TN) is a rare form of chronic neuropathic pain characterized by spontaneous or elicited paroxysms of electric shock-like or stabbing pain in a region of the face. While most cases occur in a sporadic manner and are accompanied by intracranial vascular compression of the trigeminal nerve root, alteration of ion channels has emerged as a potential exacerbating factor. Recently, whole exome sequencing analysis of familial TN patients identified 19 rare variants in the gene *CACNA1H* encoding for $Ca_v3.2$ -type calcium channels. An initial analysis of 4 of these variants pointed to a pathogenic role. In this study, we assessed the electrophysiological properties of 13 additional TN-associated $Ca_v3.2$ variants expressed in tsA-201 cells. Our data indicate that 6 out of the 13 variants analyzed display alteration of their gating properties as evidenced by a hyperpolarizing shift of their voltage dependence of activation and/or inactivation resulting in an enhanced window current supported by $Ca_v3.2$ channels. An additional variant enhanced the recovery from inactivation. Simulation of neuronal electrical membrane potential using a computational model of reticular thalamic neuron suggests that TN-associated $Ca_v3.2$ variants could enhance neuronal excitability. Altogether, the present study adds to the notion that ion channel polymorphisms could contribute to the etiology of some cases of TN and further support a role for $Ca_v3.2$ channels.

Keywords: Trigeminal neuralgia, Ion channel, Calcium channel, *CACNA1H*, $Ca_v3.2$ channel, Channelopathy

Introduction

Trigeminal neuralgia (TN) also referred as “tic douloureux” is a rare form of chronic neuropathic pain syndrome originating from the trigeminal nerve that supplies sensation to the face. TN is characterized by recurrent and chronic paroxysms of electric shock-like

or stabbing pain in the orofacial region (for reviews see [1, 2]). The pain usually lasts from a few seconds to a few minutes and may be so intense that it triggers involuntary wincing, hence the term tic. Most cases of TN are sporadic but familial forms exist and are likely to be underestimated [3]. In both situations, the etiology of TN remains largely unknown and neurovascular compression of the trigeminal root nerve represents the primary theory for the underlying cause of the disease. However, the observation that many TN patients do not show any sign of neurovascular compression, and conversely that individuals with compression do not necessarily develop symptoms, suggested the existence of additional factors. Hence, an alteration of neuronal excitability resulting from abnormal functioning of ion channels has emerged

[†]Emilio R. Mustafá, Eder Gambeta and Robin N. Stringer contributed equally to this work

*Correspondence: zamponi@ucalgary.ca; nalweiss@gmail.com

¹ Department of Pathophysiology, Third Faculty of Medicine, Charles University, Prague, Czech Republic

² Department of Clinical Neurosciences, Alberta Children's Hospital Research Institute, Hotchkiss Brain Institute, Cumming School of Medicine, University of Calgary, Calgary, Canada

Full list of author information is available at the end of the article

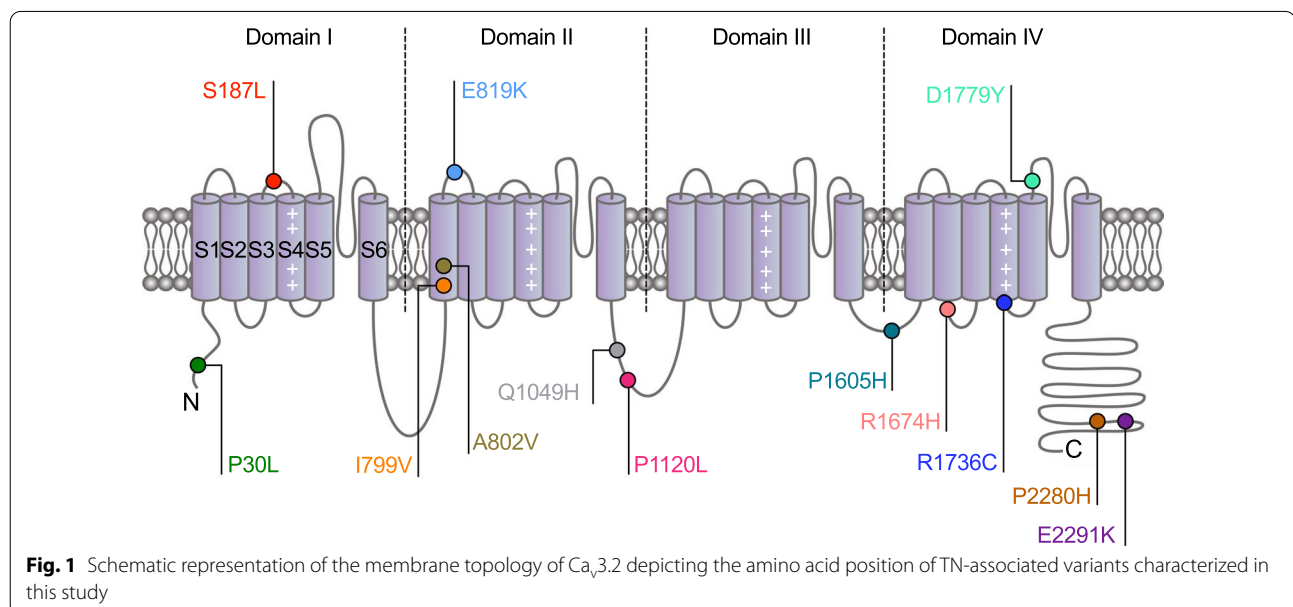


as a potential underlying mechanism [4–7] and consistent with this notion, the sodium channel blockers carbamazepine and oxcarbazepine represent the first line therapy in TN [8]. Moreover, alterations of the expression of several ion channels including sodium, calcium, and potassium channels have been reported in TN patients [9] as well as in preclinical rodent models [10–17]. In addition, rare polymorphisms in ion channel genes were identified in TN patients [18–20] suggesting the existence of predisposing genetic factors and gain-of-function mutations (GoF) were reported for $\text{Na}_v1.6$ [18], $\text{Ca}_v2.1$ [21], TRPM7 [22, 23], and TRPM8 channels [24].

Recently, TN-associated polymorphisms in the gene *CACNA1H* encoding $\text{Ca}_v3.2$ calcium channels were reported [25]. $\text{Ca}_v3.2$ channels belong to the subfamily of low-voltage-activated T-type channels and are widely expressed throughout the nervous system where they play an essential role in the control of neuronal excitability [26]. Importantly, $\text{Ca}_v3.2$ is expressed in all structures of the trigeminal pathway including trigeminal ganglion sensory neurons [27, 28], the spinal trigeminal nucleus (SpV) [17] as well as several thalamic nuclei such as the ventroposterior nucleus (VPM) [29] that receives projections from the SpV. Hence, $\text{Ca}_v3.2$ channels may be of direct relevance for the transmission of trigeminal sensory information and a role for $\text{Ca}_v3.2$ in TN-like syndrome was reported in a preclinical rodent model [17].

In this study, we aimed to provide a comprehensive analysis of TN-associated *CACNA1H* variants with regard to their impact on the functioning of $\text{Ca}_v3.2$ channels. Of the 19 variants reported [25], four had already been assessed for their impact on the

biophysical properties of $\text{Ca}_v3.2$ channels and revealed a variant-dependent effect such that G563R and P566T produced a GoF of the channel, E286K caused a mild loss-of-function (LoF), and H526Y did not cause any alteration [17, 30]. We now report the functional characterization of 13 additional variants. Seven of these variants are located within cytoplasmic regions of $\text{Ca}_v3.2$ including the N-terminal region (P30L), the loop connecting domains II and III (Q1049H and P1120L), the loop connecting domains III and IV (P1605H), the linker connecting transmembrane segments S2-S3 of domain IV (R1674H), and the C-terminal region (P2280H and E2291K). Four additional variants are mapped within important structural determinants of the channel including the transmembrane segment S1 of domain II (I799V and A802V), the end of the S4 voltage-sensor of domain IV (R1736C), and the fourth pore-forming loop (D1779Y). The two remaining variants are localized within the extracellular linkers connecting transmembrane segments S3-S4 of domain I (S187L) and S1-S2 of domain II (E819K) (Fig. 1). Electrophysiological analysis of recombinant TN-associated $\text{Ca}_v3.2$ variants in tsA-201 cells revealed a significant alteration in the gating properties of 7 out of the 13 variants analyzed. In addition, introduction of these variants in a computational model of reticular thalamic neuron (nRT) enhanced rebound burst firing of action potentials. Taken together, these data suggest that altered gating of TN-associated $\text{Ca}_v3.2$ variants may enhance neuronal excitability which could potentially contribute to the etiology of TN.



Materials and methods

Plasmid cDNA constructs and site-directed mutagenesis

The Ca_v3.2 variants were generated by site directed mutagenesis performed by GenScript using the wild-type human Ca_v3.2 (containing exon 26) in pcDNA3.1 (kindly provided by Dr. Terrance Snutch) as template. The fidelity of all constructs was confirmed by full-length sequencing of the coding region.

Cell culture and heterologous expression

Human embryonic kidney tsA-201 cells were grown in DMEM medium supplemented with 10% fetal bovine serum and 1% penicillin/streptomycin (all media purchased from Invitrogen) and maintained under standard conditions at 37 °C in a humidified atmosphere containing 5% CO₂. Heterologous expression was performed by transfecting cells with 5 µg of plasmid cDNAs encoding for Ca_v3.2 variants and empty pEGFP vector as transfection marker using the calcium/phosphate method.

Patch clamp electrophysiology

Patch clamp recordings of T-type currents in tsA-201 cells expressing Ca_v3.2 variants were performed 72 h after transfection in the whole-cell configuration at room temperature (22–24 °C) in a bath solution containing (in millimolar): 10 BaCl₂, 125 CsCl, 1 MgCl₂, 10 D-glucose, 10 4-(2-hydroxyethyl)-1-piperazineethanesulfonic acid (HEPES) (pH 7.4 with CsOH). Patch pipettes were filled with a solution containing (in millimolar): 110 CsCl, 3 Mg-ATP, 0.5 Na-GTP, 2.5 MgCl₂, 5 D-glucose, 10 EGTA, and 10 HEPES (pH 7.4 with CsOH), and had a resistance of 2–4MΩ. The calculated liquid junction potential was about – 2.6 mV and therefore was corrected from the recordings. Recordings were performed using an Axopatch 200B amplifier (Axon Instruments) and acquisition and analysis were performed using pClamp 10 and Clampfit 10 softwares, respectively (Axon Instruments). The linear leak component of the current was corrected using a P/4 subtraction protocol and current traces were digitized at 10 kHz and filtered at 2 kHz.

The voltage dependence of activation of Ca_v3.2 channels was determined by measuring the peak of the T-type current in response to 140 ms depolarizing steps from – 80 mV to +20 mV in 5 mV increments preceded by a 200 ms hyperpolarizing prepulse to – 110 mV from a holding membrane potential of – 100 mV. The current–voltage relationship (*I/V*) curve was fitted with the following modified Boltzmann Eq. (1):

$$I(V) = G_{max} \frac{(V - V_{rev})}{1 + \exp\left(\frac{V_{0.5} - V}{k}\right)} \quad (1)$$

with *I(V)* being the peak current amplitude at the command potential *V*, *G*_{max} the maximum conductance, *V*_{rev} the reversal potential, *V*_{0.5} the half-activation potential, and *k* the slope factor. The voltage dependence of the whole-cell T-type channel conductance was calculated using the following modified Boltzmann Eq. (2):

$$G(V) = \frac{G_{max}}{1 + \exp\left(\frac{V_{0.5} - V}{k}\right)} \quad (2)$$

with *G(V)* being the T-type channel conductance at the command potential *V*.

The voltage dependence of the steady-state inactivation of Ca_v3.2 channels was determined by measuring the peak T-type current amplitude in response to a 50 ms depolarizing step to –30 mV applied after a 1 s-long conditioning prepulse ranging from –110 mV to –15 mV in 5 mV increments. The current amplitude obtained during each test pulse was normalized to the maximal current amplitude and plotted as a function of the prepulse potential. The voltage dependence of the steady-state inactivation was fitted with the following two-state Boltzmann function (3):

$$I(V) = \frac{I_{max}}{1 + \exp\left(\frac{V - V_{0.5}}{k}\right)} \quad (3)$$

with *I*_{max} corresponding to the maximal peak current amplitude and *V*_{0.5} to the half-inactivation voltage.

The recovery from inactivation was assessed using a double-pulse protocol preceded by a 50 ms-long hyperpolarizing prepulse to –110 mV from a holding potential of –100 mV. The cell membrane was depolarized for 2 s at –20 mV (inactivating prepulse) to ensure complete inactivation of the channel, and then to –20 mV for 150 ms (test pulse) after an increasing time period (interpulse) ranging between 1 ms and 8 s at –110 mV. The peak current from the test pulse was plotted as a ratio of the maximum prepulse current versus interpulse interval. The data were fitted with the following single-exponential function (4):

$$\frac{I}{I_{max}} = A \times \left(1 - \exp\left(-\frac{t}{\tau}\right)\right) \quad (4)$$

where *τ* is the time constant for channel recovery from inactivation.

Computational modeling

Simulation of thalamic reticular neuron (nRT) firing was performed using the NEURON simulation environment (<https://senselab.med.yale.edu/ModelDB/>) [31] in the three-compartment model previously described [32].

The electrophysiological properties of wild-type and TG-associated $Ca_v3.2$ variants obtained experimentally were modeled using Hodgkin-Huxley equations as previously described [33] and introduced into the model. To take into account the relative expression of $Ca_v3.2$ channels in nRT neurons (about 40% of $Ca_v3.2$ and 60% of $Ca_v3.3$ [34]) and the heterozygous nature of TN-associated $Ca_v3.2$ variants, only 20% of the T-type channel conductance described in the original model was altered with experimental values obtained for WT and TN-associated $Ca_v3.2$ variants. The simulation was performed at a holding potential set to -70 mV and the electrical membrane potential of the virtual soma was monitored in response to a 200ms-long hyperpolarizing and depolarizing current injection in order to assess rebound and tonic firing, respectively.

Statistical analysis

Average data are presented as mean \pm S.E.M. for n measurements. Statistical analysis was performed using GraphPad Prism 8. A Kolmogorov–Smirnov normality test was performed and statistical significance was assessed using Kruskal–Wallis test with Dunn’s post-test. Datasets were considered significantly different for $p \leq 0.05$.

Results

Expression of TN-associated $Ca_v3.2$ variants

To assess the functional impact of TN-associated *CACNA1H* variants, tsA-201 cells were transiently transfected with plasmids encoding human $Ca_v3.2$ wild-type (WT) and TN-associated variants for electrophysiological analysis. Whole-cell patch clamp recordings in tsA-201 cells expressing wild-type (WT) and TN-associated $Ca_v3.2$ variants revealed that all variants were functionally expressed and generated a characteristic low-voltage-activated T-type current similar to WT channels (Fig. 2a–n, left panels). The maximal whole-cell macroscopic T-type channel conductance (G_{max}) obtained from the fit of the current–voltage relationships (Fig. 2a–n, right panels) revealed no significant difference between cells expressing $Ca_v3.2$ variants compared to cells expressing the WT channel except for the R1674H variant where G_{max} was reduced by 56% ($p=0.0185$) (Fig. 2o and Table 1).

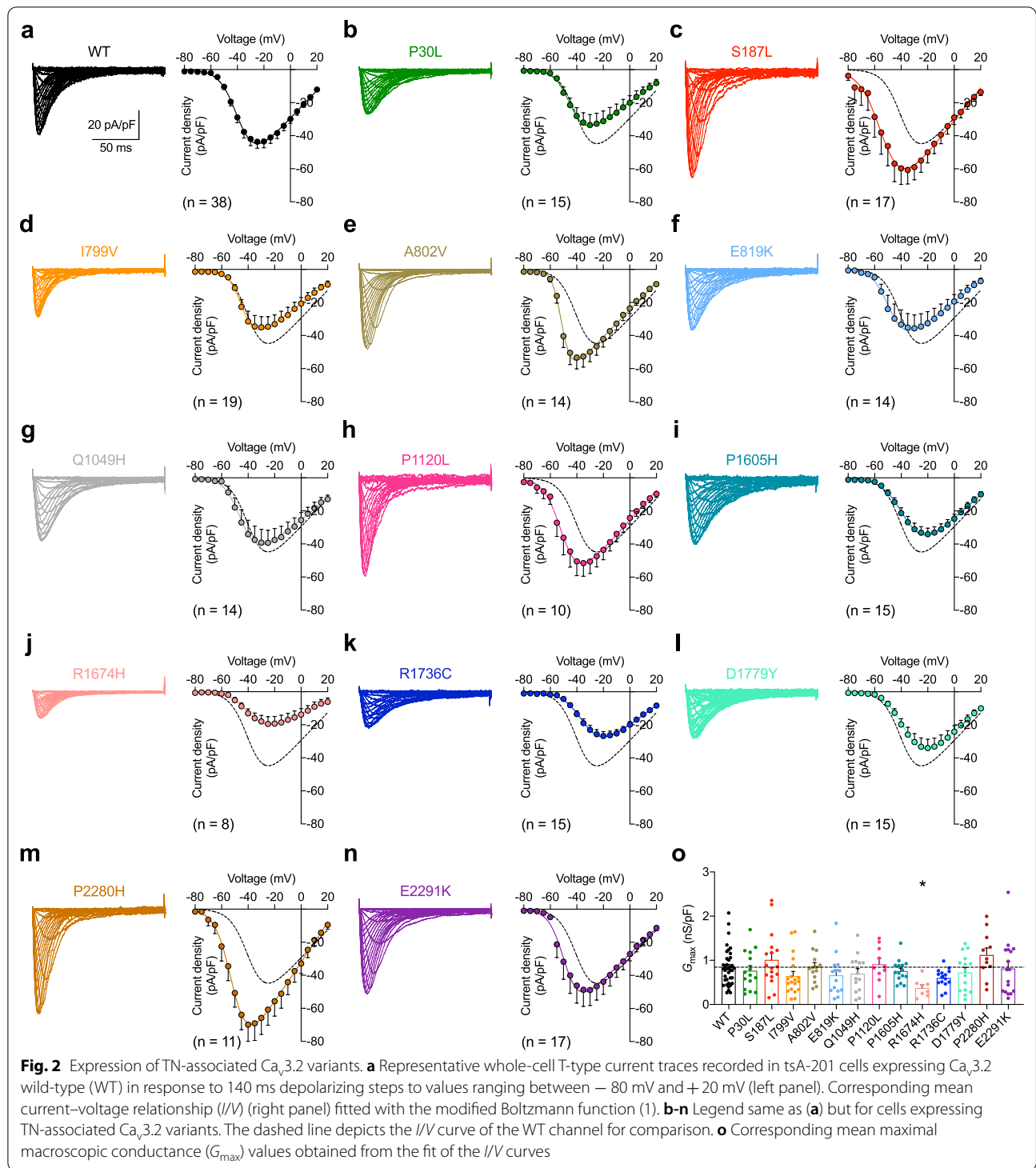
TN-associated *CACNA1H* variants alter the gating properties of $Ca_v3.2$ channels

Next, we aimed to assess the gating properties of TN-associated $Ca_v3.2$ variants. First, we analyzed the

voltage dependence of activation of the channels. In 6 (S187L, A802V, E819K, P1120L, P2280H, and E2291K) out of the 13 variants analyzed, the mean half-activation potential of the T-type current was significantly shifted toward more hyperpolarized potentials by -8.0 mV (E2291K, $p=0.0268$) up to -15.0 mV (P2280H, $p<0.0001$) relative to WT channels which is consistent with a GoF of the channels (Fig. 3a–o and Table 1). In addition, a significant decrease of the activation slope factor (k) was observed for S187L, A802V, E819K, and P2280H variants suggesting an increased coupling between the channel voltage-sensor and the pore opening again consistent with a GoF which may be particularly relevant for voltage changes close to the resting membrane potential where first openings of the channel occur (Table 1). To gain additional insights into the electrophysiological properties of TN-associated $Ca_v3.2$ variants, we then assessed their voltage dependence of inactivation. A statistically significant hyperpolarizing shift of the voltage dependence of inactivation by -12.6 mV ($p=0.0015$) relative to WT channels was observed for the P2280H variant and a similar trend albeit not statistically significant was observed for S187L (-8.6 mV, $p=0.8716$) and A802V variants (-9.2 mV, $p=0.3699$) whereas the remaining variants remained unaltered (Fig. 4a–o and Table 2). The alteration of the voltage dependence of inactivation is consistent with a LoF of the channel variants although the extent to which it may affect channel activity will largely depend on the resting membrane potential of cells, with a more pronounced effect in cells with a comparatively depolarized resting potential. In contrast, the kinetics of recovery from inactivation were accelerated by 2.7-fold for A802V ($p=0.0001$) and by 3.5-fold for Q1049H variants ($p=0.0005$) compared to WT channels, and a similar trend (albeit not statistically significant) was observed for several other variants indicative of a GoF (Fig. 5a–o and Table 2).

$Ca_v3.2$ -dependent window current is altered by TN-associated *CACNA1H* variants

Because several TN-associated $Ca_v3.2$ variants showed alterations in the voltage dependence of activation and/or inactivation, we aimed to assess the impact on the T-type window current by visualizing the overlapping area between the activation and inactivation curves (Fig. 6a–g). In all TN-associated $Ca_v3.2$ variants for which the voltage dependence of activation and/or inactivation was altered, the window current was displaced toward more hyperpolarized potentials with the peak-voltage shifted by -5 mV (P1120L) up-to



– 12 mV (P2280H) (Fig. 6h). This effect was accompanied by an increased magnitude of the window current (except for the P2280H variant) ranging from 14% (E2291K) up-to 165% increase (P1120L) (Fig. 6i).

TN-associated $Ca_v3.2$ variants increase neuronal firing in a computational model of thalamic neurons

Given that $Ca_v3.2$ channels are highly expressed in thalamic neurons where they play an essential role in

Table 1 Steady-state activation properties of TN-associated human Ca_v3.2 variants expressed in tsA-201 cells

Ca _v 3.2	Activation						
	G _{max} (nS/pF)	p	V _{0.5} (mV)	p	k (mV)	p	(n)
WT	0.84 ± 0.07		− 38.17 ± 0.80		6.38 ± 0.35		38
P30L	0.77 ± 0.11	>0.9999	− 44.18 ± 1.24	0.1251	4.70 ± 0.51	0.2024	15
S187L	1.01 ± 0.15	>0.9999	− 51.63 ± 2.56	<0.0001	3.47 ± 0.50	0.0006	17
I799V	0.65 ± 0.10	0.6889	− 41.78 ± 1.58	0.5519	5.62 ± 0.69	>0.9999	19
A802V	0.85 ± 0.09	>0.9999	− 48.82 ± 1.14	<0.0001	3.56 ± 0.45	0.0015	14
E819K	0.66 ± 0.12	>0.9999	− 48.19 ± 2.97	0.0208	4.31 ± 0.53	0.0491	14
Q1049H	0.70 ± 0.11	>0.9999	− 41.88 ± 2.42	>0.9999	4.99 ± 0.67	0.7660	14
P1120L	0.91 ± 0.13	>0.9999	− 49.55 ± 3.17	0.0106	4.23 ± 0.56	0.1175	10
P1605H	0.76 ± 0.06	>0.9999	− 34.53 ± 1.60	>0.9999	8.17 ± 0.34	0.2336	15
R1674H	0.37 ± 0.07	0.0185	− 38.23 ± 2.30	>0.9999	6.49 ± 0.99	>0.9999	8
R1736C	0.60 ± 0.05	0.8669	− 32.42 ± 1.38	0.4164	7.39 ± 0.29	>0.9999	15
D1779Y	0.72 ± 0.11	>0.9999	− 33.86 ± 1.12	>0.9999	8.08 ± 0.27	0.2457	15
P2280H	1.12 ± 0.16	>0.9999	− 53.12 ± 2.31	<0.0001	3.87 ± 0.37	0.0159	11
E2291K	0.81 ± 0.15	>0.9999	− 46.13 ± 2.01	0.0268	4.91 ± 0.69	0.1754	17

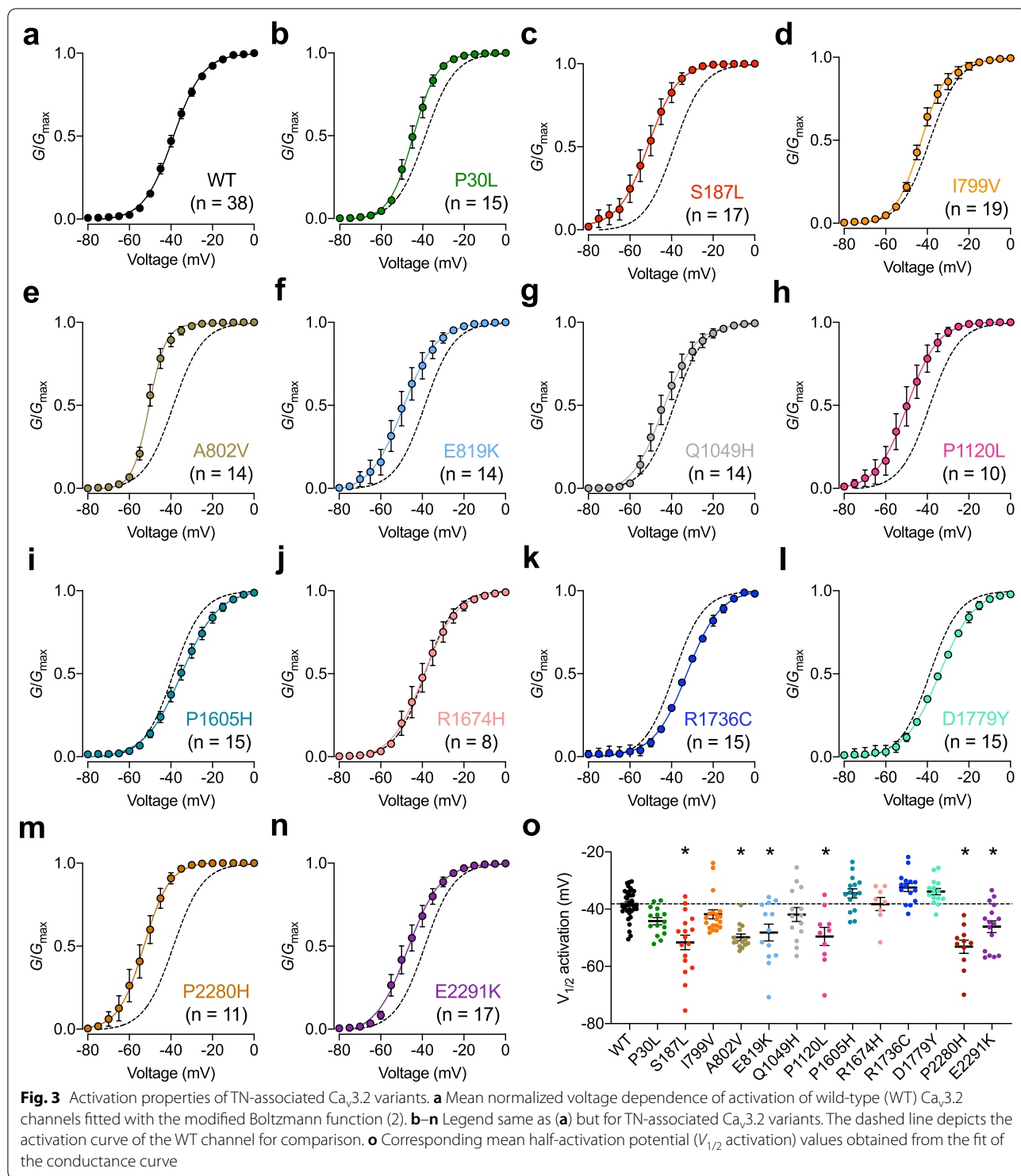
regulating neuronal excitability [35] and considering that the thalamus is a key relay station in the trigeminal sensory pathway [36], we aimed to simulate the functional consequence of TN-associated Ca_v3.2 variants on neuronal electrical activities using a computational model of reticular thalamic neuron (nRT). The simulation was performed with Ca_v3.2 variants for which an alteration of the voltage dependence of activation and/or inactivation was observed and the original model was altered in order to account for the relative contribution of Ca_v3.2 channels to the overall native T-type conductance and also to account for the heterozygous nature of TN-associated Ca_v3.2 variants (see *Methods*). Simulation of the neuronal membrane potential showed that hyperpolarizing current injections triggered rebound burst firing with WT as well as with TN-associated Ca_v3.2 variants (Fig. 7a–g). However, the minimum current necessary to trigger rebound firing (rheobase) was significantly less for TN-associated Ca_v3.2 variants (except A802V) compared to WT channels (Fig. 7h). Moreover, the firing frequency was increased (Fig. 7i). In contrast, when the firing was triggered with depolarizing current injections there was no major effect between WT and TN-associated Ca_v3.2 variants (Fig. 7j–r).

Discussion

Polymorphisms in the *CACNA1H* gene have been reported in a number of human disorders [37] and GoF mutations in Ca_v3.2 are linked to primary aldosteronism (PA) [38–40] and idiopathic generalized epilepsy (IGE) [41]. In contrast, LoF mutations were documented in

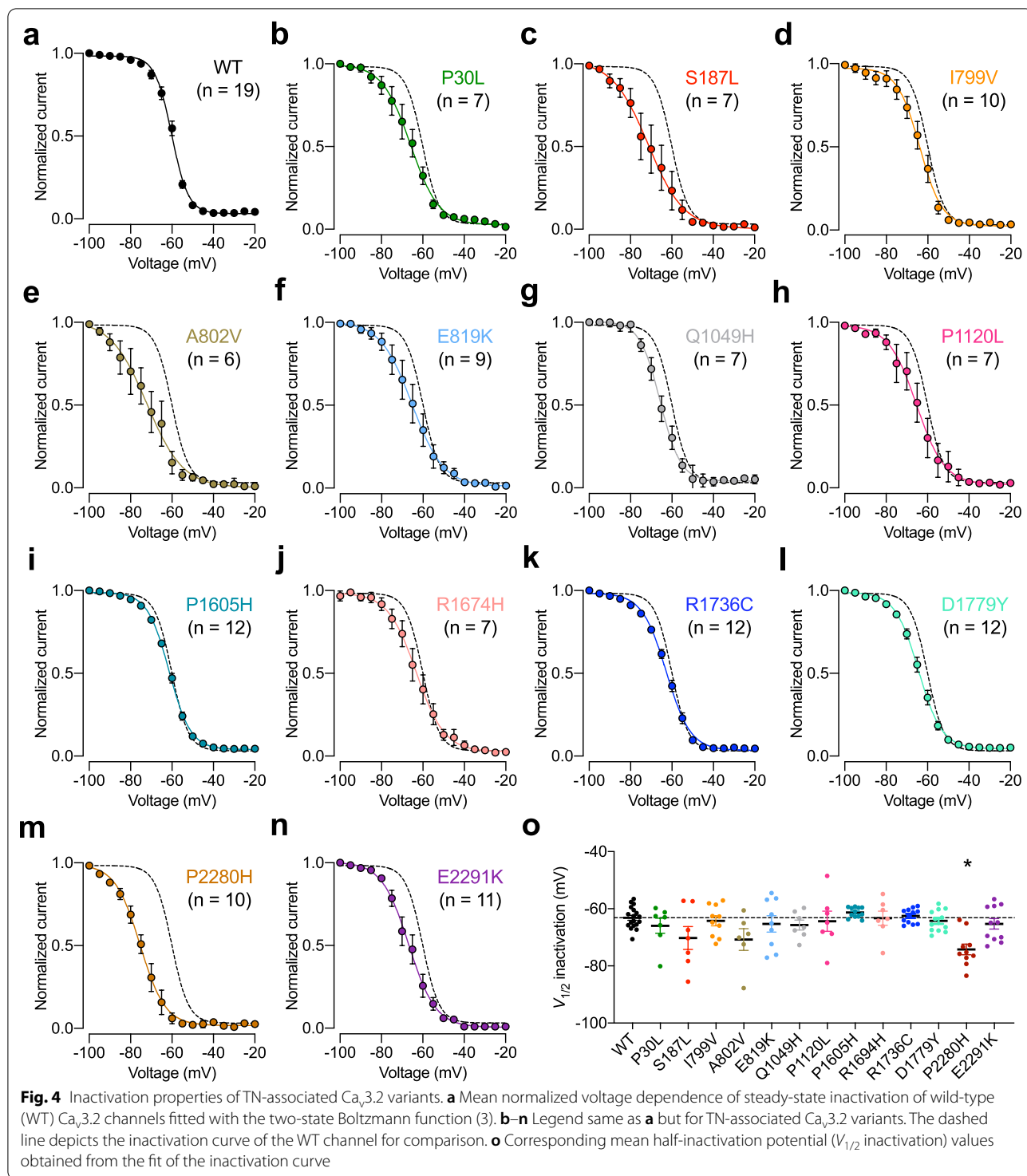
autism spectrum disorders [42], neuromuscular disorders [43–45], and developmental and epileptic encephalopathy [46].

In this study, we report the functional characterization of 13 Ca_v3.2 missense variants identified in TN patients. Patch clamp recordings of T-type currents in tsA-201 cells expressing recombinant TN-associated Ca_v3.2 variants showed that all variants were functional with no significant alteration in their maximal macroscopic conductance except for the R1674H variant for which the conductance was reduced. This effect was not further investigated but may have been caused by a decreased trafficking of the channel to the plasma membrane and/or decreased stability. In contrast, of the 13 Ca_v3.2 variants analyzed, 6 variants (S187L, A802V, E819K, P1120L, P2280H, and E2291K) displayed alterations in their gating properties evidenced by a recurrent hyperpolarized shift of the voltage dependence of activation consistent with a GoF of the channels. An additional acceleration of the recovery from inactivation was also observed for A802V and Q1049H. Although these variants showed similar alterations in their gating properties, they did not segregate into a particular region of Ca_v3.2. Nonetheless, some of the channel molecular determinants containing TN-associated variants are known to contribute to the gating of Ca_v3.2. For instance, the II-III loop containing variant P1120L and the C-terminus containing variants P2280H and E2291K were previously reported to affect the voltage dependence of T-type channels [47–49]. Moreover, the GoF effect of TN-associated variants in the C-terminus of Ca_v3.2 is reminiscent of what was reported



for several variants associated with (IGE) and PA [40, 50]. Importantly, when introduced into a computational model of nRT neuron, the 6 variants reduced the threshold for rebound burst firing implying an overall

GoF effect. This is consistent with previous findings in various types of neurons showing that upregulation of T-type channel activity underlies reduced threshold for rebound burst firing [51–55]. While our modeling was



performed in a computational model of nRT neurons, it may anticipate some of the possible effects of TN-associated $Ca_v3.2$ variants on the functioning of the trigeminal pathway for several reasons. First, although

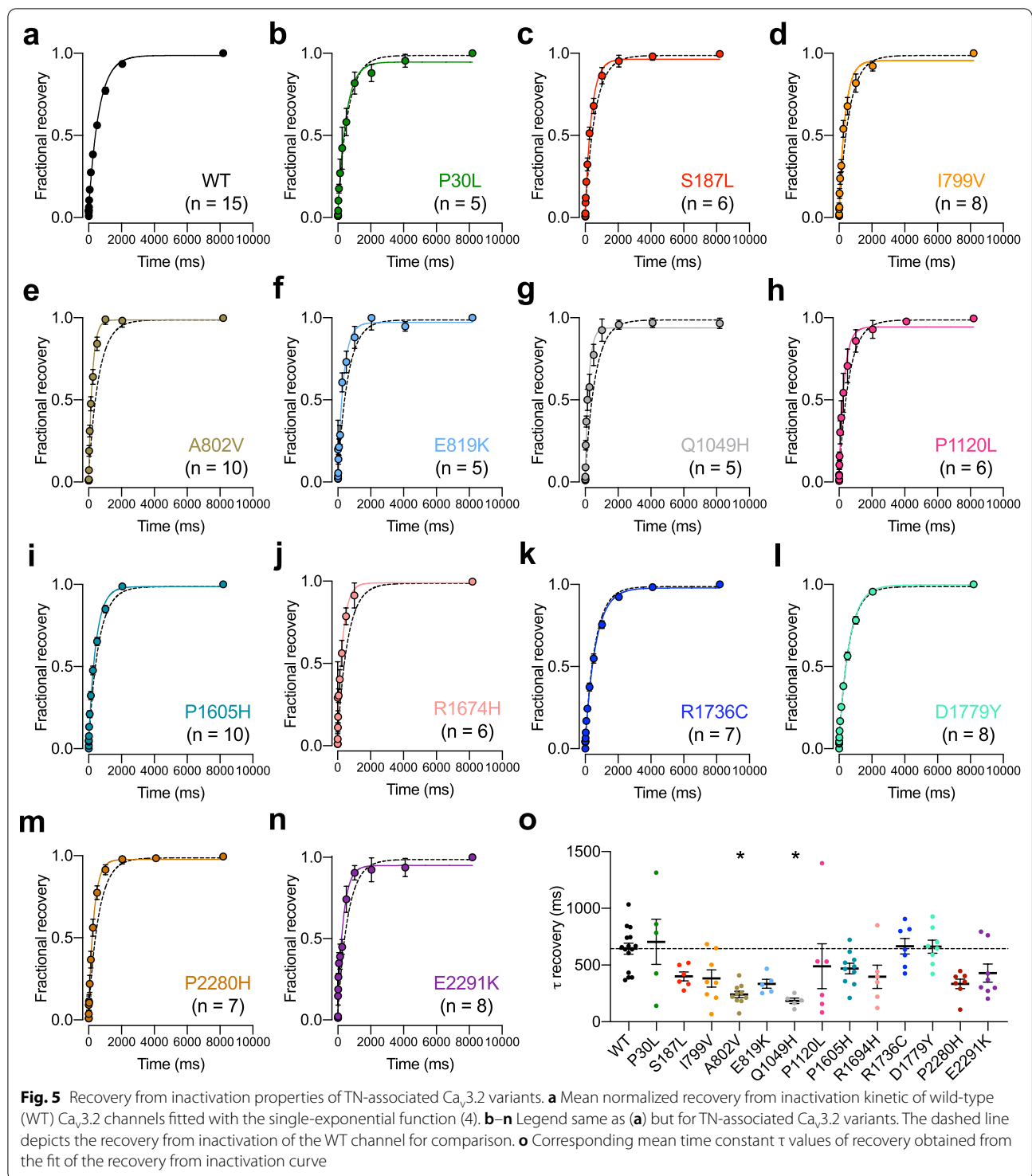
T-type dependent rebound burst firing has yet to be shown in trigeminal ganglion (TG) sensory neurons, it has been documented in dorsal root ganglion sensory neurons [56] and it is a possibility that it does also occur

Table 2 Steady-state inactivation and recovery from inactivation properties of TN-associated human Ca_v3.2 variants expressed in tsA-201 cells

Ca _v 3.2	Inactivation					Recovery from inactivation		
	V _{0.5} (mV)	p	k (mV)	p	(n)	τ (ms)	p	(n)
WT	-61.61 ± 1.75		-4.48 ± 0.22		19	644 ± 49		15
P30L	-65.95 ± 2.67	>0.9999	-4.75 ± 0.44	>0.9999	7	705 ± 200	>0.9999	5
S187L	-70.21 ± 3.99	0.8716	-4.10 ± 0.34	>0.9999	7	400 ± 39	0.6749	6
I799V	-64.22 ± 1.71	>0.9999	-4.27 ± 0.51	>0.9999	10	382 ± 76	0.1542	8
A802V	-70.79 ± 3.80	0.3699	-4.16 ± 0.39	>0.9999	6	241 ± 28	0.0001	10
E819K	-65.31 ± 2.86	>0.9999	-5.18 ± 0.55	>0.9999	9	335 ± 38	0.1564	5
Q1049H	-65.68 ± 1.74	>0.9999	-4.44 ± 0.28	>0.9999	7	185 ± 24	0.0005	5
P1120L	-64.38 ± 3.53	>0.9999	-3.64 ± 0.57	>0.9999	7	489 ± 197	0.4634	6
P1605H	-61.32 ± 0.51	>0.9999	-5.10 ± 0.19	>0.9999	12	470 ± 46	>0.9999	10
R1674H	-63.29 ± 2.49	>0.9999	-6.05 ± 1.04	>0.9999	7	397 ± 103	0.3918	6
R1736C	-62.48 ± 0.73	>0.9999	-5.50 ± 0.11	0.0191	12	665 ± 68	>0.9999	7
D1779Y	-64.23 ± 1.07	>0.9999	-5.03 ± 0.11	>0.9999	12	662 ± 58	>0.9999	8
P2280H	-74.22 ± 1.89	0.0015	-4.56 ± 0.37	>0.9999	10	334 ± 42	0.0724	7
E2291K	-65.27 ± 1.83	>0.9999	-4.23 ± 0.19	>0.9999	11	429 ± 80	0.3967	8

in TG neurons. Second, a low-threshold calcium conductance (presumably mediated by T-type channels) leading to calcium spikes and rebound burst firing has been reported in neurons of the brain stem trigeminal nuclei [57]. Third, the trigeminal pathway gates through the thalamus in particular via the VPM where T-type channels contribute to rebound burst firing [58]. And finally, alteration of thalamocortical rhythmic activities mediated by T-type channels has been implicated in the development of trigeminal pain [14]. Hence, all of these aspects suggest that alteration of rebound burst firing caused by TN-associated Ca_v3.2 variants could potentially contribute to the sensitization of the trigeminal pathway. In addition, alteration of the channel gating properties resulted in a hyperpolarizing displacement of the voltage dependence of the window current which implies an increased passive influx of calcium around the resting membrane potential of cells. Considering that the voltage range of the window current is an important determinant of neuronal electrical activities and calcium oscillations [59], this may further contribute to enhance neuronal activity. These data are consistent with a previous report showing that re-expression of a GoF TN-associated Ca_v3.2 variant in cultured TG neuron increased neuronal excitability [17]. The question then remains as to why TN patients harboring GoF Ca_v3.2 variants did not show signs of IGE or PA. It is a possibility that the gating alterations caused by these variants and affecting only the rebound burst firing in the absence of general alteration of the tonic firing is not enough to cause additional disease phenotypes.

In conclusion, our functional analysis of 13 Ca_v3.2 variants identified in TN patients revealed an overall GoF of the channel for 7 of these variants that could potentially contribute to the sensitization of the trigeminal pathway. Although these gating effects are reminiscent of what was previously reported for TN-associated variants in Na_v1.6 [18], Ca_v2.1 [21], TRPM7 [22, 23], and TRPM8 channels [24], it is important to consider that our functional analysis in a heterologous expression system provides only a snapshot of the phenotype of a mutation. Hence, additional analysis of these variants in native conditions will be necessary to further validate these findings. Moreover, it is a possibility that the variants for which we did not observe any gating alteration will show different phenotypes in a more complex physiological environment. Finally, although most of the gating alterations were in general consistent with a GoF of the channel, it is important to consider that one variant was associated with a LoF suggesting that GoF phenotypes in ion channels may not represent a universal feature in TN. For instance, the expression level of *SCN9A* (Na_v1.7) and *SCN10A* (Na_v1.8) is reduced in gingival tissue of TN patients [9], as well as in preclinical models of TN [11] implying a LoF phenotype, although this mechanism may occur as a protective mechanism to normalize neuronal excitability. Nonetheless, it is striking to note that all patients exhibiting idiopathic TN with concomitant continuous pain (iTN-2) harbored GoF Ca_v3.2 variants. In contrast, all Ca_v3.2 variants identified in patients with congenital TN and concomitant pain (cTN-2) did not cause any alteration of the channel (Table 3). While



additional studies are necessary to assess the exact role of $Ca_v3.2$ in the processing of trigeminal sensory information, our data add to the notion that rare *CACNA1H* variants may contribute to the etiology of TN. In that respect, the T-type channel blocker valproic acid was shown to be

effective to mitigate pain in some TN patients [60] suggesting that other antiepileptic T-type channel blockers ethosuximide, zonisamide, and nimodipine [26] should also be considered especially in patients resistant to first line therapies.

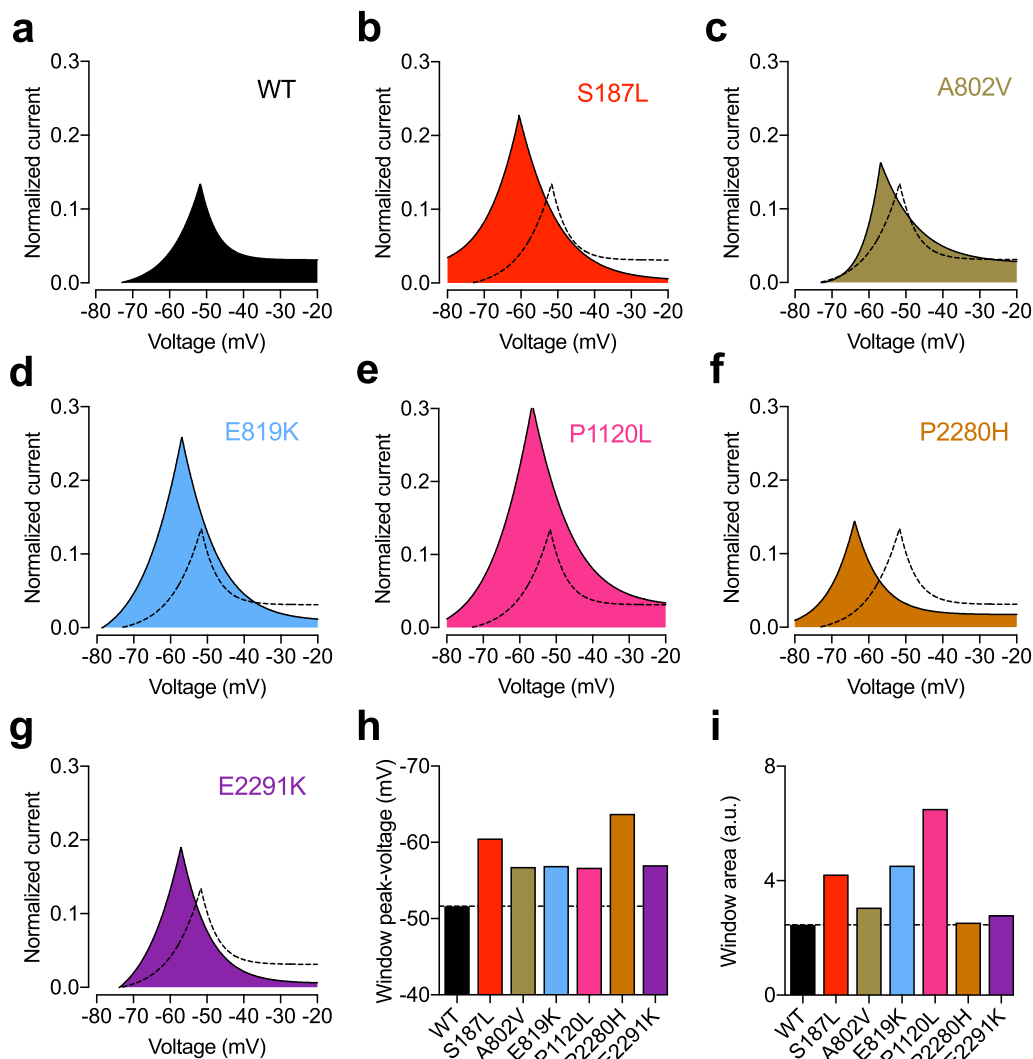


Fig. 6 Window current of TN-associated $Ca_v3.2$ variants. **a** Window current of wild-type (WT) $Ca_v3.2$ illustrated by the overlap of the mean activation and inactivation curves. **b-g** Legend same as **(a)** but for TN-associated $Ca_v3.2$ variants. The dashed line depicts the window current of the WT channel for comparison. **h** Corresponding peak-voltage values of the window current: WT (-51.6 mV), S187L (-60.5 mV), A802V (-56.8 mV), E819K (-56.9 mV), P1120L (-56.7 mV), P2280H (-63.8 mV), E2291K (-57.0 mV). **i** Corresponding magnitude values of the window current measured as the area under the curve: WT (2.5 a.u.), S187L (4.2 a.u.), A802V (3.1 a.u.), E819K (4.5 a.u.), P1120L (6.5 a.u.), P2280H (2.5 a.u.), E2291K (2.8 a.u.)

(See figure on next page.)

Fig. 7 Computer simulation of nRT neuron firing. **a** Representative electrical membrane potential of the virtual soma containing wild-type (WT) $Ca_v3.2$ channels in response to a 200 ms-long hyperpolarizing current injection of -0.65 nA (left panel) and corresponding number of spikes during the rebound as a function of the current injected (right panel). **b-g** Legend same as **a** but for TN-associated $Ca_v3.2$ variants. The dashed line depicts the number of spikes for WT channels for comparison. **h** Minimum current injection (rheobase) necessary to trigger rebound action potentials: WT (-0.585 nA), S187L (-0.568 nA), A802V (-0.606 nA), E819K (-0.561 nA), P1120L (-0.528 nA), E2280H (-0.471 nA), and E2291K (-0.559 nA). **i** Rebound firing frequency at -0.65 nA current injection: WT (15 Hz), S187L (35 Hz), A802V (10 Hz), E819K (45 Hz), P1120L (55 Hz), E2280H (55 Hz), and E2291K (20 Hz). **j-p** Legend same as **a-g** but for depolarizing current injections. Representative membrane potentials are shown in response to 0.2 nA current injection. **q** Minimum current injection (rheobase) necessary to trigger tonic action potentials: WT (0.0257 nA), S187L (0.0258 nA), A802V (0.0260 nA), E819K (0.0255 nA), P1120L (0.0251 nA), E2280H (0.0254 nA), and E2291K (0.0255 nA). **r** Action potential frequency at 0.2 nA current injection: WT (170 Hz), S187L (180 Hz), A802V (170 Hz), E819K (180 Hz), P1120L (185 Hz), E2280H (175 Hz), and E2291K (175 Hz)

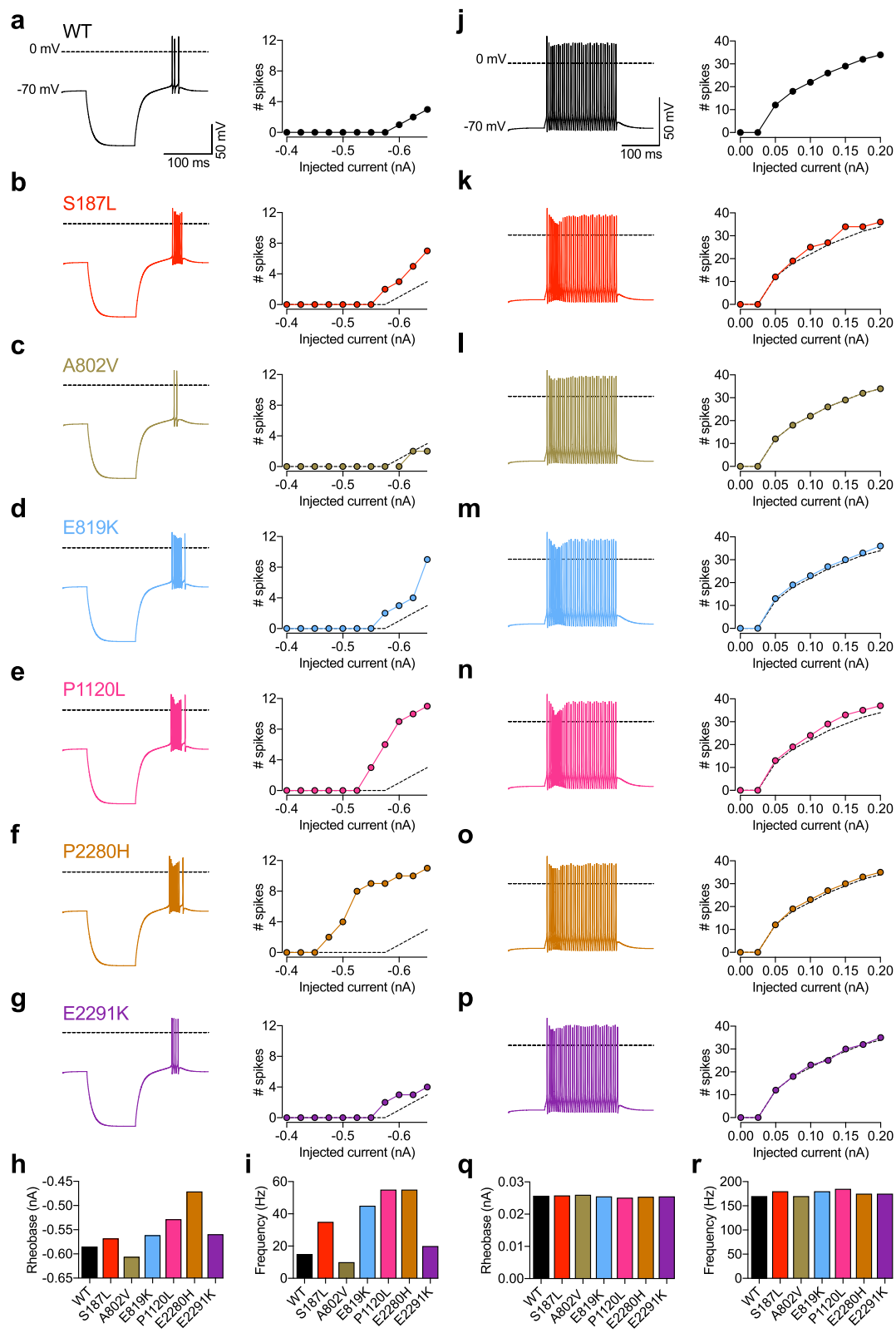


Fig. 7 (See legend on previous page.)

Table 3 Summary of gating effects of TN-associated Ca_v3.2 variants in relation to the clinical phenotype of patients

Idiopathic TN**	Ca _v 3.2 variant	Classical TN**	Ca _v 3.2 variant
iTN-1	E286K*	cTN-1	<i>E2291K</i>
iTN-1	<i>G563R*</i>		
iTN-1	R1674H	cTN-2	P30L
iTN-1	D1779Y	cTN-2	H526Y*
		cTN-2	I799V
iTN-2	<i>P566T*</i>	cTN-2	P1605H
iTN-2	<i>E819K</i>	cTN-2	R1736C
iTN-2	<i>Q1049H</i>	cTN-2	P30L
iTN-2	<i>P1120L</i>		
iTN-2	<i>P2280H</i>		

Italic: GoF

Bold: LoF

Bolditalic: Neutral

iTN idiopathic trigeminal neuralgia, *cTN* classical trigeminal neuralgia; (– 1), purely paroxysmal; (– 2) with concomitant continuous pain. *According to [17]. **According to [25]. Two GoF variants (S187L and A802V) are not included in this table since their clinical phenotype was not fully defined (atypical facial pain and TN without further information, respectively)

Abbreviations

cTN-1: Classical trigeminal neuralgia purely paroxysmal; cTN-2: Classical trigeminal neuralgia with concomitant continuous pain; GoF: Gain-of-function; IGE: Idiopathic generalized epilepsy; iTN-1: Idiopathic trigeminal neuralgia purely paroxysmal; iTN-2: Idiopathic trigeminal neuralgia with concomitant continuous pain; LoF: Loss-of-function; nRT: Reticular thalamic neuron; PA: Primary aldosteronism; SpV: Spinal trigeminal nucleus; TG: Trigeminal ganglion; TN: Trigeminal neuralgia; VPM: Ventroposterior nucleus; WT: Wild-type.

Acknowledgements

Not applicable.

Author contributions

ERM, EG, RNS, and IAS performed experiments and analyzed the data. ERM performed the computational simulation. GWZ and NW designed and supervised the study and wrote the manuscript. All authors critically revised the manuscript and contributed significantly to this work. All authors read and approved the final manuscript.

Funding

R.N.S. holds a studentship from Charles University. E.G. holds a studentship from Alberta Innovates. G.W.Z. is supported by a grant from the Canadian Institutes of Health Research and holds a Canada Research Chair. N.W. is supported by a grant from the Czech Science Foundation (GACR #22-23242S) and the National Institute for Research of Metabolic and Cardiovascular Diseases (Program EXCELES #LX22NPO5104), funded by the European Union—Next Generation EU.

Availability of data and materials

All data generated or analyzed during this study are included in this published article and its supplementary information files.

Declarations

Ethics approval and consent to participate

Not applicable.

Consent for publication

Not applicable.

Competing interests

The authors have no competing interests to declare.

Author details

¹Department of Pathophysiology, Third Faculty of Medicine, Charles University, Prague, Czech Republic. ²Department of Clinical Neurosciences, Alberta Children's Hospital Research Institute, Hotchkiss Brain Institute, Cumming School of Medicine, University of Calgary, Calgary, Canada. ³Institute of Organic Chemistry and Biochemistry, Czech Academy of Sciences, Prague, Czech Republic.

Received: 12 October 2022 Accepted: 2 November 2022

Published online: 17 November 2022

References

- Cruccu G, Di Stefano G, Truini A. Trigeminal neuralgia. *N Engl J Med*. 2020;383(8):754–62.
- Gambeta E, Chichorro JG, Zamponi GW. Trigeminal neuralgia: an overview from pathophysiology to pharmacological treatments. *Mol Pain*. 2020;16:1744806920901890.
- Eide PK. Familial occurrence of classical and idiopathic trigeminal neuralgia. *J Neurol Sci*. 2022;434: 120101.
- Rappaport HZ, Devor M. Trigeminal neuralgia: the role of self-sustaining discharge in the trigeminal ganglion. *Pain*. 1994;56(2):127–38.
- Devor M, Amir R, Rappaport ZH. Pathophysiology of trigeminal neuralgia: the ignition hypothesis. *Clin J Pain*. 2002;18(1):4–13.
- Devor M, Govrin-Lippmann R, Rappaport ZH. Mechanism of trigeminal neuralgia: an ultrastructural analysis of trigeminal root specimens obtained during microvascular decompression surgery. *J Neurosurg*. 2002;96(3):532–43.
- Burchiel KJ, Baumann TK. Pathophysiology of trigeminal neuralgia: new evidence from a trigeminal ganglion intraoperative microneurographic recording. *Case report J Neurosurg*. 2004;101(5):872–3.
- Obermann M. Treatment options in trigeminal neuralgia. *Ther Adv Neurol Disord*. 2010;3(2):107–15.
- Siqueira SR, Alves B, Malpartida HM, Teixeira MJ, Siqueira JT. Abnormal expression of voltage-gated sodium channels Nav1.7, Nav1.3 and Nav1.8 in trigeminal neuralgia. *Neuroscience*. 2009;164(2):573–7.
- Luiz AP, Kopach O, Santana-Varela S, Wood JN. The role of Nav1.9 channel in the development of neuropathic orofacial pain associated with trigeminal neuralgia. *Mol Pain*. 2015;11:72.
- Xu W, Zhang J, Wang Y, Wang L, Wang X. Changes in the expression of voltage-gated sodium channels Nav1.3, Nav1.7, Nav1.8, and Nav1.9 in rat trigeminal ganglia following chronic constriction injury. *NeuroReport*. 2016;27(12):929–34.
- Vit JP, Ohara PT, Bhargava A, Kelley K, Jasmin L. Silencing the Kir4.1 potassium channel subunit in satellite glial cells of the rat trigeminal ganglion results in pain-like behavior in the absence of nerve injury. *J Neurosci*. 2008;28(16):4161–71.
- Takeda M, Takahashi M, Nasu M, Matsumoto S. Peripheral inflammation suppresses inward rectifying potassium currents of satellite glial cells in the trigeminal ganglia. *Pain*. 2011;152(9):2147–56.
- Choi S, Yu E, Hwang E, Llinás RR. Pathophysiological implication of Cav3.1 T-type Ca²⁺ channels in trigeminal neuropathic pain. *Proc Natl Acad Sci U S A*. 2016;113(8):2270–5.
- Montera M, Benemei S, Materazzi S, De Logu F, De Siena G, Fusi C, et al. TRPA1 mediates trigeminal neuropathic pain in mice downstream of monocytes/macrophages and oxidative stress. *Brain*. 2016;139(Pt 5):1361–77.
- Montera M, Goins A, Cmarko L, Weiss N, Westlund KN, Alles SRA. Trigeminal neuropathic pain is alleviated by inhibition of Cav3.3 T-type calcium channels in mice. *Channels (Austin)*. 2021;15(1):31–7.

17. Gambeta E, Gandini MA, Souza IA, Zamponi GW. Cav32 calcium channels contribute to trigeminal neuralgia. *Pain*. 2022. <https://doi.org/10.1097/j.pain.0000000000002651>.
18. Tanaka BS, Zhao P, Dib-Hajj FB, Morisset V, Tate S, Waxman SG, et al. A gain-of-function mutation in Nav1.6 in a case of trigeminal neuralgia. *Mol Med*. 2016;22:338–48.
19. Costa GMF, Rocha LPC, Siqueira SRDT, Moreira PR, Almeida-Leite CM. No association of polymorphisms in Nav1.7 or nerve growth factor receptor genes with trigeminal neuralgia. *Pain Med*. 2019;20(7):1362–9.
20. Di Stefano G, Yuan JH, Cruccu G, Waxman SG, Dib-Hajj SD, Truini A. Familial trigeminal neuralgia—a systematic clinical study with a genomic screen of the neuronal electrogenome. *Cephalalgia*. 2020;40(8):767–77.
21. Gambeta E, Gandini MA, Souza IA, Ferron L, Zamponi GW. A CACNA1A variant associated with trigeminal neuralgia alters the gating of Cav2.1 channels. *Mol Brain*. 2021;14(1):4.
22. Gualdani R, Gailly P, Yuan JH, Yerna X, Di Stefano G, Truini A, et al. A TRPM7 mutation linked to familial trigeminal neuralgia: Omega current and hyperexcitability of trigeminal ganglion neurons. *Proc Natl Acad Sci U S A*. 2022;119(38): e2119630119.
23. Weiss N, Zamponi GW. The omega of TRPM7 channels in trigeminal neuralgia. *Pflugers Arch*. 2022. <https://doi.org/10.1007/s00424-022-02757-w>.
24. Gualdani R, Yuan JH, Effraim PR, Di Stefano G, Truini A, Cruccu G, et al. Trigeminal neuralgia TRPM8 mutation: enhanced activation, basal $[Ca^{2+}]_i$ and menthol response. *Neurol Genet*. 2021;7(1): e550.
25. Dong W, Jin SC, Allocco A, Zeng X, Sheth AH, Panchagnula S, et al. Exome sequencing implicates impaired GABA signaling and neuronal ion transport in trigeminal neuralgia. *iScience*. 2020;23(10):101552.
26. Weiss N, Zamponi GW. T-type calcium channels: from molecule to therapeutic opportunities. *Int J Biochem Cell Biol*. 2019;108:34–9.
27. Zhang Y, Ji H, Wang J, Sun Y, Qian Z, Jiang X, et al. Melatonin-mediated inhibition of Cav3.2 T-type Ca^{2+} channels induces sensory neuronal hypoexcitability through the novel protein kinase C- η isoform. *J Pineal Res*. 2018;64(4):e12476.
28. Wang H, Wei Y, Pu Y, Jiang D, Jiang X, Zhang Y, et al. Brain-derived neurotrophic factor stimulation of T-type Ca^{2+} channels in sensory neurons contributes to increased peripheral pain sensitivity. *Sci Signal*. 2019;12(600):eaaw2300.
29. Liao YF, Tsai ML, Chen CC, Yen CT. Involvement of the Cav3.2 T-type calcium channel in thalamic neuron discharge patterns. *Mol Pain*. 2011;7:43.
30. Gomez K, Khanna R. Cav32 calcium channels: new players in facial pain. *Pain*. 2022. <https://doi.org/10.1097/j.pain.0000000000002652>.
31. Hines ML, Carnevale NT. The NEURON simulation environment. *Neural Comput*. 1997;9(6):1179–209.
32. Destexhe A, Contreras D, Steriade M, Sejnowski TJ, Huguenard JR. In vivo, in vitro, and computational analysis of dendritic calcium currents in thalamic reticular neurons. *J Neurosci*. 1996;16(1):169–85.
33. Huguenard JR, McCormick DA. Simulation of the currents involved in rhythmic oscillations in thalamic relay neurons. *J Neurophysiol*. 1992;68(4):1373–83.
34. Talley EM, Solorzano G, Depaulis A, Perez-Reyes E, Bayliss DA. Low-voltage-activated calcium channel subunit expression in a genetic model of absence epilepsy in the rat. *Mol Brain Res*. 2000;75(1):159–65.
35. Cain SM, Tyson JR, Choi HB, Ko R, Lin PJC, LeDue JM, et al. Cav 3.2 drives sustained burst-firing, which is critical for absence seizure propagation in reticular thalamic neurons. *Epilepsia*. 2018;59(4):778–91.
36. Danyluk H, Andrews J, Kesarwani R, Seres P, Broad R, Wheatley BM, et al. The thalamus in trigeminal neuralgia: structural and metabolic abnormalities, and influence on surgical response. *BMC Neurol*. 2021;21(1):290.
37. Weiss N, Zamponi GW. Genetic T-type calcium channelopathies. *J Med Genet*. 2020;57(1):1–10.
38. Scholl UI, Stölting G, Nelson-Williams C, Vichot AA, Choi M, Loring E, et al. Recurrent gain of function mutation in calcium channel CACNA1H causes early-onset hypertension with primary aldosteronism. *Elife*. 2015;4: e06315.
39. Reimer EN, Walenda G, Seidel E, Scholl UI. CACNA1H(M1549V) mutant calcium channel causes autonomous aldosterone production in HAC15 cells and is inhibited by mibefradil. *Endocrinology*. 2016;157(8):3016–22.
40. Daniil G, Fernandes-Rosa FL, Chemin J, Blesneac I, Beltrand J, Polak M, et al. CACNA1H mutations are associated with different forms of primary aldosteronism. *EBioMedicine*. 2016;13:225–36.
41. Khosravani H, Zamponi GW. Voltage-gated calcium channels and idiopathic generalized epilepsies. *Physiol Rev*. 2006;86(3):941–66.
42. Splawski I, Yoo DS, Stotz SC, Cherry A, Clapham DE, Keating MT. CACNA1H mutations in autism spectrum disorders. *J Biol Chem*. 2006;281(31):22085–91.
43. Rzhetsky Y, Lazniewska J, Blesneac I, Pamphlett R, Weiss N. CACNA1H missense mutations associated with amyotrophic lateral sclerosis alter Cav3.2 T-type calcium channel activity and reticular thalamic neuron firing. *Channels (Austin)*. 2016;10(6):466–77.
44. Stringer RN, Jurkovicova-Tarabova B, Huang S, Haji-Ghassemi O, Idoux R, Liashenko A, et al. A rare CACNA1H variant associated with amyotrophic lateral sclerosis causes complete loss of Cav3.2 T-type channel activity. *Mol Brain*. 2020;13(1):33.
45. Carter MT, McMillan HJ, Tomin A, Weiss N. Compound heterozygous CACNA1H mutations associated with severe congenital amyotrophy. *Channels (Austin)*. 2019;13(1):153–61.
46. Stringer RN, Jurkovicova-Tarabova B, Souza IA, Ibrahim J, Vacik T, Fathalla WM, et al. De novo SCN8A and inherited rare CACNA1H variants associated with severe developmental and epileptic encephalopathy. *Mol Brain*. 2021;14(1):126.
47. Kang HW, Park JY, Lee JH. Distinct contributions of different structural regions to the current kinetics of the Cav3.3 T-type Ca^{2+} channel. *Biochim Biophys Acta*. 2008;1778(12):2740–8.
48. Weiss N, Hameed S, Fernández-Fernández JM, Fablet K, Karmazinova M, Poillot C, et al. A $Ca(v)3.2$ /syntaxin-1A signaling complex controls T-type channel activity and low-threshold exocytosis. *J Biol Chem*. 2012;287(4):2810–8.
49. Jurkovicova-Tarabova B, Cmarko L, Rehak R, Zamponi GW, Lacinova L, Weiss N. Identification of a molecular gating determinant within the carboxy terminal region of Cav3.3 T-type channels. *Mol Brain*. 2019;12(1):34.
50. Heron SE, Khosravani H, Varela D, Bladen C, Williams TC, Newman MR, et al. Extended spectrum of idiopathic generalized epilepsies associated with CACNA1H functional variants. *Ann Neurol*. 2007;62(6):560–8.
51. Jagodic MM, Pathirathna S, Nelson MT, Mancuso S, Joksovic PM, Rosenberg ER, et al. Cell-specific alterations of T-type calcium current in painful diabetic neuropathy enhance excitability of sensory neurons. *J Neurosci*. 2007;27(12):3305–16.
52. Canto-Bustos M, Loeza-Alcocer E, González-Ramírez R, Gandini MA, Delgado-Lezama R, Felix R. Functional expression of T-type Ca^{2+} channels in spinal motoneurons of the adult turtle. *PLoS ONE*. 2014;9: e108187.
53. Huang D, Huang S, Gao H, Liu Y, Qi J, Chen P, et al. Redox-dependent modulation of T-type Ca^{2+} channels in sensory neurons contributes to acute anti-nociceptive effect of substance P. *Antioxid Redox Signal*. 2016;25(5):233–51.
54. Nigam A, Hargus NJ, Barker BS, Ottolini M, Hounshell JA, Bertram EH, et al. Inhibition of T-type calcium channels in mEC layer II stellate neurons reduces neuronal hyperexcitability associated with epilepsy. *Epilepsy Res*. 2019;154:132–8.
55. Tracy ME, Tesic V, Stamenic TT, Joksimovic SM, Busquet N, Jevtovic-Todorovic V, et al. Cav31 isoform of T-type calcium channels supports excitability of rat and mouse ventral tegmental area neurons. *Neuropharmacology*. 2018;135:343–54.
56. Zhu T, Wei S, Wang Y. Post-inhibitory rebound firing of dorsal root ganglia neurons. *J Pain Res*. 2022;15:2029–40.
57. Guido W, Günhan-Agar E, Erzurumlu RS. Developmental changes in the electrophysiological properties of brain stem trigeminal neurons during pattern (barrelette) formation. *J Neurophysiol*. 1998;79(3):1295–306.
58. Landisman CE, Connors BW. VPM and PoM nuclei of the rat somatosensory thalamus: intrinsic neuronal properties and corticothalamic feedback. *Cereb Cortex*. 2007;17(12):2853–65.
59. Williams SR, Tóth TI, Turner JP, Hughes SW, Crunelli V. The 'window' component of the low threshold Ca^{2+} current produces input signal amplification and bistability in cat and rat thalamocortical neurones. *J Physiol*. 1997;505(Pt 3):689–705.
60. Peiris JB, Perera GL, Devendra SV, Lionel ND. Sodium valproate in trigeminal neuralgia. *Med J Aust*. 1980;2(5):278.

Publisher's Note

Springer Nature remains neutral with regard to jurisdictional claims in published maps and institutional affiliations.

MICRO REPORT

Open Access



Secretory carrier-associated membrane protein 2 (SCAMP2) regulates cell surface expression of T-type calcium channels

Leos Cmarko^{1,2} , Robin N. Stringer^{2,3} , Bohumila Jurkovicova-Tarabova⁴ , Tomas Vacik¹ ,
Lubica Lacinova⁴ and Norbert Weiss^{1,2,3,4*}

Abstract

Low-voltage-activated T-type Ca^{2+} channels are key regulators of neuronal excitability both in the central and peripheral nervous systems. Therefore, their recruitment at the plasma membrane is critical in determining firing activity patterns of nerve cells. In this study, we report the importance of secretory carrier-associated membrane proteins (SCAMPs) in the trafficking regulation of T-type channels. We identified SCAMP2 as a novel $\text{Ca}_v3.2$ -interacting protein. In addition, we show that co-expression of SCAMP2 in mammalian cells expressing recombinant $\text{Ca}_v3.2$ channels caused an almost complete drop of the whole cell T-type current, an effect partly reversed by single amino acid mutations within the conserved cytoplasmic E peptide of SCAMP2. SCAMP2-induced downregulation of T-type currents was also observed in cells expressing $\text{Ca}_v3.1$ and $\text{Ca}_v3.3$ channel isoforms. Finally, we show that SCAMP2-mediated knockdown of the T-type conductance is caused by the lack of $\text{Ca}_v3.2$ expression at the cell surface as evidenced by the concomitant loss of intramembrane charge movement without decrease of total $\text{Ca}_v3.2$ protein level. Taken together, our results indicate that SCAMP2 plays an important role in the trafficking of $\text{Ca}_v3.2$ channels at the plasma membrane.

Keywords: Ion channels, Calcium channels, T-type channels, $\text{Ca}_v3.2$ channels, Secretory carrier-associated membrane protein 2, SCAMP2, Trafficking

Through their ability to pass calcium ions (Ca^{2+}) near the resting membrane potential, low-voltage-activated T-type channels have an important physiological role in shaping firing activity patterns of nerve cells, both in the central and peripheral nervous system. The implication of T-type channels in the control of neuronal excitability is partly defined by the density of channels embedded in the plasma membrane. Therefore, a number of molecular mechanisms and signaling pathways come into play to underly precise control of cell surface expression

of T-type channels [1] and defects whether genetic or acquired can lead to severe neuronal conditions [2, 3].

Secretory carrier-associated membrane proteins (SCAMPs) form a family of integral membrane proteins essentially expressed in the trans-Golgi network and recycling endosome membranes where they regulate vesicular trafficking and vesicle recycling processes [4]. Of the five known mammalian SCAMPs, SCAMP2 shows a ubiquitous expression pattern including in neuronal tissues where SCAMP2 transcripts are observed for instance in the cerebellum, thalamus, hippocampus, and spinal cord (<https://www.proteinatlas.org/ENSG00000140497-SCAMP2/tissue>). SCAMP2 consists of four trans-membrane helices with cytoplasmic amino- and carboxy-termini and a so-called E peptide located between

*Correspondence: nalweiss@gmail.com

¹ Institute of Biology and Medical Genetics, First Faculty of Medicine, Charles University, Prague, Czech Republic
Full list of author information is available at the end of the article



© The Author(s) 2021. **Open Access** This article is licensed under a Creative Commons Attribution 4.0 International License, which permits use, sharing, adaptation, distribution and reproduction in any medium or format, as long as you give appropriate credit to the original author(s) and the source, provide a link to the Creative Commons licence, and indicate if changes were made. The images or other third party material in this article are included in the article's Creative Commons licence, unless indicated otherwise in a credit line to the material. If material is not included in the article's Creative Commons licence and your intended use is not permitted by statutory regulation or exceeds the permitted use, you will need to obtain permission directly from the copyright holder. To view a copy of this licence, visit <http://creativecommons.org/licenses/by/4.0/>. The Creative Commons Public Domain Dedication waiver (<http://creativecommons.org/publicdomain/zero/1.0/>) applies to the data made available in this article, unless otherwise stated in a credit line to the data.

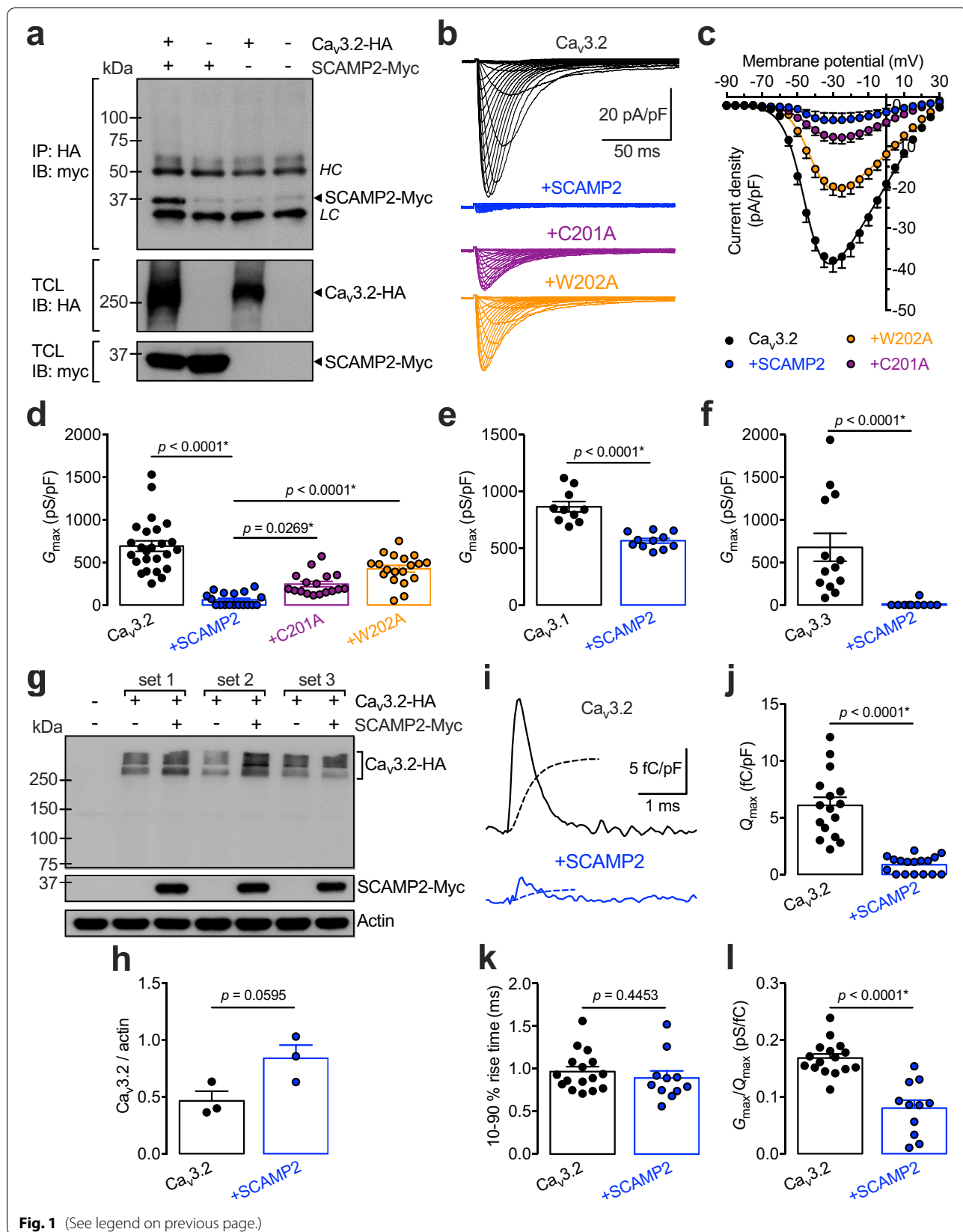
transmembrane helices 2 and 3 essential for mediating SCAMP2 function [5]. This E domain is highly conserved among SCAMP isoforms and represents an essential molecular determinant for SCAMP2-mediated inhibition of exocytosis [6]. Only a few reports have documented the role of SCAMP2 in the regulation of ion channels and transporters [7–10]. In the present study, we aimed to assess the functional role of SCAMP2 in the regulation of T-type channels.

To address this issue, we assessed whether $Ca_v3.2$ channels and SCAMP2 associate at the protein level. Co-immunoprecipitation from tsA-201 cells expressing recombinant HA-tagged $Ca_v3.2$ and Myc-tagged SCAMP2 using an anti-HA-antibody precipitated SCAMP2-Myc with $Ca_v3.2$ -HA revealing the existence of a $Ca_v3.2$ /SCAMP2 protein complex (Fig. 1a). We note that co-immunoprecipitation experiments from total cell lysates do not address whether this interaction is direct or not and it is a possibility that formation of $Ca_v3.2$ /SCAMP2 protein complex may also involve another intermediate protein. Next, we aimed to analyze the functional effect of SCAMP2 on $Ca_v3.2$ channels. Patch-clamp recordings from tsA-201 cells expressing $Ca_v3.2$ showed that co-expression of SCAMP2 produces an almost complete drop of the whole-cell T-type current (Fig. 1b and c). For instance, the maximal macroscopic conductance (G_{max}) was reduced by 91% ($p < 0.0001$) in cells co-expressing SCAMP2 (61 ± 18 pS/pF, $n = 18$) compared to cells expressing $Ca_v3.2$ alone (692 ± 62 pS/pF, $n = 25$) (Fig. 1d). Alanine mutagenesis of the E peptide of SCAMP2 at cysteine 201 (C201A) and tryptophan 202 (W202A) reduced this effect to 64% ($p = 0.0269$) and 39% ($p < 0.0001$) inhibition, respectively, indicating that SCAMP2-induced knockdown of $Ca_v3.2$ currents is at least partly mediated by the E peptide (Fig. 1b–d). These data also indicate that the reduction in $Ca_v3.2$ current density in the presence of SCAMP2 is not merely due to the co-expression of just any protein given that the W202A mutant construct has no big effect. With regard

to the effect of SCAMP2 on the other T-type channel isoforms, co-expression of SCAMP2 in cells expressing recombinant $Ca_v3.1$ and $Ca_v3.3$ reduced G_{max} by 35% ($p < 0.0001$) and 98% ($p < 0.0001$) respectively (Fig. 1e and f and Additional file 1: Fig. S1) indicative of a differential susceptibility to SCAMP2-dependent modulation ($Ca_v3.3 \approx Ca_v3.2 > Ca_v3.1$). Next, we aimed to assess the underlying mechanism by which SCAMP2 induced knockdown of the T-type conductance. The alteration of the T-type conductance in the presence of SCAMP2 could originate from an overall decreased level of $Ca_v3.2$ proteins or from a reduced expression of the channel in the plasma membrane. Western blot analysis from total cell lysates showed that $Ca_v3.2$ protein levels were not decreased by the presence of SCAMP2. Instead, we observed a non-significant trend toward higher expression levels which may have arisen from a lower rate of vesicular exocytosis therefore preventing the channel from being targeted to the proteasomal degradation machinery (Fig. 1g and h). In contrast, recording of intramembrane charge movements (Q) that provide an accurate assessment of the number of channels embedded in the plasma membrane revealed an 85% decrease ($p < 0.0001$) of Q_{max} in cells expressing SCAMP2 (from 6.1 ± 0.7 fC/pF, $n = 16$ to 0.9 ± 0.2 fC/pF, $n = 17$) (Fig. 1i and j) indicating a decreased channel expression at the cell surface. Moreover, while the kinetics of intramembrane charge movements remained unaltered (Fig. 1k), the G_{max}/Q_{max} dependency in the presence of SCAMP2 was reduced by 52% ($p < 0.0001$) (from 0.169 ± 0.007 pS/fC, $n = 16$ to 0.080 ± 0.014 pS/fC, $n = 11$) suggesting an additional alteration of the coupling between the activation of the voltage-sensor and the pore opening of the channel (Fig. 1l). This observation is consistent with a previous report showing that besides to be concentrated primarily in intracellular membranes, SCAMP2 is also found in the plasma membrane [11] and therefore could potentially modulate the gating of the channel in addition to its insertion in the membrane. We note that the reduction

(See figure on next page.)

Fig. 1 SCAMP2 regulates T-type channel expression. **a** Co-immunoprecipitation of Myc-tagged SCAMP2 (SCAMP2-Myc) from tsA-201 cells co-transfected with HA-tagged $Ca_v3.2$ channel ($Ca_v3.2$ -HA). The upper panel shows the result of the co-immunoprecipitation of SCAMP2-Myc with $Ca_v3.2$ -HA using an anti-HA antibody. The lower panels show the immunoblot of $Ca_v3.2$ -HA and SCAMP2-Myc from total cell lysates using an anti-HA and anti-Myc antibody, respectively. HC, heavy chain antibody; LC, light chain antibody. This experiment was performed four times from independent transfections and $Ca_v3.2$ /SCAMP2 interaction was consistently observed. **b** Representative T-type current traces from tsA-201 cells expressing $Ca_v3.2$ alone (black traces) and in combination with wild-type SCAMP2 (blue traces), as well as with C201A (purple traces) and W202A (orange traces) SCAMP2 mutants in response to 150 ms depolarizing steps varied from -90 mV to $+30$ mV from a holding potential of -100 mV. **c** Corresponding mean current/voltage (I/V) relationships. **d** Corresponding mean maximal macroscopic conductance values (G_{max}) obtained from the fit of the I/V curves with the modified Boltzmann Eq. (1). **e–f** Mean G_{max} values for tsA-201 cells expressing $Ca_v3.1$ and $Ca_v3.3$ channels, respectively. **g** Immunoblot of $Ca_v3.2$ -HA expressed in tsA-201 cells in the absence (–) and presence (+) of SCAMP2-Myc. The immunoblot shows the results of three independent sets of transfections. **h** Corresponding mean expression levels of $Ca_v3.2$ -HA normalized to actin. **i** Representative intramembrane charge movement traces recorded at the ionic reversal potential from cells expressing $Ca_v3.2$ alone (black trace) and in the presence of SCAMP2 (blue trace). The dotted lines depict the time course of the intramembrane charge movement integral. **j** Corresponding mean maximal intramembrane charge movement values (Q_{max}). **k** Corresponding mean 10–90% rise time values calculated from the integral time course shown in **i**. **l** Corresponding mean G_{max}/Q_{max} values



of Q_{\max} combined with the reduction of G_{\max}/Q_{\max} of the small fraction of channels that still reached the plasma membrane in the presence of SCAMP2 is very similar to the reduction of the maximal T-type conductance we previously observed (91%, Fig. 1d).

Several $Ca_v3.2$ interacting proteins including KLHL1 [12], USP5 [13], Stac1 [14], calnexin [15], and Rack-1 [16] have been reported to modulate the sorting and trafficking of the channel to the plasma membrane. In this study, we reported SCAMP2 as a novel $Ca_v3.2$ -interacting partner and potent repressor of the expression of the channel at the cell surface. Further investigations will be necessary to fully explore the importance of this regulation in native conditions. Importantly, altered expression of SCAMP2 has been reported in several types of cancer [17]. Given the importance of $Ca_v3.2$ channels in the development of peripheral painful neuropathies [18], it will be interesting to assess to what extent SCAMP2-mediated regulation of $Ca_v3.2$ could possibly contribute to cancer-related neuropathic pain.

Abbreviations

G_{\max} : Maximal macroscopic conductance; KLHL1: Kelch-like 1; Q_{\max} : Maximal intra membrane charge movement; Rack-1: Receptor for activated C kinase 1; SCAMP2: Secretory carrier membrane protein 2; Stac1: Stac adaptor protein 1; USP5: Ubiquitin-specific proteinase 5.

Supplementary Information

The online version contains supplementary material available at <https://doi.org/10.1186/s13041-021-00891-7>.

Additional file 1. Fig. S1. Functional effect of SCAMP2 on $Ca_v3.1$ and $Ca_v3.3$ channels. **a** Representative T-type current traces from tsA-201 cells expressing $Ca_v3.1$ alone (black traces) and in combination with SCAMP2 (blue traces) in response to 150 ms depolarizing steps varied from -90 mV to +30 mV from a holding potential of -100 mV. **b** Corresponding mean current/voltage (I/V) relationships. **c** Corresponding mean maximal macroscopic conductance values (G_{\max}) obtained from the fit of the I/V curves with the modified Boltzmann Eq. (1). **d-e** Same legend as for **a-c** but for cells expressing $Ca_v3.3$ channel.

Acknowledgements

We are grateful to Drs. Heidi Kaastrup Müller and Jana Haase for providing the human SCAMP2 W202A plasmid. We thank Charles University (Progres Q28).

Authors' contributions

LC, RNS and BJT performed experiments and analyzed the data. TV generated SCAMP2 C201A mutant cDNA. LL supervised recordings and analysis of intramembrane charge movement. NW designed and supervised the study and wrote the manuscript. All authors critically revised the manuscript and contributed significantly to this work. All authors read and approved the final manuscript.

Funding

This work did not receive specific funding.

Availability of data and materials

All data generated or analyzed during this study are included in this published article and its additional information files.

Declarations

Ethics approval and consent to participate

Not applicable.

Consent for publication

Not applicable.

Competing interests

The authors declare that they have no competing interests.

Author details

¹Institute of Biology and Medical Genetics, First Faculty of Medicine, Charles University, Prague, Czech Republic. ²Institute of Organic Chemistry and Biochemistry, Czech Academy of Sciences, Prague, Czech Republic. ³Department of Pathophysiology, Third Faculty of Medicine, Charles University, Prague, Czech Republic. ⁴Center of Biosciences, Institute of Molecular Physiology and Genetics, Slovak Academy of Sciences, Bratislava, Slovakia.

Received: 2 December 2021 Accepted: 20 December 2021

Published online: 03 January 2022

References

- Ferron L, Koshti S, Zamponi GW. The life cycle of voltage-gated Ca^{2+} channels in neurons: an update on the trafficking of neuronal calcium channels. *Neuronal Signal*. 2021;5(1):NS20200095.
- Weiss N, Zamponi GW. T-type calcium channels: from molecule to therapeutic opportunities. *Int J Biochem Cell Biol*. 2019;108:34–9.
- Weiss N, Zamponi GW. Genetic T-type calcium channelopathies. *J Med Genet*. 2020;57(1):1–10.
- Castle A, Castle D. Ubiquitously expressed secretory carrier membrane proteins (SCAMPs) 1–4 mark different pathways and exhibit limited constitutive trafficking to and from the cell surface. *J Cell Sci*. 2005;118(Pt 16):3769–80.
- Hubbard C, Singleton D, Rauch M, Jayasinghe S, Cafiso D, Castle D. The secretory carrier membrane protein family: structure and membrane topology. *Mol Biol Cell*. 2000;11(9):2933–47.
- Guo Z, Liu L, Cafiso D, Castle D. Perturbation of a very late step of regulated exocytosis by a secretory carrier membrane protein (SCAMP2)-derived peptide. *J Biol Chem*. 2002;277(38):35357–63.
- Müller HK, Wiborg O, Haase J. Subcellular redistribution of the serotonin transporter by secretory carrier membrane protein 2. *J Biol Chem*. 2006;281(39):28901–9.
- Diering GH, Church J, Numata M. Secretory carrier membrane protein 2 regulates cell-surface targeting of brain-enriched Na^{+}/H^{+} exchanger NHE5. *J Biol Chem*. 2009;284(20):13892–903.
- Zaarour N, Defontaine N, Demarets S, Azroyan A, Cheval L, Laghmani K. Secretory carrier membrane protein 2 regulates exocytic insertion of NKCC2 into the cell membrane. *J Biol Chem*. 2011;286(11):9489–502.
- Fjorback AW, Müller HK, Haase J, Raarup MK, Wiborg O. Modulation of the dopamine transporter by interaction with Secretory Carrier Membrane Protein 2. *Biochem Biophys Res Commun*. 2011;406(2):165–70.
- Liu L, Guo Z, Tieu Q, Castle A, Castle D. Role of secretory carrier membrane protein SCAMP2 in granule exocytosis. *Mol Biol Cell*. 2002;13(12):4266–78.
- Aromolaran KA, Benzow KA, Cribbs LL, Koob MD, Piedras-Rentería ES. T-type current modulation by the actin-binding protein Kelch-like 1. *Am J Physiol Cell Physiol*. 2010;298(6):C1353–62.
- García-Caballero A, Gadotti VM, Stenkowski P, Weiss N, Souza IA, Hodgkinson V, et al. The deubiquitinating enzyme USP5 modulates neuropathic and inflammatory pain by enhancing $Cav3.2$ channel activity. *Neuron*. 2014;83(5):1144–58.
- Rzhepetskyy Y, Lazniewska J, Proft J, Campiglio M, Flucher BE, Weiss N. A $Cav3.2/Stac1$ molecular complex controls T-type channel expression at the plasma membrane. *Channels (Austin)*. 2016;10(5):346–54.
- Proft J, Rzhepetskyy Y, Lazniewska J, Zhang FX, Cain SM, Snutch TP, et al. The $Ca_{v}1h$ mutation in the GAERS model of absence epilepsy enhances T-type Ca^{2+} currents by altering calnexin-dependent trafficking of $Cav3.2$ channels. *Sci Rep*. 2017;7(1):11513.

16. Gandini MA, Souza IA, Khullar A, Gambeta E, Zamponi GW. Regulation of Ca_v3.2 channels by the receptor for activated C kinase 1 (Rack-1). *Pflugers Arch*. 2021
17. Yue C, Xie S, Zhong J, Zhao H, Lin Z, Zhang L, et al. SCAMP2/5 as diagnostic and prognostic markers for acute myeloid leukemia. *Sci Rep*. 2021;11(1):17012.
18. Cai S, Gomez K, Moutal A, Khanna R. Targeting T-type/CaV3.2 channels for chronic pain. *Transl Res*. 2021;234:20–30.

Publisher's Note

Springer Nature remains neutral with regard to jurisdictional claims in published maps and institutional affiliations.

Ready to submit your research? Choose BMC and benefit from:

- fast, convenient online submission
- thorough peer review by experienced researchers in your field
- rapid publication on acceptance
- support for research data, including large and complex data types
- gold Open Access which fosters wider collaboration and increased citations
- maximum visibility for your research: over 100M website views per year

At BMC, research is always in progress.

Learn more biomedcentral.com/submissions



MICRO REPORT

Open Access



Functional identification of potential non-canonical N-glycosylation sites within Ca_v3.2 T-type calcium channels

Vendula Ficelova^{1,2†}, Ivana A. Souza^{3†}, Leos Cmarko^{1,2}, Maria A. Gandini³, Robin N. Stringer^{1,2,4}, Gerald W. Zamponi³  and Norbert Weiss^{1,2*} 

Abstract

Low-voltage-activated T-type calcium channels are important contributors to nervous system function. Post-translational modification of these channels has emerged as an important mechanism to control channel activity. Previous studies have documented the importance of asparagine (N)-linked glycosylation and identified several asparagine residues within the canonical consensus sequence N-X-S/T that is essential for the expression and function of Ca_v3.2 channels. Here, we explored the functional role of non-canonical N-glycosylation motifs in the conformation N-X-C based on site directed mutagenesis. Using a combination of electrophysiological recordings and surface biotinylation assays, we show that asparagines N345 and N1780 located in the motifs NVC and NPC, respectively, are essential for the expression of the human Ca_v3.2 channel in the plasma membrane. Therefore, these newly identified asparagine residues within non-canonical motifs add to those previously reported in canonical sites and suggest that N-glycosylation of Ca_v3.2 may also occur at non-canonical motifs to control expression of the channel in the plasma membrane. It is also the first study to report the functional importance of non-canonical N-glycosylation motifs in an ion channel.

Keywords: Asparagine-linked glycosylation, N-glycosylation, Non-canonical glycosylation, Calcium channel, T-type channel, ca_v3.2 Channel, Trafficking

Low-voltage-activated T-type calcium channels are widely expressed throughout the nervous system where they generate low-threshold calcium spikes that contribute to neuronal electrical excitability [1]. Over recent years, post-translational modification of the channel protein including phosphorylation [2–4], ubiquitination [5], and glycosylation [6] has emerged as an important level of control over the expression and function of the channel in the plasma membrane, and alteration of these regulations is known to contribute to the development of

several neurological disorders. Therefore, the identification of channel loci undergoing post-translational modification is essential not only to enhance our fundamental understanding of the channel, but also to gain insights into how alteration of these regulations may compromise channel function in pathological conditions.

We and others have previously documented the importance of asparagine (N)-linked glycosylation in the expression of the Ca_v3.2 T-type channels and identified several asparagines essential for the expression of the channel in the plasma membrane [7, 8]. These asparagine residues are located within the sequence N-X-S/T commonly referred to as the canonical N-glycosylation motif where the asparagine is located at the N-terminal to any amino acid (except proline) followed by either a serine (S)

*Correspondence: weiss@uochb.cas.cz

†Vendula Ficelova and Ivana A. Souza equally contributed to this work

¹ Institute of Biology and Medical Genetics, First Faculty of Medicine, Charles University, Prague, Czech Republic

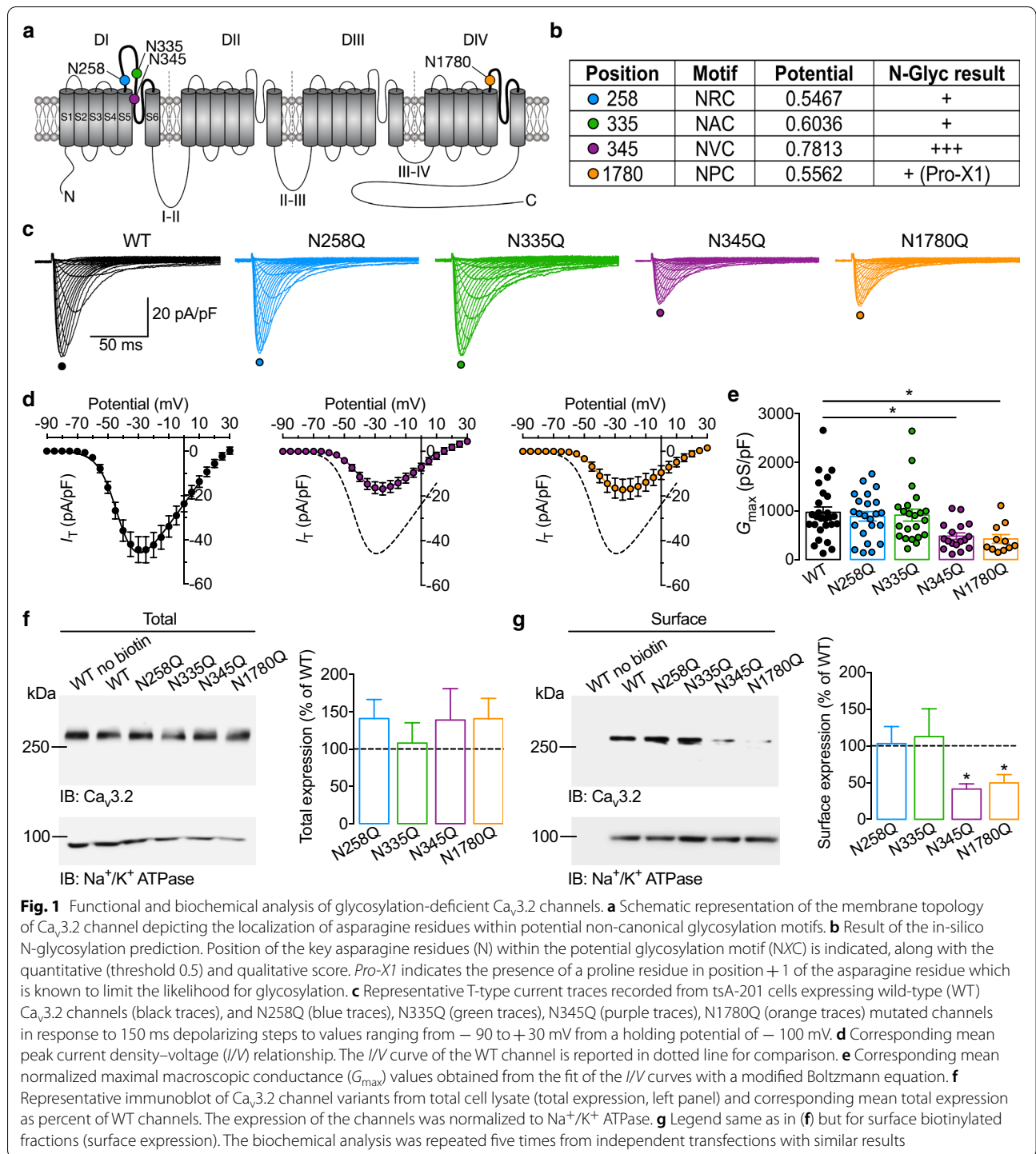
Full list of author information is available at the end of the article



or threonine (T). However, while N-glycosylation at N-X-S/T motifs is an established dogma, there is evidence for the occurrence of N-glycosylation at non-canonical motifs falling into the conformation N-X-C (cysteine) [9]. In the present study, we aimed to further explore the glycosylation loci of $Ca_v3.2$ channels and assess whether asparagines located within such non-canonical motifs contribute to the expression of the channel. The human $Ca_v3.2$ channel contains four potential non-canonical motifs defined by asparagines N258, N335 and N345 located within the first pore-forming loop (P-loop), and asparagine N1780 within the forth P-loop of the channel (Fig. 1a) and in-silico analysis using NetNGlyc 1.0 server (<https://www.cbs.dtu.dk/services/NetNGlyc/>) predicted that these sites could be potentially glycosylated (Fig. 1b). To assess the functional importance of these residues in the expression of $Ca_v3.2$ channels, we used site directed mutagenesis to disrupt these motifs. We replaced asparagine residues with glutamine (Q) and such recombinant mutated channels were expressed in tsA-201 cells for functional characterization by patch clamp electrophysiology. Representative current traces for cells expressing the wild-type (WT) channel and the various mutated variants (N258Q, N335Q, N345Q, and N1780Q) are shown in Fig. 1c. While all channel variants produced a characteristic low-threshold voltage-activated T-type current, currents recorded from cells expressing the N345Q and N1780Q variants were strongly reduced compared to cells expressing the WT channel (Fig. 1d). The maximal whole cell slope conductance was reduced by 50% ($p=0.0050$) in N345Q (480 ± 68 pS/pF, $n=17$) and by 56% ($p=0.0021$) in N1780Q-expressing cells (423 ± 90 pS/pF, $n=11$) compared to cells expressing the WT channel (970 ± 110 pS/pF, $n=27$). This decrease of the maximal conductance was associated with a mild but significant shift of the voltage-dependence of activation without any additional alteration of the voltage-dependence of inactivation and recovery from inactivation (Additional file 1: Figure S1). Furthermore, mutations at asparagines N345 and N1780 did not alter the ability of nickel to block T-type currents (Additional file 1: Figure S2). Next, we aimed to determine whether the impaired T-type conductance in cells expressing the N345Q and N1780Q channels was caused by an alteration of the channel activity or due to reduced expression of the channels in the plasma membrane. To do so, we used cell surface biotinylation followed by immunodetection of the channels. Representative immunoblots of total and surface biotinylated channels are shown in Fig. 1f and g, respectively. No immunoreactivity was detected in non-biotinylated cells expressing WT $Ca_v3.2$ channels demonstrating the absence of contamination from other cellular fractions and also the absence of non-specific interaction

of the channel with NeutrAvidin beads. While the total channel expression was statistically similar across all channel variants (Fig. 1f), the expression of the N345Q and N1780Q channels in the plasma membrane was reduced by 50% ($p=0.0031$) and 56% ($p=0.0301$) respectively, a decrease that is closely correlated with the reduction of the whole cell conductance.

Glycosylation of T-type channels has emerged as an important post-translational modification to control the expression and functioning of the channel in the plasma membrane, and it was suggested that alteration of the glycoproteome of $Ca_v3.2$ may contribute to the development of peripheral pain associated with diabetes [8, 10]. While several studies have previously reported the importance of canonical glycosylation sites in the expression and function of $Ca_v3.2$ channels [7, 8, 11, 12], the potential role for non-canonical motifs has never been explored. Here, we identified two asparagine residues, N345 and N1780 located within non-consensus glycosylation motifs in the conformation N-X-C that contribute to the expression of the channel in the plasma membrane. Although the exact underlying mechanisms by which these two asparagines influence the expression of the channel at the cell surface was not explored in this study, it is likely that they either enhance the trafficking of the channel to the cell surface, or stabilize the channel protein in the plasma membrane by slowing down its internalization as it was previously reported for other glycosylation loci [11]. Because of the large molecular weight of the full-length channel and the existence of several canonical glycosylation sites, it is challenging to demonstrate by Western blot analysis that mutagenesis of the non-canonical sites leads to small molecular weight shifts that are consistent with fewer sugar groups. We can therefore not exclude the possibility that alteration of $Ca_v3.2$ expression upon mutagenesis of asparagines N345 and N1780 may have resulted from an alteration of the channel itself rather than from disruption of its glycosylation. However, this mutagenesis approach is commonly used to functionally assess the functional importance of glycosylation motifs, and glutamine as a replacement of asparagine was chosen because of its similarity, which is therefore expected to preserve the local charge distribution and secondary structure of the channel. Moreover, we cannot totally exclude that mutagenesis of asparagines N345 and N1780 may have interfered with the ubiquitination of the channel, although this process occurs at a different locus (III-IV linker) and therefore is not expected to be directly impacted by the mutations [5]. Our observation that the total expression of mutated channels remained unaltered would also argue against an effect on the ubiquitination pathway.



Altogether, this study supports the notion that $Ca_v3.2$ channels may undergo N-glycosylation at non-canonical motifs and identified two sites defined by asparagines N345 and N1780 important for expression of the

channel at the cell surface. To our knowledge, this study is the first to document the functional role of non-canonical N-glycosylation motifs within an ion channel.

Supplementary information

Supplementary information accompanies this paper at <https://doi.org/10.1186/s13041-020-00697-z>.

Additional file 1. **Figure S1** Electrophysiological properties of Ca_v3.2 channel variants. **a** Mean normalized voltage-dependence of activation for wild-type (WT) Ca_v3.2 channels (black circles), and N258Q (blue circles), N335Q (green circles), N345Q (purple circles), N1780Q (orange circles). **b** Corresponding mean half-activation potential values obtained from the fit of the activation curves with a modified Boltzmann equation. **c-d** Legend same as for (a-b) but for the voltage-dependence of steady state inactivation. **e** Mean normalized recovery from inactivation kinetics. **f** Corresponding mean time constant values of recovery from inactivation obtained from the fit of the recovery curves with a single-exponential function. **Figure S2** Effect of nickel on Ca_v3.2 channel variants. **a** Representative T-type current traces recorded from tsA-201 cells expressing wild-type (WT, black traces), N345Q (purple traces) and N1780Q (orange traces) Ca_v3.2 variants recorded in response to 150 ms depolarizing steps to -20 mV from a holding potential of -100 mV before (Ctrl) and after application of 50 μM nickel (Ni²⁺). **b** Corresponding mean peak current inhibition.

Acknowledgements

Not applicable.

Authors' contributions

VF, LC, and RNS performed electrophysiological recordings and analyzed the data. MAG performed biotinylation experiments. IAS generated plasmid cDNAs encoding for Ca_v3.2 mutants. NW designed and supervised the study. GWZ and NW wrote the manuscript. All authors read and approved the final manuscript.

Funding

This work was supported by a grant to GWZ from the Natural Sciences and Engineering Research Council of Canada. GWZ holds a Canada Research Chair. MAG is supported by postdoctoral Fellowship from the Canadian Institutes of Health Research. NW is supported by Charles University (Progres Q28).

Availability of data and materials

All data generated or analyzed during this study are included in this published article and its supplementary information files.

Ethics approval and consent to participate

Not applicable.

Consent for publication

Not applicable.

Competing interests

The authors declare that they have no competing interests.

Author details

¹ Institute of Biology and Medical Genetics, First Faculty of Medicine, Charles University, Prague, Czech Republic. ² Institute of Organic Chemistry and Biochemistry, Czech Academy of Sciences, Prague, Czech Republic. ³ Department of Physiology and Pharmacology, Cumming School of Medicine, University of Calgary, Calgary, Canada. ⁴ Third Faculty of Medicine, Charles University, Prague, Czech Republic.

Received: 27 August 2020 Accepted: 6 November 2020

Published online: 11 November 2020

References

- Weiss N, Zamponi GW. T-type calcium channels: from molecule to therapeutic opportunities. *Int J Biochem Cell Biol.* 2019;108:34–9.
- Blesneac I, Chemin J, Bidaud I, Huc-Brandt S, Vandermoere F, Lory P. Phosphorylation of the Cav3.2 T-type calcium channel directly regulates its gating properties. *Proc Natl Acad Sci U S A.* 2015;112(44):13705–10.
- Gaifullina AS, Lazniewska J, Gerasimova EV, Burkhanova GF, Rzhepetsky Y, Tomin A, et al. A potential role for T-type calcium channels in homocysteinemia-induced peripheral neuropathy. *Pain.* 2019;160(12):2798–810.
- Gomez K, Calderón-Rivera A, Sandoval A, González-Ramírez R, Vargas-Parada A, Ojeda-Alonso J, et al. Cdk5-dependent phosphorylation of Cav3.2 T-type channels: possible role in nerve ligation-induced neuropathic allodynia and the compound action potential in primary afferent C fibers. *J Neurosci.* 2020;40(2):283–96.
- García-Caballero A, Gadotti VM, Stenkowski P, Weiss N, Souza IA, Hodgkinson V, et al. The deubiquitinating enzyme USP5 modulates neuropathic and inflammatory pain by enhancing Cav3.2 channel activity. *Neuron.* 2014;83(5):1144–58.
- Lazniewska J, Weiss N. Glycosylation of voltage-gated calcium channels in health and disease. *Biochim Biophys Acta Biomembr.* 2017;1859(5):662–8.
- Weiss N, Black SA, Bladen C, Chen L, Zamponi GW. Surface expression and function of Cav3.2 T-type calcium channels are controlled by asparagine-linked glycosylation. *Pflugers Arch.* 2013;465(8):1159–70.
- Orestes P, Osuru HP, McIntire WE, Jacus MO, Salajegheh R, Jagodic MM, et al. Reversal of neuropathic pain in diabetes by targeting glycosylation of Ca(V)_{3.2} T-type calcium channels. *Diabetes.* 2013;62(11):3828–38.
- Lowenthal MS, Davis KS, Formolo T, Kilpatrick LE, Phinney KW. Identification of novel N-glycosylation sites at noncanonical protein consensus motifs. *J Proteome Res.* 2016;15(7):2087–101.
- Stringer RN, Lazniewska J, Weiss N. Transcriptomic analysis of glycan-processing genes in the dorsal root ganglia of diabetic mice and functional characterization on Cav3.2 channels. *Channels (Austin).* 2020;14(1):132–40.
- Lazniewska J, Rzhepetsky Y, Zhang FX, Zamponi GW, Weiss N. Cooperative roles of glucose and asparagine-linked glycosylation in T-type calcium channel expression. *Pflugers Arch.* 2016;468(11–12):1837–51.
- Ondacova K, Karmazinova M, Lazniewska J, Weiss N, Lacinova L. Modulation of Cav3.2 T-type calcium channel permeability by asparagine-linked glycosylation. *Channels (Austin).* 2016;10(3):175–84.

Publisher's Note

Springer Nature remains neutral with regard to jurisdictional claims in published maps and institutional affiliations.

Ready to submit your research? Choose BMC and benefit from:

- fast, convenient online submission
- thorough peer review by experienced researchers in your field
- rapid publication on acceptance
- support for research data, including large and complex data types
- gold Open Access which fosters wider collaboration and increased citations
- maximum visibility for your research: over 100M website views per year

At BMC, research is always in progress.

Learn more biomedcentral.com/submissions



MICRO REPORT

Open Access



De novo *SCN8A* and inherited rare *CACNA1H* variants associated with severe developmental and epileptic encephalopathy

Robin N. Stringer^{1,2†}, Bohumila Jurkovicova-Tarabova^{3†}, Ivana A. Souza⁴, Judy Ibrahim⁵, Tomas Vacik⁶, Waseem Mahmoud Fathalla⁷, Jozef Hertecant^{5,8}, Gerald W. Zamponi⁴, Lubica Lacinova³ and Norbert Weiss^{1,2,3,6*}

Abstract

Developmental and epileptic encephalopathies (DEEs) are a group of severe epilepsies that are characterized by seizures and developmental delay. DEEs are primarily attributed to genetic causes and an increasing number of cases have been correlated with variants in ion channel genes. In this study, we report a child with an early severe DEE. Whole exome sequencing showed a de novo heterozygous variant (c.4873–4881 duplication) in the *SCN8A* gene and an inherited heterozygous variant (c.952G > A) in the *CACNA1H* gene encoding for Na_v1.6 voltage-gated sodium and Ca_v3.2 voltage-gated calcium channels, respectively. In vitro functional analysis of human Na_v1.6 and Ca_v3.2 channel variants revealed mild but significant alterations of their gating properties that were in general consistent with a gain- and loss-of-channel function, respectively. Although additional studies will be required to confirm the actual pathogenic involvement of *SCN8A* and *CACNA1H*, these findings add to the notion that rare ion channel variants may contribute to the etiology of DEEs.

Keywords: Ion channels, Channelopathy, Calcium channel, *CACNA1H*, Ca_v3.2 channel, Sodium channel, *SCN8A*, Na_v1.6 channel, Epilepsy, Encephalopathy

Main text

Developmental and epileptic encephalopathies (DEEs) are a group of severe epilepsies that are characterized by seizures often drug-resistant, and developmental delay leading to varying degrees of intellectual, psychiatric, behavioral, and motor disabilities [1]. DEEs are primarily attributed to genetic causes and while recessive and X-linked variants have been found, the majority of patients show de novo pathogenic variants [2]. Recently,

an increasing number of DEE cases have been correlated with variants in ion channel genes [3].

In the present study, we report a girl with an early severe DEE. She was born by emergency caesarean section at 37 weeks due to placenta previa and was the first child of non-consanguineous parents. Immediately after birth, she presented with trembling despite normal blood sugar levels. In the early postnatal period, she developed myoclonic jerks in all limbs, diagnosed as infantile spasms but did not respond to steroids. By the age of 2 months, she started having generalized tonic-clonic seizures and recurrent status epilepticus that poorly responded to antiepileptic medication including clobazam, levetiracetam, phenobarbital and topiramate. Seizures were characterized by right eye deviation and generalized tonic posturing. She also presented with

*Correspondence: nalweiss@gmail.com

†Robin N. Stringer and Bohumila Jurkovicova-Tarabova contributed equally to this work

¹ Department of Pathophysiology, Third Faculty of Medicine, Charles University, Prague, Czech Republic

Full list of author information is available at the end of the article



© The Author(s) 2021, corrected publication 2021. **Open Access** This article is licensed under a Creative Commons Attribution 4.0 International License, which permits use, sharing, adaptation, distribution and reproduction in any medium or format, as long as you give appropriate credit to the original author(s) and the source, provide a link to the Creative Commons licence, and indicate if changes were made. The images or other third party material in this article are included in the article's Creative Commons licence, unless indicated otherwise in a credit line to the material. If material is not included in the article's Creative Commons licence and your intended use is not permitted by statutory regulation or exceeds the permitted use, you will need to obtain permission directly from the copyright holder. To view a copy of this licence, visit <http://creativecommons.org/licenses/by/4.0/>. The Creative Commons Public Domain Dedication waiver (<http://creativecommons.org/publicdomain/zero/1.0/>) applies to the data made available in this article, unless otherwise stated in a credit line to the data.

(See figure on next page.)

Fig. 1 Electrophysiological properties of Na_v1.6 and Ca_v3.2 channel variants associated with developmental and epileptic encephalopathy. **a** Family pedigree chart. Filled and open symbols indicate affected and unaffected individuals, respectively. **b** Location of the Na_v1.6 G1625_I1627 duplication (red circle) and Ca_v3.2 G318S missense variants (blue circle) within the secondary membrane topology of the channels. **c** Representative sodium current traces recorded from cells expressing wild-type Na_v1.6 (Na_v1.6^{wt}, black traces) and Na_v1.6 duplication variant (Na_v1.6^{dup}, red traces) in combination with Na_vb₂. **d** Corresponding mean current–voltage (*I/V*) relationship. **e** Corresponding mean maximal macroscopic conductance (*G*_{max}) values obtained from the fit of the *I/V* curves with the modified Boltzmann Eq. (1). **f** Corresponding mean normalized voltage-dependence of activation. The voltage-dependence of activation for Na_v1.6^{wt} in the absence of Na_vb₂ is shown for comparison (dotted line). *Inset* shows corresponding mean half-activation potential values obtained from the fit of the activation curve with the modified Boltzmann Eq. (2). **g** Mean normalized voltage-dependence of steady-state inactivation for Na_v1.6^{wt} and Na_v1.6^{dup}. *Inset* shows corresponding mean half-inactivation potential values obtained from the fit of the inactivation curves with the two-state Boltzmann function (3). **h** Mean normalized recovery from inactivation kinetics. *Inset* shows corresponding mean time constant *t* values of recovery from inactivation obtained by fitting recovery curves with a single-exponential function (4). **i–n** Legend same as in (c–h) but for cells expressing wild type Ca_v3.2 (Ca_v3.2^{wt}, black) and Ca_v3.2 G318S (Ca_v3.2^{G>S}, blue) channel variants

additional complications including scoliosis, bilateral hip dislocation and recurrent pneumonia, and by the age of 3 she developed myoclonus, spastic quadriplegia with generalized hypertonia and hyperreflexia with clonus. Secondary skeletal abnormalities were also observed including flattening of the head and chest, severe kyphoscoliosis and flexion contractures. An MRI brain scan showed generalized brain atrophy with marked insular atrophy and bright white matter on flair. Blood tests were in general normal and only creatine phosphokinase levels were increased, probably as secondary consequence of seizures. The patient died at the age of 4. Whole exome sequencing (EGL Genetics) showed a de novo heterologous duplication (c.4873_4881dup) in *SCN8A* (Fig. 1a) causing the duplication of amino acid G1625_I1627 (p.G1625_I1627dup) within the highly conserved transmembrane IVS4 segment (voltage sensor) of the voltage-gated sodium channel Na_v1.6 (Fig. 1b). This variant has never been reported in the Genome Aggregation Database (gnomAD) and was predicted to be deleterious (PROVEAN algorithm). In addition, a rare heterozygous missense variant (c.952G>A) in *CACNA1H* (Fig. 1a) was inherited from the father who was asymptomatic. This variant that caused the substitution of a glycine at position 318 by a serine (p.G318S) within the first pore-forming loop of the voltage-gated calcium channel Ca_v3.2 (Fig. 1b) has never been reported and was not predicted to be deleterious. To assess the impact of these mutations, the G1625_I1627 duplication and G318S missense variant were introduced into the human Na_v1.6 (UniProt Q9UQD0-1) and Ca_v3.2 (UniProt O95180-1) channels, respectively, and recombinant channels were expressed in HEK cells for electrophysiological analysis. The sodium conductance recorded from cells expressing the duplication variant (Na_v1.6^{dup}) in combination with the human Na_vb₂ ancillary subunit (UniProt O60939) was similar to the one measured from cells expressing the wild-type channel (Na_v1.6^{wt})

(Fig. 1c–e and Additional file 1: Table S1). However, the mean half activation potential of Na_v1.6^{dup} was shifted toward more hyperpolarized potentials by -5.4 mV ($p=0.0005$) (Fig. 1f and Additional file 1: Table S1) to values similar to Na_v1.6^{wt} expressed without the Na_vb₂ subunit (Additional file 1: Fig. S1 and Table S1). In contrast, we did not observe any gating alteration of Na_v1.6^{dup} in the absence of Na_vb₂. While the current literature on the effect of Na_vb on the regulation of Na_v1.6 is rather sparse and conflicting [4, 5], these results suggest that phenotypic expression of *SCN8A* duplication variant may depend on the molecular composition of Na_v1.6, possibly by disrupting Na_vb-dependent regulation of the channel. Other gating properties including steady-state inactivation and recovery from inactivation were not affected (Fig. 1g, h and Additional file 1: Table S1). In addition, recording of T-type currents from cells expressing the Ca_v3.2 G318S variant (Ca_v3.2^{G>S}) did not reveal any alteration of the T-type conductance compared to cells expression the wild-type channel (Ca_v3.2^{wt}) (Fig. 1i–k and Additional file 1: Table S1). However, the mean half activation potential of the Ca_v3.2^{G>S} variant was shifted toward more positive potentials by $+4.3$ mV ($p=0.0048$) (Fig. 1l and Additional file 1: Table S1) without any additional alteration of the other gating properties (Fig. 1m, n and Additional file 1: Table S1).

In summary, we reported the case of a child with severe DEE in whom a de novo mutation in *SCN8A* and an inherited rare *CACNA1H* variant were found. Pathogenic variants in *SCN8A* have originally been described in patients with DEE [6–9]. Most are de novo missense variants clustered in the highly conserved transmembrane domains of Na_v1.6 and are in general consistent with a gain-of-function pathogenic mechanism predicted to increase neuronal excitability and seizure susceptibility [6, 10, 11]. Our observation that the *SCN8A* duplication variant produced a hyperpolarizing shift of the voltage-dependence of activation of

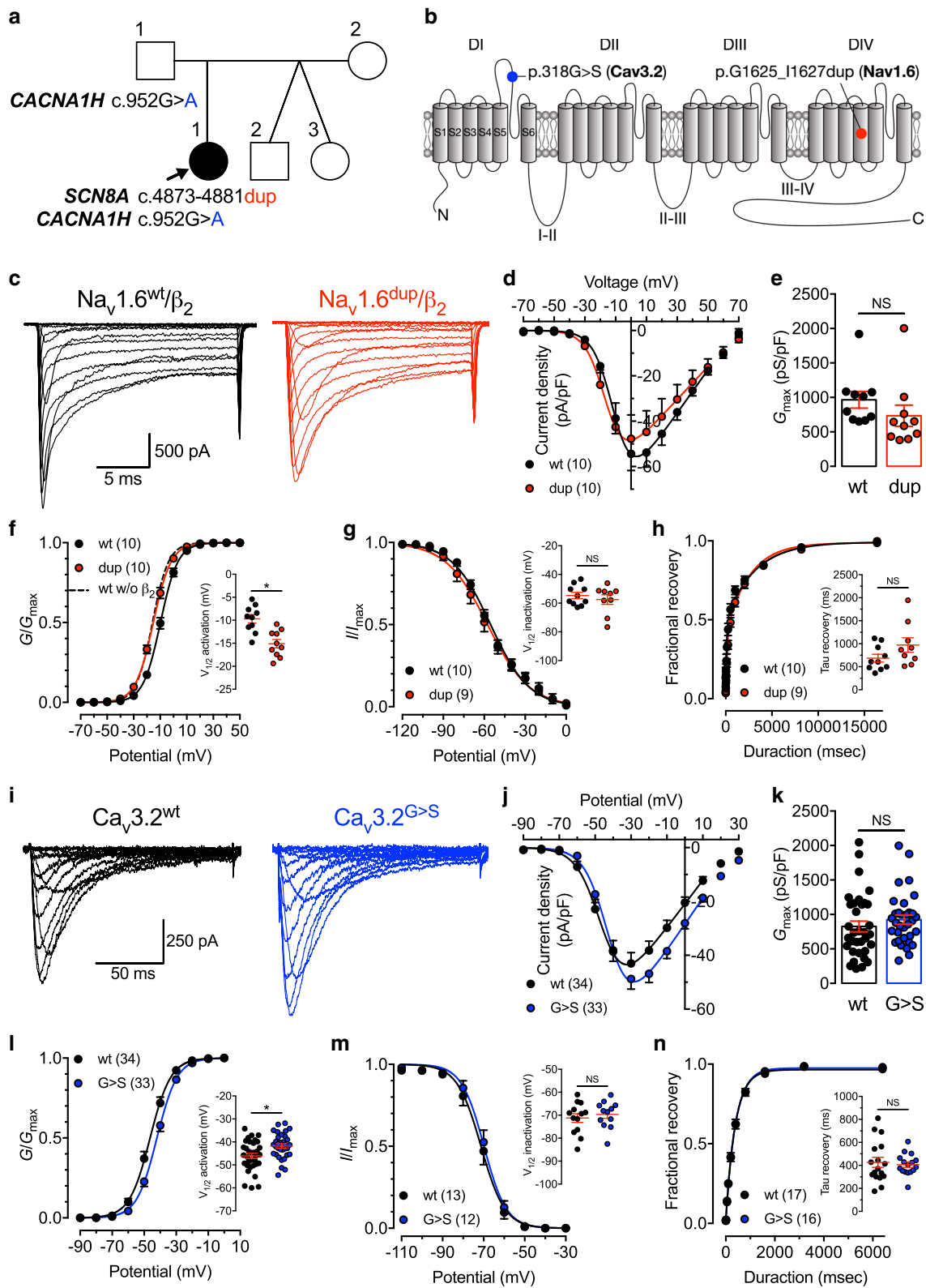


Fig. 1 (See legend on previous page.)

Na_v1.6 is also consistent with a gain-of-function (GoF) of the channel. Although future studies will be required to further assess the importance of the molecular composition of the channel in the phenotypic expression of *SCN8A* variants, the results presented here strengthen the notion that GoF *SCN8A* mutations may represent a general pathogenic mechanism in DEEs. In contrast, *CACNA1H* has never been associated with DEEs. Instead, GoF *CACNA1H* variants have been linked to absence epilepsy and primary aldosteronism [12] while loss-of-function (LoF) variants have been reported in autism spectrum disorders [13], amyotrophic lateral sclerosis [14, 15], and congenital amyotrophy [16]. It is not clear to which extent the LoF *CACNA1H* variant we identified in our patient may have contributed to the disease. Given that the father from whom the child inherited this variant was asymptomatic, this variant may not have had a major contribution to the development of the disease on its own. However, it is a possibility that it may have precipitated its development by interacting with other genes. This notion is supported by previous studies showing that *CACNA1G* (Ca_v3.1) and *CACNA1A* (Ca_v2.1) are genetic modifiers of epilepsy associated with Dravet syndrome [17–19]. While additional studies using primary neurons will be required to uncover the detailed underlying pathogenic mechanisms of Na_v1.6 and Ca_v3.2 variants, the current findings add to the notion that rare ion channel variants may contribute to the etiology of DEEs.

Abbreviations

DEEs: Developmental and epileptic encephalopathies; GoF: Gain-of-function; LoF: Loss-of-function.

Supplementary Information

The online version contains supplementary material available at <https://doi.org/10.1186/s13041-021-00838-y>.

Additional file 1: Fig. S1. Electrophysiological properties of Nav1.6 variant expressed in the absence of Navb2. a Representative sodium current traces recorded from cells expressing wild-type Nav1.6 (Nav1.6wt, black traces) and Nav1.6 duplication variant (Nav1.6dup, red traces). b Corresponding mean current–voltage (*I/V*) relationship. c Corresponding mean maximal macroscopic conductance (*G*_{max}) values obtained from the fit of the *I/V* curves with the modified Boltzmann Eq. (1). d Corresponding mean normalized voltage dependence of activation. Inset shows corresponding mean half-activation potential values obtained from the fit of the activation curve with the modified Boltzmann Eq. (2). e Mean normalized voltage-dependence of steady-state inactivation for Nav1.6wt and Nav1.6dup. Inset shows corresponding mean half-inactivation potential values obtained from the fit of the inactivation curves with the two-state Boltzmann function (3). f Mean normalized recovery from inactivation kinetics. Inset shows corresponding mean time constant *t* values of recovery from inactivation obtained by fitting recovery curves with a single-exponential function (4). **Table S1.** Electrophysiological properties of human Nav1.6 and Cav3.2 variants expressed in tsA-201 cells. **p* < 0.05.

Acknowledgements

We thank Charles University (Progres Q28).

Authors' contributions

R.N.S. and B.J.T. performed electrophysiological recordings and analyzed the data. I.V.A. and T.V. generated Ca_v3.2 and Na_v1.6 variant cDNAs, respectively. J.A.I., W.M.F., and J.H. performed medical examination. N.W., G.W.Z., and L.L. designed the study. N.W. supervised the study and wrote the manuscript. All authors critically revised the manuscript and contributed significantly to this work. All authors read and approved the final manuscript.

Funding

This work did not receive specific funding.

Availability of data and materials

All data generated or analyzed during this study are included in this published article and its additional information files.

Declarations

Ethics approval and consent to participate

Not applicable.

Consent for publication

Written consent to publish information related to the patient was obtained from the father.

Competing interests

The authors declare that they have no competing interests.

Author details

¹Department of Pathophysiology, Third Faculty of Medicine, Charles University, Prague, Czech Republic. ²Institute of Organic Chemistry and Biochemistry, Czech Academy of Sciences, Prague, Czech Republic. ³Center of Biosciences, Institute of Molecular Physiology and Genetics, Slovak Academy of Sciences, Bratislava, Slovakia. ⁴Department of Physiology and Pharmacology, Cumming School of Medicine, University of Calgary, Calgary, Canada. ⁵Department of Pediatrics, Tawam Hospital, Al-Ain, United Arab Emirates. ⁶Institute of Biology and Medical Genetics, First Faculty of Medicine, Charles University, Prague, Czech Republic. ⁷Department of Pediatric Neurology, Mafraq Hospital, Abu Dhabi, United Arab Emirates. ⁸Department of Pediatrics, College of Medicine and Health Sciences, United Arab Emirates University, Al-Ain, United Arab Emirates.

Received: 29 June 2021 Accepted: 1 August 2021

Published online: 16 August 2021

References

- Raga S, Specchio N, Rheims S, Wilmshurst JM. Developmental and epileptic encephalopathies: recognition and approaches to care. *Epileptic Disord.* 2021;23(1):40–52.
- Happ HC, Carvill GL. A 2020 view on the genetics of developmental and epileptic encephalopathies. *Epilepsy Curr.* 2020;20(2):90–6.
- Morrison-Levy N, Borlot F, Jain P, Whitney R. Early-onset developmental and epileptic encephalopathies of infancy: an overview of the genetic basis and clinical features. *Pediatr Neurol.* 2021;116:85–94.
- Zhao J, O'Leary ME, Chahine M. Regulation of Nav1.6 and Nav1.8 peripheral nerve Na⁺ channels by auxiliary β-subunits. *J Neurophysiol.* 2011;106(2):608–19.
- Smith MR, Smith RD, Plummer NW, Meisler MH, Goldin AL. Functional analysis of the mouse Scn8a sodium channel. *J Neurosci.* 1998;18(16):6093–102.
- Veeramah KR, O'Brien JE, Meisler MH, Cheng X, Dib-Hajj SD, Waxman SG, et al. De novo pathogenic SCN8A mutation identified by whole-genome sequencing of a family quartet affected by infantile epileptic encephalopathy and SUDEP. *Am J Hum Genet.* 2012;90(3):502–10.

7. Meisler MH, Helman G, Hammer MF, Fureman BE, Gaillard WD, Goldin AL, et al. SCN8A encephalopathy: research progress and prospects. *Epilepsia*. 2016;57(7):1027–35.
8. Wang J, Gao H, Bao X, Zhang Q, Li J, Wei L, et al. SCN8A mutations in Chinese patients with early onset epileptic encephalopathy and benign infantile seizures. *BMC Med Genet*. 2017;18(1):104.
9. Kim HJ, Yang D, Kim SH, Kim B, Kim HD, Lee JS, et al. Genetic and clinical features of SCN8A developmental and epileptic encephalopathy. *Epilepsy Res*. 2019;158: 106222.
10. Wagnon JL, Barker BS, Hounshell JA, Haaxma CA, Shealy A, Moss T, et al. Pathogenic mechanism of recurrent mutations of SCN8A in epileptic encephalopathy. *Ann Clin Transl Neurol*. 2016;3(2):114–23.
11. Barker BS, Ottolini M, Wagnon JL, Hollander RM, Meisler MH, Patel MK. The SCN8A encephalopathy mutation p.Ile1327Val displays elevated sensitivity to the anticonvulsant phenytoin. *Epilepsia*. 2016;57(9):1458–66.
12. Weiss N, Zamponi GW. Genetic T-type calcium channelopathies. *J Med Genet*. 2020;57(1):1–10.
13. Splawski I, Yoo DS, Stotz SC, Cherry A, Clapham DE, Keating MT. CACNA1H mutations in autism spectrum disorders. *J Biol Chem*. 2006;281(31):22085–91.
14. Rzhetsky Y, Lazniewska J, Blesneac I, Pamphlett R, Weiss N. CACNA1H missense mutations associated with amyotrophic lateral sclerosis alter Cav3.2 T-type calcium channel activity and reticular thalamic neuron firing. *Channels (Austin)*. 2016;10(6):466–77.
15. Stringer RN, Jurkovicova-Tarabova B, Huang S, Haji-Ghassemi O, Idoux R, Liashenko A, et al. A rare CACNA1H variant associated with amyotrophic lateral sclerosis causes complete loss of Cav3.2 T-type channel activity. *Mol Brain*. 2020;13(1):33.
16. Carter MT, McMillan HJ, Tomin A, Weiss N. Compound heterozygous CACNA1H mutations associated with severe congenital amyotrophy. *Channels (Austin)*. 2019;13(1):153–61.
17. Ohmori I, Ouchida M, Kobayashi K, Jitsumori Y, Mori A, Michiue H, et al. CACNA1A variants may modify the epileptic phenotype of Dravet syndrome. *Neurobiol Dis*. 2013;50:209–17.
18. Calhoun JD, Hawkins NA, Zachwieja NJ, Kearney JA. Cacna1g is a genetic modifier of epilepsy caused by mutation of voltage-gated sodium channel Scn2a. *Epilepsia*. 2016;57(6):e103–7.
19. Calhoun JD, Hawkins NA, Zachwieja NJ, Kearney JA. Cacna1g is a genetic modifier of epilepsy in a mouse model of Dravet syndrome. *Epilepsia*. 2017;58(8):e111–5.

Publisher's Note

Springer Nature remains neutral with regard to jurisdictional claims in published maps and institutional affiliations.

Ready to submit your research? Choose BMC and benefit from:

- fast, convenient online submission
- thorough peer review by experienced researchers in your field
- rapid publication on acceptance
- support for research data, including large and complex data types
- gold Open Access which fosters wider collaboration and increased citations
- maximum visibility for your research: over 100M website views per year

At BMC, research is always in progress.

Learn more biomedcentral.com/submissions



RESEARCH

Open Access



A rare *CACNA1H* variant associated with amyotrophic lateral sclerosis causes complete loss of Ca_v3.2 T-type channel activity

Robin N. Stringer^{1,2}, Bohumila Jurkovicova-Tarabova³, Sun Huang⁴, Omid Haji-Ghassemi⁵, Romane Idoux¹, Anna Liashenko¹, Ivana A. Souza⁴, Yuriy Rzhetsky¹, Lubica Lacinova³, Filip Van Petegem⁵, Gerald W. Zamponi⁴, Roger Pamphlett⁶ and Norbert Weiss^{1*}

Abstract

Amyotrophic lateral sclerosis (ALS) is a neurodegenerative disorder characterized by the progressive loss of cortical, brain stem and spinal motor neurons that leads to muscle weakness and death. A previous study implicated *CACNA1H* encoding for Ca_v3.2 calcium channels as a susceptibility gene in ALS. In the present study, two heterozygous *CACNA1H* variants were identified by whole genome sequencing in a small cohort of ALS patients. These variants were functionally characterized using patch clamp electrophysiology, biochemistry assays, and molecular modeling. A previously unreported c.454GTAC > G variant produced an inframe deletion of a highly conserved isoleucine residue in Ca_v3.2 (p.ΔI153) and caused a complete loss-of-function of the channel, with an additional dominant-negative effect on the wild-type channel when expressed in *trans*. In contrast, the c.3629C > T variant caused a missense substitution of a proline with a leucine (p.P1210L) and produced a comparatively mild alteration of Ca_v3.2 channel activity. The newly identified ΔI153 variant is the first to be reported to cause a complete loss of Ca_v3.2 channel function. These findings add to the notion that loss-of-function of Ca_v3.2 channels associated with rare *CACNA1H* variants may be risk factors in the complex etiology of ALS.

Keywords: ALS, Amyotrophic lateral sclerosis, Motor neuron disease, *CACNA1H*, Mutation, Calcium channel, Ca_v3.2 channel, T-type channel, Biophysics

Introduction

Amyotrophic lateral sclerosis (ALS), also known as motor neuron disease or Lou Gehrig's disease, is a heterogeneous neuromuscular disease characterized by the degeneration of cortical, brain stem and spinal motor neurons that leads to muscle weakness and paralysis. Disease onset averages between 40 and 70 years of age [1], and the annual incidence worldwide is estimated to

be between one to three per 100,000 people [2]. ALS is best regarded as a complex genetic disorder with a Mendelian pattern of inheritance in approximately 5–10% of patients (familial ALS, fALS), but most patients have no discernable family history of the disease which is then referred to being “sporadic” or “isolated” in nature (sALS) [3]. However, the observation that established fALS genes are also implicated in sALS makes the distinction between fALS and sALS more abstruse [4]. For instance, mutations in the most common ALS genes (*SOD1*, *FUS*, *TARDBP*, *C9orf72*, *VCP*, and *PFN1*) account for up to 70% of fALS patients and about 10% of

* Correspondence: weiss@uochb.cas.cz

¹Institute of Organic Chemistry and Biochemistry, Czech Academy of Sciences, Flemingovo nam 2, 16610 Prague, Czech Republic
Full list of author information is available at the end of the article



© The Author(s). 2020 **Open Access** This article is licensed under a Creative Commons Attribution 4.0 International License, which permits use, sharing, adaptation, distribution and reproduction in any medium or format, as long as you give appropriate credit to the original author(s) and the source, provide a link to the Creative Commons licence, and indicate if changes were made. The images or other third party material in this article are included in the article's Creative Commons licence, unless indicated otherwise in a credit line to the material. If material is not included in the article's Creative Commons licence and your intended use is not permitted by statutory regulation or exceeds the permitted use, you will need to obtain permission directly from the copyright holder. To view a copy of this licence, visit <http://creativecommons.org/licenses/by/4.0/>. The Creative Commons Public Domain Dedication waiver (<http://creativecommons.org/publicdomain/zero/1.0/>) applies to the data made available in this article, unless otherwise stated in a credit line to the data.

that rare *CACNA1H* variants may represent a risk factor for ALS [11, 12]. In the present study, using whole genome sequencing of a small cohort of ALS patients, we identified two additional heterozygous variants in *CACNA1H*. The first variant (c.3629C > T, p.P1210L) was identified in a man with ALS onset aged 55 years who died aged 62 years. He had no family history of ALS, though his father had Alzheimer's disease and his mother bipolar disorder. The P1210L variant is located in a non-conserved region of the intracellular linker connecting transmembrane domains II and III (II-III loop) of Ca_v3.2 (Fig. 1a and b). This variant has previously been reported in 188 out of 240,876 individuals in the gnomAD database (<https://gnomad.broadinstitute.org/>), including 144 of 193,008 alleles only from individuals who were not ascertained for having a neurological condition in a neurological case/control study. Furthermore, in silico analysis predicted the amino acid change to be neutral (Fig. 1c), suggesting that this variant is likely to not have a major pathological role. The second variant (c.454GTAC > G, p.ΔI153) was identified in a man with ALS onset aged 53 years who died aged 54 years. Although he had no family history of ALS, his mother developed insulin-dependent diabetes mellitus and narcolepsy, and his father presented with early onset dementia, a condition known to precede motor impairment in some people with ALS [14]. This mutation produces an inframe deletion of the isoleucine 153 located in the second transmembrane helix of Ca_v3.2, a region highly conserved across Ca_v3.2 channel orthologs (Fig. 1a and b). The ΔI153 variant has only been reported in 1 out of 198,036 individuals in the gnomAD database and this deletion was predicted to be deleterious on the channel (Fig. 1c). Hexanucleotide repeat number in C9orf72, the most common genetic cause of ALS, was normal in both patients.

The ΔI153 mutation causes a complete loss of Ca_v3.2 function

In the first series of experiments we assessed the functional expression of Ca_v3.2 P1210L and ΔI153 channel variants expressed in tsA-201 cells by whole-cell patch clamp electrophysiology. Cells expressing the P1210L channel variant displayed a characteristic low-threshold voltage-activated T-type current (Fig. 2a and b) that only differed from cells expressing the wild-type (WT) channel by a 32% reduction ($p = 0.0125$, Mann-Whitney test) of the maximal conductance (G_{\max}) (from 571.3 ± 58.4 pS/pF, $n = 42$ to 387.7 ± 33.9 pS/pF, $n = 41$) (Fig. 2c). The main electrophysiological properties, including voltage-dependence of activation and inactivation (Fig. 2d), and recovery from inactivation (Fig. 2e), remained unaffected. In cells expressing the ΔI153 channel variant, we did not record any T-type conductance (Fig. 2a-c). It is noteworthy that experimental conditions

known to favor the expression of misfolded proteins, such as treatment of cells with the proteasome inhibitor MG132 or decrease of cell incubation temperature to 30°C, were used but failed to restore a T-type conductance. Additionally, co-expression of the ΔI153 channel variant with Stac1 or with a calnexin-derived peptide that has previously been reported to potentiate the expression of Ca_v3.2 in the plasma membrane [15, 16] also failed to restore T-type currents (data not shown). The lack of functional expression of the ΔI153 channel variant could have been inherent in our experimental conditions using recombinant channels, so we aimed to further assess the phenotypic effect of the ΔI153 mutation on native Ca_v3.2 channels in a neuronal environment. Therefore, we used a CRISPR/Cas9 approach to introduce the ΔI153 mutation in native Ca_v3.2 channels in cultured dorsal root ganglion (DRG) neurons. DRG neurons were used as a model system since these neurons are known to display a T-type conductance that is almost exclusively carried by Ca_v3.2 channel subtype [17]. Consistent with our observation with recombinant Ca_v3.2 channels, T-type currents recorded from Ca_v3.2 ΔI153 DRG neurons 3 days after gene editing were reduced by 73% (Mann-Whitney $p < 0.0001$) compared to wild type neurons (from 15.4 ± 2.5 pA/pF, $n = 12$ to 4.1 ± 0.8 pA/pF, $n = 12$) (Fig. 2f and g).

Collectively, these data revealed a mild loss of channel function associated with the P1210L variant, and the deleterious effect of the ΔI153 mutation leading to a complete loss of Ca_v3.2 activity.

The ΔI153 mutation disrupts Ca_v3.2 biogenesis

The alteration of T-type currents in ALS-associated Ca_v3.2 variants could originate from an overall decreased expression of channel proteins, reduced channel density in the plasma membrane, altered gating of the channel, or from a combination of several of these. Therefore, we first assessed the expression levels of P1210L and ΔI153 channel variants in tsA-201 cells by western blot (Fig. 3a). Immunoblot analysis from total cell lysates showed that the P1210L channel variant was present at a similar level as the WT channel (Fig. 3b). In contrast, the expression level of the ΔI153 channel variant was reduced by 78% (Mann-Whitney $p = 0.0286$), suggesting that this variant may undergo extensive degradation (Fig. 3b). Next, we aimed to assess the expression of Cav3.2 channel variants at the cell surface. Therefore, we analyzed charge movements (Q) that refer to the movement of the channel voltage-sensor in the plasma membrane in response to electrical membrane depolarizations. Total charges (Q_{\max}) were assessed at the reversal potential of the ionic current, where we can consider Q_{rev} to be equal to Q_{\max} , providing an accurate assessment of the total number of channels in the plasma membrane (Fig. 3c). In cells expressing the P1210L

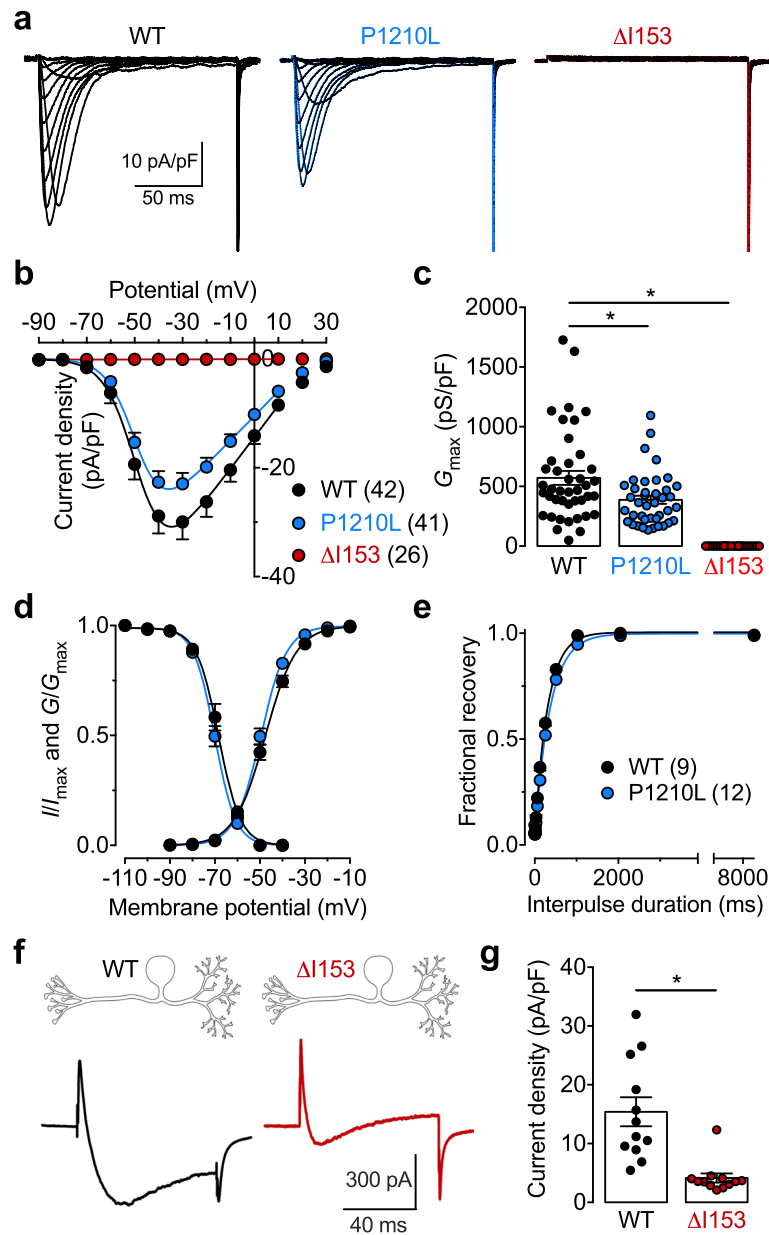


Fig. 2 Electrophysiological characterization of Ca_v3.2 P1210L and ΔI153 variants. **a** Representative T-type current traces recorded in response to 150 ms depolarizing steps to values ranging between -90 mV and +30 mV from a holding potential of -100 mV for wild-type (WT, black traces), P1210L (blue traces), and ΔI153 (red traces) channel variants expressed in tsA-201 cells. **b** Corresponding mean current-voltage relationship (*I/V*) for WT (black circles), P1210L (blue circles), and ΔI153 (red circles) channels. **c** Corresponding mean maximal macroscopic conductance (G_{max}) obtained from the fit of the *I/V* curves with the modified Boltzmann eq. (1). **d** Mean normalized voltage-dependence of activation and inactivation for WT (black circles) and P1210L channels (blue circles). **e** Mean normalized recovery from inactivation kinetics. **f** Representative T-type current traces recorded from WT (black trace) and ΔI153 DRG neurons (red trace) 3 days after editing of *Cacna1h* by CRISPR/Cas9 in response to 80 ms depolarizing steps to -25 mV from a holding potential of -90 mV. **g** Corresponding mean peak T-type current density at -25 mV in WT and ΔI153 mutant DRG neurons

variant, we observed a 27% reduction of Q_{max} (t-test $p = 0.0467$) compared to cells expressing the WT channel (from 12.0 ± 1.3 fC/pF, $n = 19$ to 8.7 ± 0.8 fC/pF, $n = 18$) (Fig. 3d). This reduction of Q_{max} is similar to the reduction of the maximal T-type conductance we previously observed (32%, Fig. 2c), suggesting that the decrease of

the T-type conductance in cells expressing the P1210L channel variant is likely caused by a reduced expression of the channel in the plasma membrane. This notion is further supported by the observation that neither the G_{max}/Q_{max} dependency (Fig. 3e), nor the kinetics of charge movements (Fig. 3f), were modified, indicating

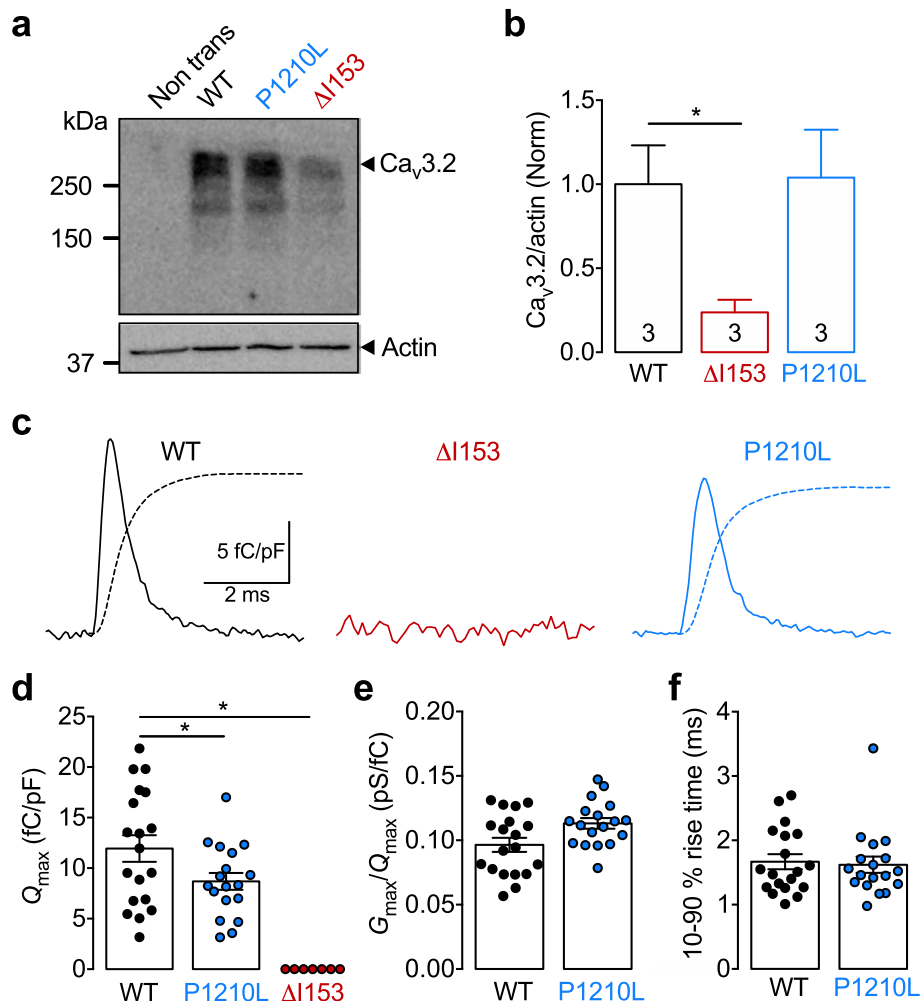


Fig. 3 Expression of $Ca_v3.2$ P1210L and $\Delta I153$ variants. **a** Representative immunoblot of $Ca_v3.2$ from tsA-201 cells expressing wild-type (WT), P1210L, and $\Delta I153$ channel variants. **b** Corresponding mean expression levels of P1210L and $\Delta I153$ variants relative to WT channels. **c** Representative charge movement traces recorded at the ionic reversal potential from cells expressing wild-type (WT, black trace), P1210L (blue trace), and $\Delta I153$ (red trace) channel variants. The dotted line depicts the time course of the integral for each trace. **d** Corresponding mean Q_{max} values calculated for each investigated cell. **e** Corresponding mean G_{max}/Q_{max} ratios. **f** Corresponding mean 10–90% rise times calculated from the integral time course shown in panel **c**

that the gating properties of the P1210L channel variant remained unaltered. In contrast, we did not detect any charge movement in cells expressing the $\Delta I153$ channel variant (Fig. 3c and d), suggesting that despite being biochemically expressed, this variant is not present in the plasma membrane.

Altogether, these data are consistent with a mildly decreased surface expression of the P1210L variant without additional alterations. Importantly, these data demonstrate the profound deleterious effect of the $\Delta I153$ mutation on the biogenesis and surface trafficking of $Ca_v3.2$ channels.

Dominant-negative effect of the $\Delta I153$ channel variant

Given the heterozygosity of the $\Delta I153$ mutation and the defective trafficking of the $\Delta I153$ channel variant, we

aimed to test whether this variant could have a dominant-negative effect on WT channels. Therefore, we co-expressed the WT and $\Delta I153$ channels in tsA-201 cells in a 1:1 ratio (equal amount of cDNAs) and compared T-type currents with cells expressing the WT channel in combination with a cation-impermeant but trafficking-competent channel (PM). Recording of T-type currents in cells expressing a combination of WT: $\Delta I153$ channels (Fig. 4a) revealed a 35% reduction (Mann-Whitney $p = 0.0080$) of the maximal T-type conductance compared to cells expressing a combination of WT:PM channels (from 569 ± 73 pS/pF, $n = 38$ to 372 ± 27 pS/pF, $n = 58$) (Fig. 4b and c), indicating that the $\Delta I153$ variant produced a dominant-negative effect on the WT channel when expressed *in trans*. In contrast, the voltage-dependence of

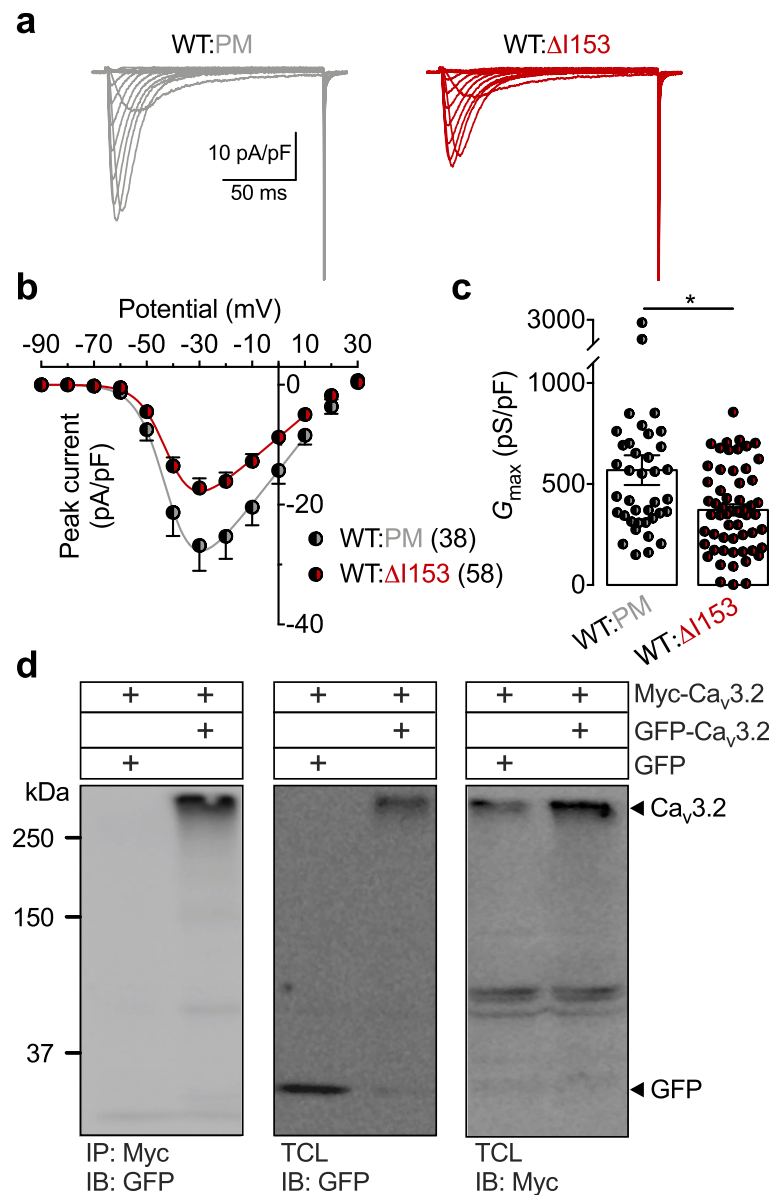


Fig. 4 Electrophysiological characterization of $\text{Ca}_v3.2$ WT and $\Delta I153$ expressed in *trans*. **a** Representative T-type current traces recorded from tsA-201 cells expressing WT channels in combination with either the $\Delta I153$ variant (WT: $\Delta I153$, red traces) or the cation-impermeant but trafficking-competent $\text{Ca}_v3.2$ pore mutant (WT:PM; grey traces) in a ratio 1:1. **b** Corresponding mean current-voltage relationship (I/V) for WT: $\Delta I153$ (black/red circles), and WT:PM (black/grey circles) conditions. **c** Corresponding mean maximal macroscopic conductance (G_{max}). **d** Co-immunoprecipitation of $\text{Ca}_v3.2$ from tsA-201 cells co-transfected with a Myc-tagged and GFP-tagged $\text{Ca}_v3.2$. The left panel shows the result of the co-immunoprecipitation of Myc- $\text{Ca}_v3.2$ with GFP- $\text{Ca}_v3.2$ using an anti-Myc antibody. The middle and right panels show the immunoblot of GFP- $\text{Ca}_v3.2$ and Myc- $\text{Ca}_v3.2$ using anti-GFP and anti-Myc antibody, respectively

activation and inactivation remained unaltered. Given the comparatively mild phenotype produced by the P1210L mutation, the P1210L variant was not tested in combination with the WT channel. Finally, to test whether this dominant-negative effect could be mediated by an interaction between $\text{Ca}_v3.2$ subunits, we performed co-immunoprecipitations from tsA-201 cells co-expressing Myc-tagged and GFP-tagged $\text{Ca}_v3.2$ to discriminate

between the two channels. We observed that the GFP-tagged $\text{Ca}_v3.2$ was immunoprecipitated with the Myc-tagged $\text{Ca}_v3.2$ using a specific anti-Myc antibody, revealing the ability of $\text{Ca}_v3.2$ channels to dimerize (Fig. 4d).

Collectively, these data revealed the dominant-negative effect of the $\Delta I153$ variant on the WT channel, a phenomenon likely to be mediated by the interaction between $\text{Ca}_v3.2$ subunits.

Discussion

While several common genes are implicated in familial ALS, the occurrence of rare genetic variants in patients with no family history of the disease has emerged as a potential contributing factor in sporadic ALS [11]. In this study, we report two heterozygous *CACNA1H* variants identified by whole genome sequencing of a small cohort of ALS patients. Functional analysis revealed mild to severe alterations of $Ca_v3.2$ variants that were consistent with a loss-of-function of the channels.

The P1210L missense mutation was located in a variable region of $Ca_v3.2$ and was not predicted to be deleterious. Our electrophysiological analysis showed a moderate reduction of the expression of the P1210L channel variant at the cell surface and an associated reduction in the T-type conductance. We cannot entirely rule out the possibility that the phenotypic expression of the P1210L variant could have differed when introduced into a different $Ca_v3.2$ splice variant [18], or when functionally assessed under different experimental conditions [19], but our experimental data together with the relatively high occurrence of this variant in the general population strongly suggest that it is indeed unlikely to be pathogenic. In contrast, the $\Delta I153$ variant had never been reported and was predicted to be deleterious. Electrophysiological analysis revealed a complete loss of functional expression of the $\Delta I153$ variant, and recording of charge movements suggested that this variant was absent from the cell surface. Furthermore, our biochemical analysis revealed a dramatic decrease of the expression level of the channel protein, suggesting that this variant may have undergone extensive degradation. Of particular importance was the dominant-negative effect produced by the $\Delta I153$ variant on the WT channel when the two channels were expressed in *trans*. This effect was likely to be mediated by the ability of $Ca_v3.2$ subunits to dimerize, which could have prevented the proper trafficking of the WT channel to the cell surface in the presence of the impaired $\Delta I153$ variant. In this regard, it is worth considering that this dominant-negative effect may also have an effect on other ion channels. Indeed, $Ca_v3.2$ channels are known to biochemically interact with several calcium- and voltage-activated potassium and sodium channel subunits [20–23] whose surface trafficking and activity could be affected by the $Ca_v3.2$ $\Delta I153$ variant.

The molecular mechanisms underlying the deleterious effect of the $\Delta I153$ variant can be appreciated by examining the 3-dimensional environment of I153, and the possible impact of its deletion in the homology model of $Ca_v3.2$ we have developed, using the 3.3 Å CryoEM structure of $Ca_v3.1$ [24]. In this model, I153 is located within the transmembrane S2 alpha helix of domain I (Fig. 5a), where it is surrounded by hydrophobic residues near the membrane-cytosol interface (Fig. 5b). The

nearby hydrophobic residues are highly conserved between L- and T-type channels and I153 shows a clear involvement in the helical packing (Fig. 5b). Therefore, deletion of I153 that results in a net loss of hydrophobicity within the transmembrane segment is likely to alter helix packing in domain I which would result in the misfolding of the channel. Additionally, deletion of I153 would also affect downstream residues in the helix due to a change in the helical register, thus further affecting the helical packing in the voltage-sensing domain.

From a clinical point of view, the loss-of-channel function associated with the $\Delta I153$ variant could have several pathological implications. First, $Ca_v3.2$ is present in several central neurons, including reticular thalamic neurons [25], where they contribute to NMDA receptor-mediated synaptic transmission [26]. Given that gain-of-function mutations associated with childhood absence epilepsy were shown to enhance synaptic activities [26], the reciprocal theory would suggest that loss-of-channel function could, in contrast, decrease synaptic transmission. Along these lines, neuroimaging studies have revealed decreased thalamic activity in ALS [27–32], and a recent MRI study reported alterations of thalamic connectivities that mirrored the progressive motor functional decline in ALS [33]. Second, although the functional expression of $Ca_v3.2$ in mammalian motor neurons remains elusive, several studies suggest that T-type channels may have a functional role. For instance, $Ca_v3.1$ channels are present in turtle spinal motor neurons where they contribute to cellular excitability [34]. In addition, a low-threshold voltage-activated calcium conductance was reported at nodes of Ranvier in mouse spinal motor neurons, suggesting the presence of T-type channels [35]. Third, a T-type channel ortholog is present in motor neurons of the nematode *C. elegans* [36] where it contributes to motor-related functions [37, 38]. Finally, a recent study documented the role of T-type channels in the maintenance of neuronal progenitor cells [39]. A loss-of-function of $Ca_v3.2$ could compromise the architecture of nerve cells and precipitate neuronal degeneration.

In conclusion, this newly identified $\Delta I153$ variant is the first to be reported to cause a complete loss of $Ca_v3.2$ channel function [40]. Although its pathogenic role in the context of ALS remains to be established, these findings add to the notion that rare *CACNA1H* variants represent a risk factor for ALS. Furthermore, several T-type channels blockers are currently being used for the treatment of epilepsy [41]. The question then arises as to whether long term use of these molecules may present a risk to the development of ALS. This notion should be given particular attention, especially considering that several other T-type channel blockers are currently evaluated in clinical trials for the management of epilepsy and chronic pain symptoms.

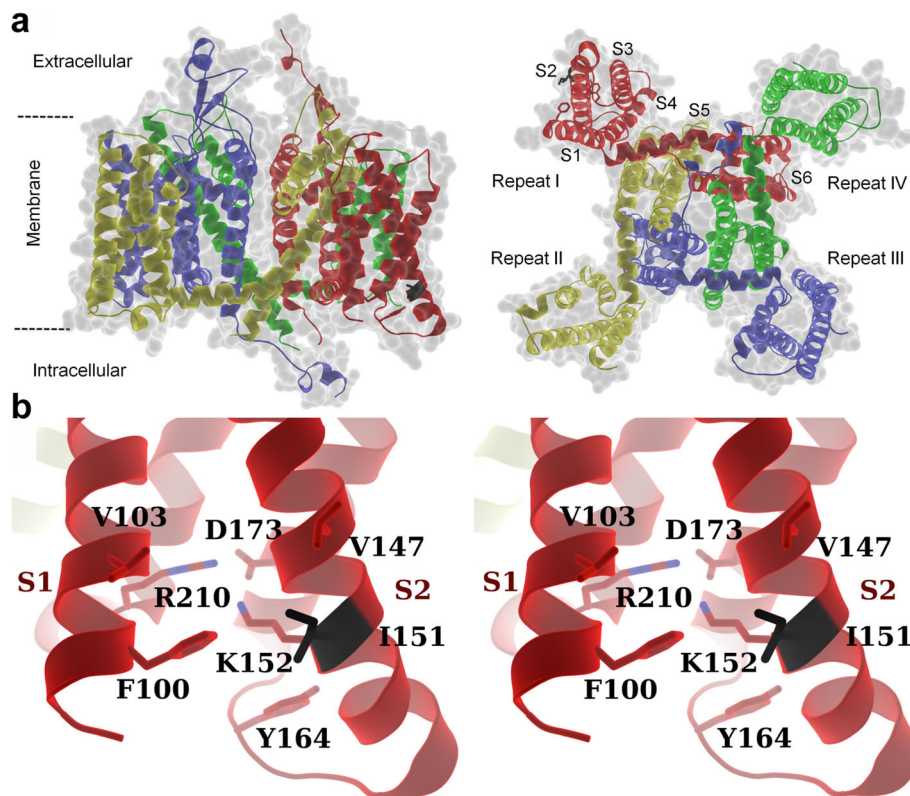


Fig. 5 Homology model of human $\text{Ca}_v3.2$. **a** Cartoon representation of secondary structural elements of human $\text{Ca}_v3.2$ (Uniprot O95180) homology model (residues 97–1974) based on $\text{Ca}_v3.1$ (PDB: 6KZO), showing side (left panel) and bottom (right panel) views of the channel. The four domains of $\text{Ca}_v3.2$ are colored in red, yellow, blue and green. The S1-S6 helices are indicated in red for domain I. Some of the flexible loops connecting the transmembrane helices are not shown, or could not be modeled, due to poor model accuracy or lack of structural information, respectively. The isoleucine 153 (Ile153) is shown in black. **b** Stereo diagram of Ile153 and nearby hydrophobic residues showing its involvement in the helical packing

Methods

Plasmids cDNA constructs and site-directed mutagenesis

The $\text{Ca}_v3.2$ P1210L and ΔI153 channel variants were created by introducing the respective mutations into the human wild-type HA-tagged $\text{Ca}_v3.2$ in pcDNA3.1 [42] by PCR-based site-directed mutagenesis using Q5[®] Site-Directed Mutagenesis Kit (New England Biolabs) and the following mutagenic primers: ΔI153 : 5'-TCAAGATGGTGGCCTTGG-3' (forward) and 5'-CCATCTCCACCGCAAAAAG-3' (reverse); P1210L: 5'-GCCGCCCTCCtGCCTACCAAGTGC-3' (forward) and 5'-CGGCCGCAGGGGCCGTGG-3' (reverse). The cation-impermeant $\text{Ca}_v3.2$ channel was generated by replacing the glutamic acid 378 in domain I with a lysine (E378K) by site-directed mutagenesis. Final constructs were verified by sequencing of the coding sequence of the plasmid cDNAs.

Cell culture and heterologous expression

Human embryonic kidney tsA-201 cells were grown in DMEM medium supplemented with 10% fetal bovine serum and 1% penicillin/streptomycin (all media purchased

from Invitrogen) and maintained under standard conditions at 37 °C in a humidified atmosphere containing 5% CO_2 . Heterologous expression of $\text{Ca}_v3.2$ channels was performed by transfecting cells with 5 μg plasmid cDNAs encoding for $\text{Ca}_v3.2$ channel variants using the calcium/phosphate method. For experiments aiming at investigating the dominant negative effect of the ΔI153 variant, cells were co-transfected with 2.5 μg plasmid cDNA encoding for WT channels with either 2.5 μg plasmid cDNA encoding for the ΔI153 channel variant or 2.5 μg plasmid cDNA encoding for a non-conducting but trafficking-competent $\text{Ca}_v3.2$ (PM).

Patch clamp electrophysiology

Patch clamp recordings of T-type currents in tsA-201 cells expressing $\text{Ca}_v3.2$ channel variants were performed 72 h after transfection in the whole-cell configuration at room temperature (22–24 °C) as previously described [43]. The bath solution contained (in millimolar): 5 BaCl_2 , 5 KCl , 1 MgCl_2 , 128 NaCl , 10 TEA-Cl , 10 D-glucose , 10 4-(2-hydroxyethyl)-1-piperazineethanesulfonic acid (HEPES) (pH 7.2 with NaOH). Patch pipettes

were filled with a solution containing (in millimolar): 110 CsCl, 3 Mg-ATP, 0.5 Na-GTP, 2.5 MgCl₂, 5 D-glucose, 10 EGTA, and 10 HEPES (pH 7.4 with CsOH), and had a resistance of 2–4 MΩ. Recordings were performed using an Axopatch 200B amplifier (Axon Instruments) and acquisition and analysis were performed using pClamp 10 and Clampfit 10 software, respectively (Axon Instruments). The linear leak component of the current was corrected online and current traces were digitized at 10 kHz and filtered at 2 kHz. The voltage dependence of activation of Ca_v3.2 channels was determined by measuring the peak T-type current amplitude in response to 150 ms depolarizing steps to various potentials applied every 10 s from a holding membrane potential of –100 mV. The current-voltage relationship (*I*/*V*) curve was fitted with the following modified Boltzmann eq. (1):

$$I(V) = G_{max} \frac{(V - V_{rev})}{1 + \exp\left(\frac{V_{0.5} - V}{k}\right)} \quad (1)$$

with *I*(*V*) being the peak current amplitude at the command potential *V*, *G*_{max} the maximum conductance, *V*_{rev} the reversal potential, *V*_{0.5} the half-activation potential, and *k* the slope factor. The voltage dependence of the whole-cell Ba²⁺ conductance was calculated using the following modified Boltzmann eq. (2):

$$G(V) = \frac{G_{max}}{1 + \exp\left(\frac{V_{0.5} - V}{k}\right)} \quad (2)$$

with *G*(*V*) being the Ba²⁺ conductance at the command potential *V*.

The voltage dependence of the steady-state inactivation of Ca_v3.2 channels was determined by measuring the peak T-type current amplitude in response to a 150 ms depolarizing step to –20 mV applied after a 5 s-long conditioning prepulse ranging from –120 mV to –30 mV. The current amplitude obtained during each test pulse was normalized to the maximal current amplitude and plotted as a function of the prepulse potential. The voltage dependence of the steady-state inactivation was fitted with the following two-state Boltzmann function (3):

$$I(V) = \frac{I_{max}}{1 + \exp\left(\frac{V - V_{0.5}}{k}\right)} \quad (3)$$

with *I*_{max} corresponding to the maximal peak current amplitude and *V*_{0.5} to the half-inactivation voltage.

The recovery from inactivation was assessed using a double-pulse protocol from a holding potential of –100

mV. The cell membrane was depolarized for 2 s at 0 mV (inactivating prepulse) to ensure complete inactivation of the channel, and then to –20 mV for 150 ms (test pulse) after an increasing time period (interpulse) ranging between 0.1 ms and 2 s at –100 mV. The peak current from the test pulse was plotted as a ratio of the maximum prepulse current versus interpulse interval. The data were fitted with the following single-exponential function (4):

$$\frac{I}{I_{max}} = A \times \left(1 - \exp\left(-\frac{t}{\tau}\right)\right) \quad (4)$$

where τ is the time constant for channel recovery from inactivation.

Measurement of charge movements

Recording of charge movements was performed 72 h after transfection as previously described [44, 45]. The bath solution contained (in millimolar): CsCl 95; TEACl 40, BaCl₂ 5; MgCl₂ 1; HEPES 10; glucose 10; pH 7.4 (adjusted with CsOH). Patch pipettes had a resistance ranging from 1.8 MΩ to 2.2 MΩ when filled with a solution containing (in millimolar): CH₃SO₃Cs 130; Na-ATP 5; TEACl 10; HEPES 10; EGTA 10; MgCl₂ 5; pH 7.4 (adjusted with CsOH). Osmolarity of the intracellular solution was approximately 300 mOsmol/L. Osmolarity of the extracellular solution was adjusted by adding sucrose so that the final value was about 2–3 mOsmol/L lower than the osmolarity of the corresponding intracellular solution. Recordings were performed using HEKA EPC10 amplifier (HEKA Electronics). Acquisition and analysis were performed using Patchmaster v90.2 and Fitmaster v2x73.1 and Origin Pro 2015 software, respectively. Only cells with an input resistance less than 5 MΩ were considered. The input resistance and capacity transients were compensated by up to 70% with in-built circuits of the EPC 10 amplifier. Remaining artifacts were subtracted using a -P/8 procedure. ON-gating currents were recorded in response to a series of 5 depolarizing pulses at the reversal potential of the ionic current assessed for each cell, and total gating charge *Q*_{ON} was calculated as the integral of area below the averaged current traces.

CRISPR/Cas9 genome editing in DRG neurons

Male rats (6-week-old) were purchased from Charles River and DRG neurons were harvested as described previously [46]. The next day, neurons were transfected with Crispr-Cas9 plasmids (Cas9-sgRNA plasmid and donor plasmid purchased from GeneCopoeia) using Lipofectamine 2000 from Invitrogen (Cat. 11,668–019). The sequence of Crispr RNA was CGTGGAGATG

GTGATCAAGA. The donor plasmid contained the homologous arms of the genomic DNA without I153. Whole-cell voltage-clamp recordings of T-type currents were performed 3 days post transfection. The external solution contained (in mM): 40 TEACl, 65 CsCl, 20 BaCl₂, 1 MgCl₂, 10 HEPES, 10 D-glucose, pH 7.4. The internal solution contained (in mM): 140 CsCl, 2.5 CaCl₂, 1 MgCl₂, 5 EGTA, 10 HEPES, 2 Na-ATP, 0.3 Na-GTP, pH 7.3. We used GFP fluorescence to specifically identify neurons that were transfected with the CRISPR plasmids. The overall percentage of GFP positive neurons in a dish was relatively low, and hence we cannot use bulk genomic sequencing for verification. However, given the large functional effect on current densities, we are confident that the use of GFP fluorescence is an appropriate means of identifying neurons that were targeted with these plasmids. We specifically targeted medium diameter neurons for our analysis. The mean capacitance of the neurons that we recorded from was 24.79 ± 4.40 pF for control neurons versus 21.89 ± 1.31 pF for CRISPR-edited neurons.

SDS-PAGE and immunoblot analysis

Immunoblot of HA-tagged Ca_v3.2 channel was performed as previously described [16]. Briefly, total cell lysate from tsA-201 cells expressing HA-Ca_v3.2 channels was separated on a 5–20% gradient SDS-PAGE gel and transferred onto PVDF membrane (Millipore). Detection of HA-Ca_v3.2 was performed using a primary rat monoclonal anti-HA antibody (1:1000, Roche) and secondary HRP-conjugated antibody (1:10,000, Jackson ImmunoResearch). Immunoreactive products were detected by enhanced chemiluminescence and analyzed using ImageJ software.

For co-immunoprecipitation, cell lysates containing GFP-tagged and Myc-tagged Ca_v3.2 were incubated for 3 h with a biotinylated mouse monoclonal anti-Myc antibody (Santa Cruz Biotechnology), and then for 45 min with streptavidin beads (Invitrogen) at 4 °C, and washed with PBS/Tween-20 buffer. Beads were resuspended in Laemmli buffer and immunoprecipitation samples were separated on SDS-PAGE gel.

Generation of human Ca_v3.2 homology model

The homology model of the human Ca_v3.2 channel was prepared using the Ca_v3.1 structure as a template (PDB: 6KZO) in conjunction with Swiss-Model server (<https://swissmodel.expasy.org/>) [47]. Figures were prepared using Pymol (v2.2 Schrödinger, LLC).

Statistics

Data values are presented as mean \pm SEM for *n* measurements. Statistical analysis was performed using GraphPad Prism 7. For datasets passing the D'Agostino &

Pearson omnibus normality test, statistical significance was determined using either Student's t-test or a Mann-Whitney test. Datasets were considered significantly different for $p \leq 0.05$.

Abbreviations

ALS: Amyotrophic lateral sclerosis; DRG: Dorsal root ganglia; GFP: Green fluorescent protein; G_{max} : Maximal macroscopic conductance; MRI: Magnetic resonance imaging; PM: Pore mutant; Q_{max} : Maximal charge movements; Q_{rev} : Charge movements at the reversal calcium potential; WT: Wild-type

Acknowledgements

We thank the patients and family members for their contribution to this study.

Authors' contributions

N.W., L.L., F.V.P., G.W.Z., and R.P. designed and conceptualized the study. R.N.S., R.I., B.J.T., O.H., S.H., I.A.S., A.L., Y.R., and N.W. collected data, performed analysis and interpreted the results. N.W. and R.P. wrote the manuscript. All authors critically revised the manuscript and contributed significantly to this work. The authors read and approved the final manuscript.

Funding

N.W. is supported by the Institute of Organic Chemistry and Biochemistry. L.L. is supported by a grant VEGA 2/0143/19. N.W. and L.L. are supported by a bilateral SAS-CAS project (SAV-18-22). G.W.Z. is supported by a grant from the Natural Sciences and Engineering Research Council and holds a Canada Research Chair.

Availability of data and materials

The data used and/or analyzed during the current study are available from the corresponding author on reasonable request.

Ethics approval and consent to participate

The whole genome sequencing of white blood cell DNA that gave rise to the finding of the genetic variants further characterised in the present study was undertaken by RP in a joint University of Sydney (Australia) and the Genome Institute Washington University (St Louis, USA) project using DNA samples from the Australian Motor Neuron Disease DNA Bank, with approval from the Sydney South West Area Health Service Human Research Ethics Committee. Informed written consent was obtained from each individual for their DNA to be used for research purposes.

Consent for publication

Not applicable.

Competing interests

The authors declare that they have no competing interests.

Author details

¹Institute of Organic Chemistry and Biochemistry, Czech Academy of Sciences, Flemingovo nam 2, 16610 Prague, Czech Republic. ²Third Faculty of Medicine, Charles University, Prague, Czech Republic. ³Center of Biosciences, Institute of Molecular Physiology and Genetics, Academy of Sciences, Bratislava, Slovakia. ⁴Department of Physiology and Pharmacology, Cumming School of Medicine, University of Calgary, Calgary, Canada. ⁵Department of Biochemistry and Molecular Biology, University of British Columbia, Vancouver, Canada. ⁶Discipline of Pathology, Brain and Mind Centre, The University of Sydney, Sydney, NSW, Australia.

Received: 25 November 2019 Accepted: 2 March 2020

Published online: 06 March 2020

References

- Marin B, Fontana A, Arcuti S, Copetti M, Boumédiène F, Couratier P, et al. Age-specific ALS incidence: a dose-response meta-analysis. *Eur J Epidemiol.* 2018;33(7):621–34.
- Marin B, Boumédiène F, Logroscino G, Couratier P, Babron MC, Leutenegger AL, et al. Variation in worldwide incidence of amyotrophic lateral sclerosis: a meta-analysis. *Int J Epidemiol.* 2017;46(1):57–74.

3. Hardiman O, Al-Chalabi A, Chio A, Corr EM, Logroscino G, Robberecht W, et al. Amyotrophic lateral sclerosis. *Nat Rev Dis Primers*. 2017;3:17071.
4. Talbot K. Familial versus sporadic amyotrophic lateral sclerosis—a false dichotomy. *Brain*. 2011;134(Pt 12):3429–31.
5. Nguyen HP, Van Broeckhoven C, van der Zee J. ALS genes in the genomic era and their implications for FTD. *Trends Genet*. 2018;34(6):404–23.
6. Gibson SB, Downie JM, Tsetsou S, Feusier JE, Figueroa KP, Bromberg MB, et al. The evolving genetic risk for sporadic ALS. *Neurology*. 2017;89(3):226–33.
7. Sproviero W, Shatunov A, Stahl D, Shoai M, van Rheenen W, Jones AR, et al. ATXN2 trinucleotide repeat length correlates with risk of ALS. *Neurobiol Aging*. 2017;51:178.e1–9.
8. van Es MA, Veldink JH, Saris CG, Blauw HM, van Vught PW, Birve A, et al. Genome-wide association study identifies 19p13.3 (UNC13A) and 9p21.2 as susceptibility loci for sporadic amyotrophic lateral sclerosis. *Nat Genet*. 2009;41(10):1083–7.
9. Greenway MJ, Andersen PM, Russ C, Ennis S, Cashman S, Donaghy C, et al. ANG mutations segregate with familial and ‘sporadic’ amyotrophic lateral sclerosis. *Nat Genet*. 2006;38(4):411–3.
10. Corcia P, Camu W, Halimi JM, Vourc’h P, Antar C, Vedrine S, et al. SMN1 gene, but not SMN2, is a risk factor for sporadic ALS. *Neurology*. 2006;67(7):1147–50.
11. Steinberg KM, Yu B, Koboldt DC, Mardis ER, Pamphlett R. Exome sequencing of case-unaffected-parents trios reveals recessive and de novo genetic variants in sporadic ALS. *Sci Rep*. 2015;5:9124.
12. Rzhetsky Y, Lazniewska J, Blesneac I, Pamphlett R, Weiss N. CACNA1H missense mutations associated with amyotrophic lateral sclerosis alter Cav3.2 T-type calcium channel activity and reticular thalamic neuron firing. *Channels (Austin)*. 2016;10(6):466–77.
13. Meltz Steinberg K, Nicholas TJ, Koboldt DC, Yu B, Mardis E, Pamphlett R. Whole genome analyses reveal no pathogenetic single nucleotide or structural differences between monozygotic twins discordant for amyotrophic lateral sclerosis. *Amyotroph Lateral Scler Frontotemporal Degener*. 2015;16(5–6):385–92.
14. Nitirini R. Frontotemporal dementia and amyotrophic lateral sclerosis: revisiting one of the first case reports with neuropathology examination. *Dement Neuropsychol*. 2014;8(1):83–6.
15. Rzhetsky Y, Lazniewska J, Proft J, Campiglio M, Flucher BE, Weiss N. A Ca_v3.2/STac1 molecular complex controls T-type channel expression at the plasma membrane. *Channels (Austin)*. 2016;10(5):346–54.
16. Proft J, Rzhetsky Y, Lazniewska J, Zhang FX, Cain SM, Snutch TP, et al. The Cacna1h mutation in the GAERS model of absence epilepsy enhances T-type Ca²⁺ currents by altering calnexin-dependent trafficking of Ca_v3.2 channels. *Sci Rep*. 2017;7(1):11513.
17. Bourinet E, Alloui A, Monteil A, Barrère C, Couette B, Poirot O, et al. Silencing of the Cav3.2 T-type calcium channel gene in sensory neurons demonstrates its major role in nociception. *EMBO J*. 2005;24(2):315–24.
18. Powell KL, Cain SM, Ng C, Sirdesai S, David LS, Kyi M, et al. A Cav3.2 T-type calcium channel point mutation has splice-variant-specific effects on function and segregates with seizure expression in a polygenic rat model of absence epilepsy. *J Neurosci*. 2009;29(2):371–80.
19. Souza IA, Gandini MA, Wan MM, Zamponi GW. Two heterozygous Cav3.2 channel mutations in a pediatric chronic pain patient: recording condition-dependent biophysical effects. *Pflugers Arch*. 2016;468(4):635–42.
20. Anderson D, Mehaffey WH, Iftinca M, Rehak R, Engbers JD, Hameed S, et al. Regulation of neuronal activity by Cav3-Kv4 channel signaling complexes. *Nat Neurosci*. 2010;13(3):333–7.
21. Engbers JD, Anderson D, Asmara H, Rehak R, Mehaffey WH, Hameed S, et al. Intermediate conductance calcium-activated potassium channels modulate summation of parallel fiber input in cerebellar Purkinje cells. *Proc Natl Acad Sci U S A*. 2012;109(7):2601–6.
22. Rehak R, Bartoletti TM, Engbers JD, Berecki G, Turner RW, Zamponi GW. Low voltage activation of KCa1.1 current by Cav3-KCa1.1 complexes. *PLoS One*. 2013;8(4):e61844.
23. García-Caballero A, Gandini MA, Huang S, Chen L, Souza IA, Dang YL, et al. Cav3.2 calcium channel interactions with the epithelial sodium channel ENaC. *Mol Brain*. 2019;12(1):12.
24. Zhao Y, Huang G, Wu Q, Wu K, Li R, Lei J, et al. Cryo-EM structures of apo and antagonist-bound human Ca_v3.1. *Nature*. 2019;576(7787):492–7.
25. Talley EM, Cribbs LL, Lee JH, Daud A, Perez-Reyes E, Bayliss DA. Differential distribution of three members of a gene family encoding low voltage-activated (T-type) calcium channels. *J Neurosci*. 1999;19(6):1895–911.
26. Wang G, Bochorishvili G, Chen Y, Salvati KA, Zhang P, Dubel SJ, et al. CaV3.2 calcium channels control NMDA receptor-mediated transmission: a new mechanism for absence epilepsy. *Genes Dev*. 2015;29(14):1535–51.
27. Turner MR, Cagnin A, Turkheimer FE, Miller CC, Shaw CE, Brooks DJ, et al. Evidence of widespread cerebral microglial activation in amyotrophic lateral sclerosis: an [11C](R)-PK11195 positron emission tomography study. *Neurobiol Dis*. 2004;15(3):601–9.
28. Chang JL, Lomen-Hoerth C, Murphy J, Henry RG, Kramer JH, Miller BL, et al. A voxel-based morphometry study of patterns of brain atrophy in ALS and ALS/FTLD. *Neurology*. 2005;65(1):75–80.
29. Sharma KR, Saigal G, Maudsley AA, Govind V. 1H MRS of basal ganglia and thalamus in amyotrophic lateral sclerosis. *NMR Biomed*. 2011;24(10):1270–6.
30. Sharma KR, Sheriff S, Maudsley A, Govind V. Diffusion tensor imaging of basal ganglia and thalamus in amyotrophic lateral sclerosis. *J Neuroimaging*. 2013;23(3):368–74.
31. Bede P, Elamin M, Byrne S, McLaughlin RL, Kenna K, Vajda A, et al. Basal ganglia involvement in amyotrophic lateral sclerosis. *Neurology*. 2013;81(24):2107–15.
32. Menke RA, Körner S, Filippini N, Douaud G, Knight S, Talbot K, et al. Widespread grey matter pathology dominates the longitudinal cerebral MRI and clinical landscape of amyotrophic lateral sclerosis. *Brain*. 2014;137(Pt 9):2546–55.
33. Tu S, Menke RAL, Talbot K, Kiernan MC, Turner MR. Regional thalamic MRI as a marker of widespread cortical pathology and progressive frontotemporal involvement in amyotrophic lateral sclerosis. *J Neurol Neurosurg Psychiatry*. 2018;89(12):1250–8.
34. Canto-Bustos M, Loeza-Alcocer E, González-Ramírez R, Gandini MA, Delgado-Lezama R, Felix R. Functional expression of T-type Ca₂₊ channels in spinal motoneurons of the adult turtle. *PLoS One*. 2014;9:e108187.
35. Zhang Z, David G. Stimulation-induced Ca (2+) influx at nodes of Ranvier in mouse peripheral motor axons. *J Physiol*. 2016;594(1):39–57.
36. Shtonda B, Avery L. CCA-1, EGL-19 and EXP-2 currents shape action potentials in the *Caenorhabditis elegans* pharynx. *J Exp Biol*. 2005;208(Pt 11):2177–90.
37. Steger KA, Shtonda BB, Thacker C, Snutch TP, Avery L. The *C. elegans* T-type calcium channel CCA-1 boosts neuromuscular transmission. *J Exp Biol*. 2005;208(Pt 11):2191–203.
38. Nicoletti M, Loppini A, Chiodo L, Folli V, Ruocco G, Filippi S. Biophysical modeling of *C. elegans* neurons: Single ion currents and whole-cell dynamics of AWCon and RMD. *PLoS One*. 2019;14(7):e0218738.
39. Kim JW, Oh HA, Lee SH, Kim KC, Eun PH, Ko MJ, et al. T-type calcium channels are required to maintain viability of neural progenitor cells. *Biomol Ther (Seoul)*. 2018;26(5):439–45.
40. Weiss N, Zamponi GW. Genetic T-type calcium channelopathies. *J Med Genet*. 2020;57(1):1–10.
41. Weiss N, Zamponi GW. T-type calcium channels: from molecule to therapeutic opportunities. *Int J Biochem Cell Biol*. 2019;108:34–9.
42. Dubel SJ, Altier C, Chaumont S, Lory P, Bourinet E, Nargeot J. Plasma membrane expression of T-type calcium channel alpha (1) subunits is modulated by high voltage-activated auxiliary subunits. *J Biol Chem*. 2004;279(28):29263–9.
43. Carter MT, McMillan HJ, Tomin A, Weiss N. Compound heterozygous CACNA1H mutations associated with severe congenital amyotrophy. *Channels (Austin)*. 2019;13(1):153–61.
44. Ondacova K, Karmazinova M, Lazniewska J, Weiss N, Lacinova L. Modulation of Cav3.2 T-type calcium channel permeability by asparagine-linked glycosylation. *Channels (Austin)*. 2016;10(3):175–84.
45. Jurkovicova-Tarabova B, Cmarko L, Rehak R, Zamponi GW, Lacinova L, Weiss N. Identification of a molecular gating determinant within the carboxy terminal region of Ca_v3.3 T-type channels. *Mol Brain*. 2019;12(1):34.
46. Altier C, Khosravani H, Evans RM, Hameed S, Peloquin JB, Vartian BA, et al. ORL1 receptor-mediated internalization of N-type calcium channels. *Nat Neurosci*. 2006;9(1):31–40.
47. Waterhouse A, Bertoni M, Bienert S, Studer G, Tauriello G, Gumienny R, et al. SWISS-MODEL: homology modelling of protein structures and complexes. *Nucleic Acids Res*. 2018;46(W1):W296–303.

Publisher's Note

Springer Nature remains neutral with regard to jurisdictional claims in published maps and institutional affiliations.

Synthesis and pharmacological evaluation of quinoline-based calcium channel blockers with analgesic properties

Leoš Cmarko^{1,2,3}, Mikhail Klychnikov², Kimberly Gomez^{4,5}, Robin N. Stringer^{1,2},
Samantha Perez-Miller^{4,5}, Miroslav Hájek², Michel De Waard³, Rajesh Khanna^{4,5}, Ullrich
Jahn², Norbert Weiss^{1*}

¹Department of Pathophysiology, Third Faculty of Medicine, Charles University, Prague, Czech Republic;

²Institute of Organic Chemistry and Biochemistry, Czech Academy of Sciences, Prague, Czech Republic;

³Nantes Université, CNRS, INSERM, l'institut du thorax, Nantes, France;

⁴Department of Molecular Pathobiology, College of Dentistry, New York University, NY, United States;

⁵NYU Pain Research Center, New York University, New York, United States.

*Correspondence to: Norbert Weiss (nalweiss@gmail.com)

ORCID ID:

Leoš Cmarko <https://orcid.org/0000-0003-4272-2784>

Robin N. Stringer <https://orcid.org/0000-0002-0887-7670>

Mikhail Klychnikov <https://orcid.org/0000-0001-6108-236X>

Kimberly Gomez <https://orcid.org/0000-0003-1867-5041>

Samantha Perez-Miller <https://orcid.org/0000-0002-9034-3693>

Miroslav Hájek <https://orcid.org/0000-0002-8906-243X>

Michel De Waard <https://orcid.org/0000-0002-2782-9615>

Rajesh Khanna <https://orcid.org/0000-0002-9066-2969>

Ullrich Jahn <https://orcid.org/0000-0001-8386-1348>

Norbert Weiss <https://orcid.org/0000-0002-0040-1109>

ABSTRACT

In the neurons of the dorsal root ganglia (DRG), various voltage-gated calcium channels (VGCCs) play a role in the processing of peripheral nociceptive information, serving as validated targets for pain therapeutics. Despite significant efforts to develop selective pharmacological blockers of VGCC subtypes for pain management, progress in clinical translation has been slow. Alternatively, polypharmacological blockers targeting multiple VGCC subtypes may offer additional advantages over highly selective inhibitors due to their synergistic activity. Previously, we identified surfen (bis(2-methyl-4-amino-quinolin-6-yl)urea) as a broad-spectrum VGCC blocker with analgesic properties. In this study, a series of 15 quinoline-based surfen analogs were rationally synthesized and evaluated for their pharmacological activity on VGCCs. Our results demonstrate that compound **S13** exhibits improved cell tolerance compared to the reference compound surfen, while maintaining blocking activities on several recombinant VGCCs subtypes, including the primary pain-relevant Cav2.2 (N-type) and Cav3.2 (T-type) channels. Molecular docking analyses predicted direct binding of **S13** to Cav2.2 and Cav3.2, suggesting potential interactions with ion-conducting pathways. Additional electrophysiology analyses of acutely dissociated DRG neurons in culture confirmed the blocking activity of **S13** on both native low-voltage-activated (LVA) and high-voltage-activated (HVA) VGCCs, while sparing sodium and potassium channels. Notably, we show that intrathecal administration of **S13** in a preclinical rat model of nerve ligation-induced mechanical allodynia produced substantial antinociceptive effects. Altogether, these findings underscore the potential of broad-spectrum VGCC blockers for pain therapy, and establish the quinoline-based backbone structure of **S13** as the basis for the development of novel analgesics.

KEYWORDS

Calcium channels, Voltage-gated calcium channels, Quinoline, Molecular docking, Pain, Neuropathy

INTRODUCTION

Voltage-gated calcium channels (VGCCs) play an essential role in processing peripheral nociceptive information within the neurons of the dorsal root ganglia (DRG) ¹⁰. Among the diverse VGCCs expressed in DRG neurons ^{14, 47}, two stand out as primary contributors to pain signaling in primary afferent nociceptive nerve fibers: the low-voltage-activated (LVA) Ca_v3.2 (T-type) and the high-voltage-activated (HVA) Ca_v2.2 (N-type) channels. For example, Ca_v3.2 channels, found in the soma and along the axon ³², drive neuronal excitability ²⁶. Moreover, presynaptic Ca_v3.2 channels directly participate in nociceptive transmission between primary afferent fibers and second-order neurons of the lamina I and II in the dorsal horn of the spinal cord ²⁰. Likewise, Ca_v2.2 channels, predominantly located in presynaptic nerve terminals, facilitate the release of key pronociceptive neurotransmitters such as glutamate, substance P, and calcitonin gene-related peptide (CGRP) ^{13, 24, 33, 39}. Beyond Ca_v3.2 and Ca_v2.2 channels, there is also evidence pointing to the involvement other VGCC members, especially the HVA Ca_v1.2 ^{7, 29, 31} and Ca_v2.3 channels ⁶ to the processing of peripheral nociception. Consequently, selective inhibition of VGCC subtypes with small organic molecules or peptides has been recognized for its potential in mediating analgesia in a wide range of preclinical rodent pain models ^{27, 48}. Significant effort has been directed towards the development of selective VGCC blockers for pain therapy. However, progress in clinical development of new drugs for chronic pain treatment has been slow. Despite promising preclinical drug candidates, no selective small-molecule channel blockers have received clinical approval thus far ⁴⁰. The limitations of established rodent pain models in predicting drug responses may be one factor, but it is also evident that these molecules often fail due to their adverse side effects.

An alternative approach may hinge on broad-spectrum calcium channel blockers with relatively lower affinity. Such molecules offer dual advantages: 1) their lower affinity may be less harmful to tissues beyond the pain pathway, which generally display a more limited diversity of VGCCs, and 2) their analgesic effect arises from the synergistic blocking of multiple VGCC subtypes.

Our previous findings indicate that surfen (bis(2-methyl-4-amino-quinolin-6-yl)urea) possesses analgesic properties in mouse models of acute and chronic inflammatory pain ³⁰. These analgesic effects were primarily attributed to the ability of

surfen to inhibit VGCCs, irrespective of the specific channel isoform. As part of our ongoing endeavors to develop broad-spectrum calcium channel blockers for pain therapy, we rationally designed and synthesized a series of surfen analogs to generate structure-activity relationships, and assessed their pharmacological activity on heterologous and native VGCCs. Among these 16 compounds, **S13** emerged as noteworthy, showing enhanced tolerance in cell toxicity assays compared to surfen, all the while retaining its ability to inhibit VGCCs. Molecular docking analyses provide further support for presumptive direct binding of **S13** to the channels. Importantly, in vivo evaluation of **S13** revealed potent analgesic effects in a preclinical rat pain model of neuropathic pain.

RESULTS AND DISCUSSION

Chemical synthesis of quinoline-based compounds. The synthesis of the quinoline derivatives **S1** was performed according to the literature³⁵ by condensation of 5-nitro-2-aminobenzonitrile and acetone in the presence of tin tetrachloride and subsequent reduction of the nitro group to amino with Al/Ni alloy under basic conditions (**Figure 1A-B**). Quinoline **S1** and commercially available 4-desamino derivatives **S2** were subsequently subjected to selective N-acylation reaction at N6. Ureas **S5-S11** were synthesized by reaction with isocyanates (X=O), potassium cyanate (X = O, R² = H) or isothiocyanates (X = S). N-Quinolin-6-yl amides **S12** and **S14-S16** and carbamate **S13** were prepared by N-acylation with acid chlorides or phenyl chloroformate, respectively (see Supplemental information).

Screening of quinoline-based compounds on recombinant Ca_v3.2 channels. To evaluate the pharmacological activities of quinoline-based compounds, we conducted a primary screen on recombinant Ca_v3.2 channels expressed in tsA-201 cells using patch-clamp electrophysiology. The compounds were applied acutely at 30 μM and the steady-state inhibition was recorded (**Figure 2A**). Clear trends emerged from the results. The N'-aminoquinolinyl unit in surfen **S4** can be easily substituted by the sterically similar, yet significantly more hydrophobic, β-naphthyl unit in **S6** or the sterically less demanding N'-phenyl unit in urea **S5** without losing blocking activity. The carbonyl oxygen atom in **S4-S6** appeared to play a crucial role for the pharmacological action, as the thiourea **S7** displayed significantly less blocking activity. However, substituting the distal nitrogen atom in N'-phenylurea **S5** with a CH₂ group in phenylacetamide **S12** or an oxygen atom to O-phenyl carbamate **S13** resulted only in a slight decrease in channel blocking activity, while **S13** showed a more favorable biological profile (*vide infra*). Urea **S9**, featuring the sterically significantly different α-naphthyl group compared to surfen **S4**, **S5**, or **S6**, showed almost no blocking activity, demonstrating the importance of steric features at the N'-aryl group. However, substituting the N'-aryl unit in ureas **S4-S6** with aliphatic amide groups as in **S8** and **S15**, benzamide units as in **S14**, or having no N'-substituent at all as in **S10**, largely abolished the pharmacological activity on VGCCs. Finally, the importance

of the free amino group at the 4-position of the quinoline ring is highlighted by the loss of blocking activity if it is absent, as observed in **S11**, or if acylated, as in **S16** (**Figure 2B**).

S13 is a broad-spectrum calcium channel blocker. Among the four surfen derivatives that produced greater than 50% inhibition of $\text{Ca}_v3.2$ channels (**Figure 3A**), **S13** showed significantly less cytotoxicity against various human cell lines in vitro. Notably, the half-maximal (IC_{50}) cytotoxic concentration of **S13** was approximately 5 to 7 times higher than that of our reference compound **S4** (surfen) (**Figure 3B**). Consequently, **S13** was selected as the lead compound for further analysis. To assess the pharmacological profile of **S13** across the voltage-gated calcium channel family, we conducted patch-clamp recordings in tsA-201 cells expressing recombinant channels to assess **S13** against $\text{Ca}_v1.2$ (L-type), $\text{Ca}_v2.1$ (P/Q-type), and $\text{Ca}_v2.2$ (N-type), as well as $\text{Ca}_v3.1$, $\text{Ca}_v3.2$, and $\text{Ca}_v3.3$ (T-type) channels. Acute application of **S13** (30 μM) resulted in pronounced inhibition of all channels, with the exception of $\text{Ca}_v2.1$, which appeared to be comparatively less sensitive (**Figure 4A**). The time course for **S13**-mediated inhibition of LVA channels was nearly instantaneous, whereas it occurred progressively over 3 to 4 minutes for HVA channels. While we cannot totally dismiss the possibility of two markedly different mechanisms of inhibition between LVA and HVA channels, one possibility for this difference could be due to **S13** binding to the channels with distinct accessibility (see Molecular docking section below for in-depth discussion). Notably, **S13** blocked the two prominent channels involved in the processing of peripheral nociception, $\text{Ca}_v3.2$ and $\text{Ca}_v2.2$ channels, by 67% and 58%, respectively (**Figure 4B**). The relative IC_{50} values were approximately 17 μM (Hill coefficient 1.8) for $\text{Ca}_v3.2$ channels (**Figure 4C**) and 25 μM (Hill coefficient 2.5) for $\text{Ca}_v2.2$ channels (**Figure 4D**).

Next, we conducted a further assessment of the effects of **S13** on the gating properties of recombinant $\text{Ca}_v3.2$ and $\text{Ca}_v2.2$ channels. T-type currents recorded in $\text{Ca}_v3.2$ -expressing cells treated with 30 μM **S13** for 2 minutes were significantly reduced across a wide range of membrane potentials compared to cells treated with the vehicle (**Figure 5A**), and the maximal macroscopic T-type conductance (G_{max}) was reduced by 68% ($p < 0.0001$) (**Figure 5B**). Furthermore, **S13** caused an additional depolarized shift of the voltage dependence of activation by 10.0 mV ($p < 0.0001$) (**Figure 5C**), along with a

depolarized shift of the voltage dependence of inactivation by 7.5 mV ($p < 0.0001$) (**Figure 5D**). Likewise, **S13** caused inhibition of N-type currents in cells expressing $\text{Ca}_v2.2$ channels (**Figure 5E**) and decreased the maximal N-type conductance by 44% ($p = 0.0004$) (**Figure 5F**). The voltage dependence of activation remained unaltered (**Figure 5G**), and only the voltage dependence of inactivation was slightly shifted, by 3.5 mV ($p = 0.0038$), in cells treated with **S13** (**Figure 5H**). Altogether, these data indicate that **S13** is effective in blocking several VGCC members including those involved in the processing of peripheral nociception.

Molecular docking of S13 to $\text{Ca}_v2.2$ and $\text{Ca}_v3.2$ channels. We used computational docking to predict binding sites for **S13**, focusing on the two primary pain-relevant channels, $\text{Ca}_v2.2$ and $\text{Ca}_v3.2$ which were most strongly inhibited by **S13**. Because a structure of $\text{Ca}_v3.2$ has not yet been published, we used our previously generated homology model ⁹. Based on electrophysiology data showing minimal ($\text{Ca}_v2.2$) or moderate ($\text{Ca}_v3.2$) effects on channel gating (**Figure 5**), we docked **S13** to the extracellular vestibule and the pore (including open fenestrations) in each structure using Glide with enhanced sampling (see Methods). The top scoring sites were within the central pore for $\text{Ca}_v2.2$ (**Fig 6A**) and in the open fenestration between domains IV and I for $\text{Ca}_v3.2$ (**Fig 6B**). Each of these sites were then redocked using the Schrödinger Induced-Fit (flexible-receptor) protocol, resulting in improved docking scores for both targets due to optimization of favorable contacts (**Fig 6A-D**). In both receptors, the best **S13** pose is predicted to contact residues in the domain I S6 helix, partially obscuring the ion-conducting pathway, albeit with **S13** in different orientations (**Fig 6C-D**). This site differs from ligand binding sites observed in $\text{Ca}_v2.2$ and $\text{Ca}_v3.1$ or $\text{Ca}_v3.3$ structures to date. Cryo-EM structures of $\text{Ca}_v2.2$ showed that PD173212 and “blocker 1” bound within the open DIII-DIV fenestration and partially within the pore ⁸. One overlap does occur for predicted **S13** and bound PD173212 which are both within hydrophobic contact distance of the Phe345 side-chain (**Fig 6E**). In the cases of $\text{Ca}_v3.1$ with bound Z944 ⁵¹ and $\text{Ca}_v3.3$ with mibefradil, otilonium bromide, or pimozone ¹⁵, these ligands bind to the central pore and also enter into fenestration DII-DIII to varying degrees (**Fig 6F**). In the $\text{Ca}_v3.2$ model, **S13** docks in the pore and the DIV-DI fenestration (**Fig 6F**). In this pose, **S13** is in the

vicinity of two conserved contacts made by mibefradil and pimozide at Asn412 in DI-S6 (Asn388 in Cav3.1, Asn391 in Cav3.3) and at Leu1851 DIV-S6 (Leu1891 in Cav3.1, Leu1791 in Cav3.3). Interestingly, Cryo-EM structures have uncovered changes in pore-lining S6 helices with ligand binding, such as α/π transitions^{46, 50, 51}, straightening of kinks⁵⁰, and axial rotation⁵¹. S6 transitions have also been observed in other p-loop channels, including the highly structurally related Navs^{18, 44, 49}, and may impact opening and closing of the intracellular gate^{4, 43}. Thus, interaction with the S6 helix suggests that **S13** could impair calcium current via direct channel block as well as through restriction of conformational transitions of the DI-S6 helix. Further, the predicted fenestration site for **S13** for Cav3.2 is also of interest as the fenestrations, first proposed 45 years ago by Hille¹⁶, have been found to be utilized to anchor various channel inhibitors and drugs within the pore of both Cav^{8, 15, 46, 51} and Nav channels^{19, 21, 23, 49}, demonstrating the importance of these sites for drug targeting. Recent studies in Nav channels suggest that opening and closing of these hydrophobic drug access pathways may also be linked to α/π transitions and kinking in the S6 helices^{5, 42} highlighting additional layers of complexity to inhibition of voltage-gated channels and raising a third possible mechanism for channel block by **S13**.

Finally, we venture to speculate that the slower onset of inhibition by **S13** observed for Cav2.2 channels could be due to slower entry into the pore or effects of VGCC ancillary subunits Cav β and Cav $\alpha_2\delta$. We did not investigate docking to the latter based on the ability of **S13** to inhibit T-type channels, which are typically impervious to regulation by Cav ancillary subunits²². Finally, we also note several caveats of our *in-silico* studies. In addition to the obvious predictive nature of docking and uncertainties in homology modeling, we note that the Cav structures are missing about 40% of the amino acids (mainly the intracellular loops) precluding investigation into possible ligand binding sites in these regions. Thus, although our docking models are intriguing, the predicted binding sites remain to be experimentally validated.

S13 blocks voltage-activated calcium currents in DRG neurons but not sodium and potassium currents. Next, our aim was to confirm that **S13** not only inhibits recombinant calcium channels but is also effective on native channels in cultured mouse DRG

neurons. We assessed the effects of **S13** on voltage-activated calcium currents in medium-sized DRG neurons, corresponding to thinly myelinated nociceptive A δ fibers known to express both LVA and HVA calcium channels². In line with our observations on recombinant VGCCs, acute application of 30 μ M **S13** resulted in a significant reduction of both LVA and HVA calcium currents (**Figure 7A**). The maximal steady-state inhibition was 62% and 64% for LVA and HVA currents, respectively (**Figure 7C**). Our findings, showing that **S13** effectively inhibits LVA calcium currents, confirm its action on native Ca_v3.2 channels since Ca_v3.2 is the primary T-type channel isoform responsible for carrying LVA currents in DRG neurons². On the other hand, the HVA calcium conductance in rodent DRG neurons comprises a combination of N-type (39%), P/Q-type (20%), L-type (22%), and R-type (19%) currents¹⁴. Therefore, our observation that **S13** blocked 64% of the total HVA current suggests that **S13** is also effective on multiple native HVA channels, as none of them individually accounts for more than 40% of the total HVA current conductance. In contrast, **S13** had very minimal effects on total voltage-activated sodium and potassium currents (**Figure 7B**), causing only 8% and 9% inhibition, respectively (**Figure 7C**). Nonetheless, we note that **S13** induced a mild yet consistent slowdown of the inactivation kinetics of the sodium current. Altogether, these findings confirm that **S13** primarily functions as a broad-spectrum VGCC blocker, effectively reducing the calcium conductance in nociceptive DRG neurons.

S13 shows antinociceptive effects in a preclinical pain model of SNL-induced mechanical hyperalgesia. The data above revealed that pronociceptive VGCCs are the primary target of **S13**. Therefore, we sought to determine whether treatment with **S13** would demonstrate efficacy in a preclinical rat model of neuropathic pain induced by spinal nerve ligation (SNL). SNL induces partial denervation of the sensory zone of the spinal nerve, resulting in mechanical allodynia as evidenced by a pronounced decreased of the paw withdrawal thresholds (PWT) within 10 days post-surgery (**Figure 8A**). In this allodynic state, intrathecal treatment of male animals with **S13** (10 μ g/5 μ L) resulted in a significant increase in PWT within 1 h after treatment (**Figure 8A**). The reversal of allodynia persisted for approximately 3 h post-treatment, as evidenced by the increase of the PWT integral compared to vehicle-treated animals (**Figure 8B**). We then conducted

a similar experiment with female rats to determine whether there were any sex-based differences in the analgesic effects observed for **S13**. As shown in **Figure 8C-D**, **S13** was also effective at reversing mechanical hyperalgesia in female rats, indicating that its analgesic actions in rats are independent of sex. Collectively, these data demonstrate the antinociceptive potential of **S13** in experimentally induced neuropathic pain.

CONCLUSIONS

Previous studies have documented the analgesic effects of mixed VGCC blockers. For example, A-1264087, which acts as a mixed blocker of Ca_v2.1, Ca_v2.2, and Ca_v3 channels, has been shown to mitigate SNL-induced mechanical hyperalgesia^{45, 52}. Similarly, TROX-1 exhibits inhibition of Ca_v2.1, Ca_v2.2, and Ca_v2.3 channels with comparable efficacy⁴¹ and has been demonstrated to reverse inflammatory-induced hyperalgesia and nerve-injury-induced allodynia^{1, 28}. In addition to these synthetic compounds, the natural product physalin F serves as a dual blocker of Ca_v2.2 and Ca_v2.3 channels, offering relief from mechanical hyperalgesia in rodent models of neuropathic pain³⁶. Moreover, indirect modulation of Ca_v2.2 channels with a peptidomimetic was shown to be analgesic in models of neuropathic and inflammatory pain¹³. In this study, we introduce **S13**, a promising quinoline-based compound that exhibits activity against several pronociceptive VGCCs. **S13** effectively inhibits voltage-activated calcium currents in nociceptive DRG neurons while sparing sodium and potassium currents. Notably, **S13** demonstrates substantial potential as an analgesic agent in a preclinical rat model of SNL-induced neuropathic pain, successfully alleviating mechanical allodynia in both male and female animals. These findings further underscore the therapeutic promise of broad-spectrum calcium channel blockers in mitigating neuropathic pain and suggest that the quinoline backbone structure may serve as a valuable platform for the development of novel derivatives with analgesic properties for further preclinical investigation.

MATERIAL AND METHODS

Synthesis of quinoline-based compounds. See Supplemental information.

Compound preparation. All compounds were dissolved in DMSO at a stock concentration of 30 mM, aliquoted, and stored at -20°C. For patch clamp recordings, compounds were diluted directly into the bath solution at the desired concentration, ensuring that the final DMSO concentration never exceeded 1/1000.

Heterologous expression of voltage-gated calcium channels. Human embryonic kidney tsA-201 cells were grown in DMEM high glucose medium supplemented with 10% (v/v) heat-inactivated fetal bovine serum and 1% penicillin/streptomycin (all media purchased from Invitrogen) and maintained under standard conditions at 37°C in a humidified atmosphere containing 5% CO₂. Cells were transfected using the calcium/phosphate method with plasmid cDNAs encoding for the human Ca_v1.2 and Ca_v2.1 (along with Ca_vβ and Ca_vα2δ-1 ancillary subunits), Ca_v3.1, Ca_v3.2, and Ca_v3.3 channels. Patch-clamp recordings were performed 72h after transfection. The CHO cell line stably expressing the rat Ca_v2.2 channel is a generous gift from Dr. Klugbauer (University of Freiburg) and was previously described ²⁵.

Isolation of DRG neurons. Lumbar L4-L6 dorsal root ganglia (DRGs) from adult C57 male and female mice were harvested as previously described ³⁸ and dissociated enzymatically with 1 mg/mL collagenase (Sigma-Aldrich) in DMEM medium for 1 h at 37°C, followed by mechanical trituration. Cells were seeded onto 12 mm glass coverslips coated with Poly-L-Lysine (Sigma-Aldrich) in DMEM medium supplemented with 10% FBS and 1% penicillin-streptomycin (Thermo-Fisher). The cells were maintained at 37°C in 5% CO₂ for 24 h before patch-clamp recordings.

Whole-cell patch clamp recordings (manual). Whole-cell patch clamp recordings were performed at room temperature (18-22 °C) using an Axopatch 200B amplifier in voltage-clamp mode and acquisition was performed using pClamp 10 (Axon Instruments). The

linear leak component of the current was corrected using a P/4 subtraction protocol and current traces were digitized at 10 kHz and filtered at 2 kHz. Recording of recombinant VGCCs was performed in a bath solution containing (in millimolar): 5 BaCl₂, 5 KCl, 1 MgCl₂, 128 NaCl, 10 TEA-Cl, 10 D-glucose, 10 4-(2-hydroxyethyl)-1-piperazineethanesulfonic acid (HEPES) (pH 7.2 with NaOH). Patch pipettes were filled with a solution containing (in millimolar): 110 CsCl, 3 Mg-ATP, 0.5 Na-GTP, 2.5 MgCl₂, 5 D-glucose, 10 EGTA, and 10 HEPES (pH 7.4 with CsOH), and had a resistance of 2–4 MΩ. For recording of VGCCs in DRG neurons, the extracellular solution contained (in mM): 2 CaCl₂, 160 TEA-Cl, 10 Glucose and 10 HEPES (pH 7.4). The intracellular solution contained (in mM): 134 CsCl, 10 EGTA, 10 HEPES, 4 Mg-ATP and 0.1 Leupeptin (pH 7.2). For recording of voltage gated sodium channels in DRG neurons, the extracellular solution contained (in mM): 128 NaCl, 2 CaCl₂, 5 KCl, 1 MgCl₂, 10 TEA-Cl, 10 Glucose and 10 HEPES (pH 7.4). The intracellular solution contained (in mM): 110 CsF, 2.5 MgCl₂, 5 Glucose, 10 EGTA, 10 HEPES, 3 Mg-ATP, 0.5 Na₂-GTP (pH 7.4). For recording of voltage-gated potassium channels in DRG neurons, the extracellular solution contained (in mM): 138 NaCl, 2 CaCl₂, 5 KCl, 1 MgCl₂, 10 Glucose and 10 HEPES (pH 7.4). The intracellular solution contained (in mM): 140 KCl, 4 NaCl, 1 MgCl₂, 10 EGTA, 10 HEPES and 2 Na₂-GTP (pH 7.4).

Whole-cell patch clamp recordings (automated). Some of the recordings of recombinant Ca_v3.2 and Ca_v2.2 channels (presented in Figure 5) were conducted using the SyncroPatch 384PE (Nanion) at room temperature (18-22°C). Pulse generation and data acquisition were carried out with PatchControl384 v1.9.7 software (Nanion) and the Biomek v1.0 interface (Beckman Coulter). The extracellular solution contained (in mM): 10 CaCl₂, 140 NaCl, 4 KCl, 1 MgCl₂, 5 Glucose and 10 HEPES (pH 7.4). The intracellular solution contained (in mM): 10 CsCl, 110 CsF, 10 NaCl, 10 EGTA, and 10 HEPES (pH 7.2).

Electrophysiological analysis. The voltage dependence of activation of recombinant Ca_v3.2 and Ca_v2.2 channels was determined by measuring the peak of the currents in response to depolarizing steps from a holding potential of -120 mV (Ca_v3.2) and -100 mV

(Ca_v2.2). The current-voltage relationship (I/V) curve was fitted with the following modified Boltzmann equation (1):

$$(1) \quad I(V) = G_{max} \frac{(V - V_{rev})}{1 + \exp\left(\frac{V_{0.5} - V}{k}\right)}$$

with $I(V)$ being the peak current amplitude at the command potential V , G_{rev} the maximum conductance, V_{rev} the reversal potential, $V_{0.5}$ the half-activation potential, and k the slope factor. The voltage dependence of the whole-cell calcium conductance was calculated using the following modified Boltzmann equation (2):

$$(2) \quad G(V) = \frac{G_{max}}{1 + \exp\left(\frac{V_{0.5} - V}{k}\right)}$$

with $G(V)$ being the conductance at the command potential V . The voltage dependence of the steady-state inactivation was determined by measuring the peak of the current amplitude in response to a 200 ms depolarizing step to +10 mV (Ca_v3.2) and +40 mV (Ca_v2.2) applied after a 1 s-long conditioning prepulse ranging from -120 mV to +80 mV. The current amplitude obtained during each test pulse was normalized to the maximal current amplitude and plotted as a function of the prepulse potential. The voltage dependence of the steady-state inactivation was fitted with the following two-state Boltzmann function (3):

$$(3) \quad I(V) = \frac{I_{max}}{1 + \exp\left(\frac{V - V_{0.5}}{k}\right)}$$

with I_{max} corresponding to the maximal peak current amplitude and $V_{0.5}$ to the half-inactivation voltage.

Cytotoxicity assay. Cervix cancer (HeLa), hepatocellular carcinoma (Hep G2), acute lymphoblastic leukemia (CCRF-CEM), and acute promyelocytic leukemia (HL-60) human cell lines were purchased from ATCC (LGC Standards Sp. z o.o., Poland). HeLa cells were cultured in DMEM high glucose medium, CCRF-CEM and HL-60 cells in RPMI-1640 medium (Dutch modification), and Hep G2 cells in α MEM medium supplemented with 10% (v/v) heat-inactivated fetal bovine serum (FBS) and 2 mM glutamine at 37°C in a humidified atmosphere containing 5% CO₂. All media and supplements were purchased from Sigma-Aldrich. The CellTiter-Glo[®] 2.0 Cell Viability Assay kit (Promega) was used to measure the cytotoxicity of tested compounds. Following the seeding of cells (20 μ L) into white 384-well plates (Thermo Fisher Scientific Nunc[™]), cells were grown for 24 h before the addition of compounds or DMSO (used as a vehicle control) into each well. Post 72 h treatment, CellTiter-Glo[®] reagent (20 μ L) was added to each well, and the content was mixed on an orbital shaker in the dark for 2 min at 400 rpm. Subsequently, the luminescent signal was allowed to stabilize for 10 min at room temperature. Luminescence readings were taken using a microplate reader (Cytation 3, BioTek, USA). In this assay, the luminescence directly correlates with the cell number. Cytotoxicity is expressed using IC₅₀ values, representing the concentration of a tested compound that reduces the number of viable cells by half. The data were normalized, and IC₅₀ values were calculated using nonlinear regression analysis, assuming a sigmoidal concentration-response curve with a variable Hill slope (GraphPadPRISM[®] 7 software).

Molecular docking analysis. Protein and ligand preparation and docking were conducted using the Schrödinger Docking Suite (Schrödinger Release 2023-2: Schrödinger, LLC, New York, NY, 2023). Ligands were prepared using LigPrep with possible ionization states at pH 7.0³⁴. The cryo-EM structure of Ca_v2.2 (PDB ID: 7mix¹²) was prepared using the Protein Preparation Wizard³⁴. The homology model of Ca_v3.2 was described previously⁹. Docking was conducted using Glide in Standard Precision (SP) mode with enhanced sampling (4x) to obtain up to 100 poses per site¹¹. Schrödinger Induced-Fit Docking (IFD) was used for flexible receptor docking³⁷. In this approach, 20 docking runs are each followed by optimization of the amino acid positions and

conformations within 5 Å of the newly docked site, and the resulting ligand-receptor complexes are ranked by the energies of the resulting induced-fit complexes.

Animals. All experiments and procedures were performed in accordance with the guidelines recommended by the National Institutes of Health, the International Association for the Study of Pain, and the National Center for the Replacement, Refinement, and Reduction of Animals in Research (NC3Rs) guidelines. Pathogen-free adult male and female Sprague-Dawley rats (100-150 g; Charles River Laboratories, Wilmington, MA) were used for behavioral experiments. Animals were housed in the New York University's Kriser Dental Center Animal Facility in light/dark cycle (12-h light: 12-h dark cycle; lights on at 07:00 h) and temperature ($23 \pm 3^\circ\text{C}$) controlled rooms, with standard rodent chow and water *ad libitum*. The Institutional Animal Care and Use Committees of the College of Dentistry at New York University approved all experiments.

L5/L6 spinal nerve ligation. Male and female rats (~150 g) were deeply anesthetized with isoflurane (4% for induction and 2% for maintenance). The lower half of the animal's back was shaved. After surgical preparation, the left L5 and L6 spinal nerves were exposed by removing the paraspinal muscles and ligated with a 5-0 silk suture in a region distal to the DRG¹⁷. After hemostasis was confirmed, muscle and fascia were closed in layers using 5-0 absorbable suture, and the skin was closed with wound clips. Animals were allowed to recover for 10 days.

Intrathecal administration. Ten days after spinal nerve ligation, **S13** was injected intrathecally (10 µg/5 µL) between L4/L5 intervertebral level into isoflurane anesthetized rats (4% for induction and 2% for maintaining) and behavior was measured every hour for 6 hours.

Measurement of mechanical allodynia. Mechanical allodynia was assessed by measuring rats' paw withdrawal threshold in response to probing with a series of fine calibrated filaments (von Frey, Stoelting, Wood Dale, IL). Rats were placed in suspended plastic cages with a wire mesh floor, and each von Frey filament was applied

perpendicularly to the plantar surface of the paw. The “up-down” method (sequential increase and decrease of the stimulus strength) was used to determine the withdrawal threshold. Dixon’s nonparametric method was used for data analysis, as described by Chaplan et al. ³. Data were expressed as the paw withdrawal threshold. Mechanical allodynia was manifested as a decrease in paw withdrawal threshold.

Data analysis and statistics. Data values are presented as mean \pm S.E.M for n measurements. Statistical significance was evaluated by one-way or two-way ANOVA followed by a Turkey’s test with GraphPad Prism 7 and datasets were considered significantly different for $p < 0.05$.

AUTHOR CONTRIBUTIONS

M.K. synthesized the compounds. L.C. and R.N.S. performed electrophysiological recordings and analyzed the data. K.G. performed the behavioral analysis. S.P.M. performed the molecular docking analysis. M.H. performed the cytotoxicity analysis. N.W., U.J., R.K., and M.D.W. supervised the study. N.W. wrote the first draft of the manuscript. All authors edited and approved the final manuscript.

FUNDING

L.C. is supported by a Barrande fellowship (Campus France). N.W. and E.J. are supported by a grant from the Ministry of Education, Youth and Sport of the Czech Republic (#LUAUS23322). N.W. is supported by the National Institute for Research of Metabolic and Cardiovascular Diseases (Program EXCELES #LX22NPO5104), funded by the European Union – Next Generation EU. K.G. was supported by the National Institute Of Neurological Disorders And Stroke of the National Institutes of Health under Award Number K99NS134965.

ACKNOWLEDGMENTS

We are grateful to Dr. Emanuela Jahn (IOCB Prague) for her help with the chemical synthesis and fruitful discussions.

REFERENCES

- (1) Abbadie, C.; McManus, O.B.; Sun, S.Y.; Bugianesi, R.M.; Dai, G.; Haedo, R.J.; Herrington, J.B.; Kaczorowski, G.J.; Smith, M.M.; Swensen, A.M.; Warren, V.A.; Williams, B.; Arneric, S.P.; Eduljee, C.; Snutch, T.P.; Tringham, E.W.; Jochnowitz, N.; Liang, A.; Euan MacIntyre, D.; McGowan, E.; Mistry, S.; White, V.V.; Hoyt, S.B.; London, C.; Lyons, K.A.; Bunting, P.B.; Volksdorf, S.; Duffy, J.L. Analgesic effects of a substituted N-triazole oxindole (TROX-1), a state-dependent, voltage-gated calcium channel 2 blocker. *J Pharmacol Exp Ther* **2010**, 334, 545-555.
- (2) Bourinet, E.; Alloui, A.; Monteil, A.; Barrère, C.; Couette, B.; Poirot, O.; Pages, A.; McRory, J.; Snutch, T.P.; Eschalier, A.; Nargeot, J. Silencing of the Cav3.2 T-type calcium channel gene in sensory neurons demonstrates its major role in nociception. *EMBO J* **2005**, 24, 315-324.
- (3) Chaplan, S.R.; Bach, F.W.; Pogrel, J.W.; Chung, J.M.; Yaksh, T.L. Quantitative assessment of tactile allodynia in the rat paw. *J Neurosci Methods* **1994**, 53, 55-63.
- (4) Choudhury, K.; Delemotte, L. Modulation of Pore Opening of Eukaryotic Sodium Channels by π -Helices in S6. *J Phys Chem Lett* **2023**, 14, 5876-5881.
- (5) Choudhury, K.; Howard, R.J.; Delemotte, L. An α - π transition in S6 shapes the conformational cycle of the bacterial sodium channel NavAb. *J Gen Physiol* **2023**, 155, e202213214.
- (6) de Amorim Ferreira, M.; Ferreira, J. Role of Cav2.3 (R-type) Calcium Channel in Pain and Analgesia: A Scoping Review. *Curr Neuropharmacol* **2023**,
- (7) Dobremez, E.; Bouali-Benazzouz, R.; Fossat, P.; Monteils, L.; Dulluc, J.; Nagy, F.; Landry, M. Distribution and regulation of L-type calcium channels in deep dorsal horn neurons after sciatic nerve injury in rats. *Eur J Neurosci* **2005**, 21, 3321-3333.
- (8) Dong, Y.; Gao, Y.; Xu, S.; Wang, Y.; Yu, Z.; Li, Y.; Li, B.; Yuan, T.; Yang, B.; Zhang, X.C.; Jiang, D.; Huang, Z.; Zhao, Y. Closed-state inactivation and pore-blocker modulation mechanisms of human Cav2.2. *Cell Rep* **2021**, 37, 109931.
- (9) Duran, P.; Loya-López, S.; Ran, D.; Tang, C.; Calderon-Rivera, A.; Gomez, K.; Stratton, H.J.; Huang, S.; Xu, Y.M.; Wijeratne, E.M.K.; Perez-Miller, S.; Shan, Z.; Cai, S.; Gabrielsen, A.T.; Dorame, A.; Masterson, K.A.; Alsbiei, O.; Madura, C.L.; Luo, G.; Moutal, A.; Streicher, J.; Zamponi, G.W.; Gunatilaka, A.A.L.; Khanna, R.

- The natural product argentatin C attenuates postoperative pain via inhibition of voltage-gated sodium and T-type voltage-gated calcium channels. *Br J Pharmacol* **2023**, 180, 1267-1285.
- (10) Ferron, L.; Zamponi, G.W. (2022) in *Voltage-Gated Calcium Channels* Eds.), pp. 491-514, Springer,
- (11) Friesner, R.A.; Banks, J.L.; Murphy, R.B.; Halgren, T.A.; Klicic, J.J.; Mainz, D.T.; Repasky, M.P.; Knoll, E.H.; Shelley, M.; Perry, J.K.; Shaw, D.E.; Francis, P.; Shenkin, P.S. Glide: a new approach for rapid, accurate docking and scoring. 1. Method and assessment of docking accuracy. *J Med Chem* **2004**, 47, 1739-1749.
- (12) Gao, S.; Yao, X.; Yan, N. Structure of human Cav2.2 channel blocked by the painkiller ziconotide. *Nature* **2021**, 596, 143-147.
- (13) Gomez, K.; Santiago, U.; Nelson, T.S.; Allen, H.N.; Calderon-Rivera, A.; Hestehave, S.; Rodríguez Palma, E.J.; Zhou, Y.; Duran, P.; Loya-Lopez, S.; Zhu, E.; Kumar, U.; Shields, R.; Koseli, E.; McKiver, B.; Giuvelis, D.; Zuo, W.; Inyang, K.E.; Dorame, A.; Chefdeville, A.; Ran, D.; Perez-Miller, S.; Lu, Y.; Liu, X.; Handoko; Arora, P.S.; Patek, M.; Moutal, A.; Khanna, M.; Hu, H.; Laumet, G.; King, T.; Wang, J.; Damaj, M.I.; Korczeniewska, O.A.; Camacho, C.J.; Khanna, R. A peptidomimetic modulator of the Cav2.2 N-type calcium channel for chronic pain. *Proc Natl Acad Sci U S A* **2023**, 120, e2305215120.
- (14) Hartung, J.E.; Moy, J.K.; Loeza-Alcocer, E.; Nagarajan, V.; Jostock, R.; Christoph, T.; Schroeder, W.; Gold, M.S. Voltage-gated calcium currents in human dorsal root ganglion neurons. *Pain* **2022**, 163, e774-e785.
- (15) He, L.; Yu, Z.; Geng, Z.; Huang, Z.; Zhang, C.; Dong, Y.; Gao, Y.; Wang, Y.; Chen, Q.; Sun, L.; Ma, X.; Huang, B.; Wang, X.; Zhao, Y. Structure, gating, and pharmacology of human CaV3.3 channel *Nature Communications* **2022**, 13,
- (16) Hille, B. Local anesthetics: hydrophilic and hydrophobic pathways for the drug-receptor reaction. *J Gen Physiol* **1977**, 69, 497-515.
- (17) Ho Kim, S.; Mo Chung, J. An experimental model for peripheral neuropathy produced by segmental spinal nerve ligation in the rat. *Pain* **1992**, 50, 355-363.

- (18) Huang, G.; Wu, Q.; Li, Z.; Jin, X.; Huang, X.; Wu, T.; Pan, X.; Yan, N. Unwinding and spiral sliding of S4 and domain rotation of VSD during the electromechanical coupling in Nav1.7. *Proc Natl Acad Sci U S A* **2022**, 119, e2209164119.
- (19) Huang, X.; Jin, X.; Huang, G.; Huang, J.; Wu, T.; Li, Z.; Chen, J.; Kong, F.; Pan, X.; Yan, N. Structural basis for high-voltage activation and subtype-specific inhibition of human Nav1.8. *Proc Natl Acad Sci U S A* **2022**, 119, e2208211119.
- (20) Jacus, M.O.; Uebele, V.N.; Renger, J.J.; Todorovic, S.M. Presynaptic Cav3.2 channels regulate excitatory neurotransmission in nociceptive dorsal horn neurons. *J Neurosci* **2012**, 32, 9374-9382.
- (21) Jiang, D.; Shi, H.; Tonggu, L.; Gamal El-Din, T.M.; Lenaeus, M.J.; Zhao, Y.; Yoshioka, C.; Zheng, N.; Catterall, W.A. Structure of the Cardiac Sodium Channel. *Cell* **2020**, 180, 122-134.e10.
- (22) Leuranguer, V.; Bourinet, E.; Lory, P.; Nargeot, J. Antisense depletion of beta-subunits fails to affect T-type calcium channels properties in a neuroblastoma cell line. *Neuropharmacology* **1998**, 37, 701-708.
- (23) Li, X.; Xu, F.; Xu, H.; Zhang, S.; Gao, Y.; Zhang, H.; Dong, Y.; Zheng, Y.; Yang, B.; Sun, J.; Zhang, X.C.; Zhao, Y.; Jiang, D. Structural basis for modulation of human Nav1.3 by clinical drug and selective antagonist. *Nat Commun* **2022**, 13, 1286.
- (24) Maggi, C.A.; Tramontana, M.; Cecconi, R.; Santicoli, P. Neurochemical evidence for the involvement of N-type calcium channels in transmitter secretion from peripheral endings of sensory nerves in guinea pigs. *Neurosci Lett* **1990**, 114, 203-206.
- (25) Mallmann, R.T.; Wilmes, T.; Lichvarova, L.; Bühner, A.; Lohmüller, B.; Castonguay, J.; Lacinova, L.; Klugbauer, N. Tetraspanin-13 modulates voltage-gated CaV2.2 Ca²⁺ channels. *Sci Rep* **2013**, 3, 1777.
- (26) Nelson, M.T.; Joksovic, P.M.; Perez-Reyes, E.; Todorovic, S.M. The endogenous redox agent L-cysteine induces T-type Ca²⁺ channel-dependent sensitization of a novel subpopulation of rat peripheral nociceptors. *J Neurosci* **2005**, 25, 8766-8775.
- (27) Patel, R.; Montagut-Bordas, C.; Dickenson, A.H. Calcium channel modulation as a target in chronic pain control. *Br J Pharmacol* **2018**, 175, 2173-2184.

- (28) Patel, R.; Rutten, K.; Valdor, M.; Schiene, K.; Wigge, S.; Schunk, S.; Damann, N.; Christoph, T.; Dickenson, A.H. Electrophysiological characterization of activation state-dependent Ca(v)2 channel antagonist TROX-1 in spinal nerve injured rats. *Neuroscience* **2015**, *297*, 47-57.
- (29) Radwani, H.; Lopez-Gonzalez, M.J.; Cattaert, D.; Roca-Lapirot, O.; Dobremez, E.; Bouali-Benazzouz, R.; Eiríksdóttir, E.; Langel, Ü.; Favereaux, A.; Errami, M.; Landry, M.; Fossat, P. Cav1.2 and Cav1.3 L-type calcium channels independently control short- and long-term sensitization to pain. *J Physiol* **2016**, *594*, 6607-6626.
- (30) Rivas-Ramirez, P.; Gadotti, V.M.; Zamponi, G.W.; Weiss, N. Surfen is a broad-spectrum calcium channel inhibitor with analgesic properties in mouse models of acute and chronic inflammatory pain. *Pflugers Arch* **2017**, *469*, 1325-1334.
- (31) Roca-Lapirot, O.; Radwani, H.; Aby, F.; Nagy, F.; Landry, M.; Fossat, P. Calcium signalling through L-type calcium channels: role in pathophysiology of spinal nociceptive transmission. *Br J Pharmacol* **2018**, *175*, 2362-2374.
- (32) Rose, K.E.; Lunardi, N.; Boscolo, A.; Dong, X.; Erisir, A.; Jevtovic-Todorovic, V.; Todorovic, S.M. Immunohistological demonstration of CaV3. 2 T-type voltage-gated calcium channel expression in soma of dorsal root ganglion neurons and peripheral axons of rat and mouse *Neuroscience* **2013**, *250*, 263-274.
- (33) Santicoli, P.; Del Bianco, E.; Tramontana, M.; Geppetti, P.; Maggi, C.A. Release of calcitonin gene-related peptide like-immunoreactivity induced by electrical field stimulation from rat spinal afferents is mediated by conotoxin-sensitive calcium channels *Neuroscience letters* **1992**, *136*, 161-164.
- (34) Sastry, G.M.; Adzhigirey, M.; Day, T.; Annabhimoju, R.; Sherman, W. Protein and ligand preparation: parameters, protocols, and influence on virtual screening enrichments. *J Comput Aided Mol Des* **2013**, *27*, 221-234.
- (35) Sestili, I.; Borioni, A.; Mustazza, C.; Rodomonte, A.; Turchetto, L.; Sbraccia, M.; Riitano, D.; Del Giudice, M.R. A new synthetic approach of N-(4-amino-2-methylquinolin-6-yl)-2-(4-ethylphenoxyethyl)benzamide (JTC-801) and its analogues and their pharmacological evaluation as nociceptin receptor (NOP) antagonists. *Eur J Med Chem* **2004**, *39*, 1047-1057.

- (36) Shan, Z.; Cai, S.; Yu, J.; Zhang, Z.; Vallecillo, T.G.M.; Serafini, M.J.; Thomas, A.M.; Pham, N.Y.N.; Bellampalli, S.S.; Moutal, A.; Zhou, Y.; Xu, G.B.; Xu, Y.M.; Luo, S.; Patek, M.; Streicher, J.M.; Gunatilaka, A.A.L.; Khanna, R. Reversal of Peripheral Neuropathic Pain by the Small-Molecule Natural Product Physalin F via Block of CaV2.3 (R-Type) and CaV2.2 (N-Type) Voltage-Gated Calcium Channels. *ACS Chem Neurosci* **2019**, *10*, 2939-2955.
- (37) Sherman, W.; Day, T.; Jacobson, M.P.; Friesner, R.A.; Farid, R. Novel procedure for modeling ligand/receptor induced fit effects. *J Med Chem* **2006**, *49*, 534-553.
- (38) Sleight, J.N.; West, S.J.; Schiavo, G. A video protocol for rapid dissection of mouse dorsal root ganglia from defined spinal levels. *BMC Res Notes* **2020**, *13*, 302.
- (39) Smith, M.T.; Cabot, P.J.; Ross, F.B.; Robertson, A.D.; Lewis, R.J. The novel N-type calcium channel blocker, AM336, produces potent dose-dependent antinociception after intrathecal dosing in rats and inhibits substance P release in rat spinal cord slices *Pain* **2002**, *96*, 119-127.
- (40) Stevens, E.B.; Stephens, G.J. Recent advances in targeting ion channels to treat chronic pain. *Br J Pharmacol* **2018**, *175*, 2133-2137.
- (41) Swensen, A.M.; Herrington, J.; Bugianesi, R.M.; Dai, G.; Haedo, R.J.; Ratliff, K.S.; Smith, M.M.; Warren, V.A.; Arneric, S.P.; Eduljee, C.; Parker, D.; Snutch, T.P.; Hoyt, S.B.; London, C.; Duffy, J.L.; Kaczorowski, G.J.; McManus, O.B. Characterization of the substituted N-triazole oxindole TROX-1, a small-molecule, state-dependent inhibitor of Ca(V)₂ calcium channels. *Mol Pharmacol* **2012**, *81*, 488-497.
- (42) Tao, E.; Corry, B. Characterizing fenestration size in sodium channel subtypes and their accessibility to inhibitors. *Biophys J* **2022**, *121*, 193-206.
- (43) Tikhonov, D.B.; Zhorov, B.S. P-Loop Channels: Experimental Structures, and Physics-Based and Neural Networks-Based Models. *Membranes (Basel)* **2022**, *12*, 229.
- (44) Wu, Q.; Huang, J.; Fan, X.; Wang, K.; Jin, X.; Huang, G.; Li, J.; Pan, X.; Yan, N. Structural mapping of Nav1.7 antagonists. *Nat Commun* **2023**, *14*, 3224.
- (45) Xu, J.; Chu, K.L.; Zhu, C.Z.; Niforatos, W.; Swensen, A.; Searle, X.; Lee, L.; Jarvis, M.F.; McGaraughty, S. A mixed Ca²⁺ channel blocker, A-1264087, utilizes

- peripheral and spinal mechanisms to inhibit spinal nociceptive transmission in a rat model of neuropathic pain. *J Neurophysiol* **2014**, 111, 394-404.
- (46) Yao, X.; Gao, S.; Yan, N. Structural basis for pore blockade of human voltage-gated calcium channel Cav1.3 by motion sickness drug cinnarizine. *Cell Res* **2022**, 32, 946-948.
- (47) Yusaf, S.P.; Goodman, J.; Pinnock, R.D.; Dixon, A.K.; Lee, K. Expression of voltage-gated calcium channel subunits in rat dorsal root ganglion neurons *Neuroscience letters* **2001**, 311, 137-141.
- (48) Zamponi, G.W. Targeting voltage-gated calcium channels in neurological and psychiatric diseases. *Nat Rev Drug Discov* **2016**, 15, 19-34.
- (49) Zhang, J.; Shi, Y.; Huang, Z.; Li, Y.; Yang, B.; Gong, J.; Jiang, D. Structural basis for Nav1.7 inhibition by pore blockers. *Nat Struct Mol Biol* **2022**, 29, 1208-1216.
- (50) Zhao, Y.; Huang, G.; Wu, J.; Wu, Q.; Gao, S.; Yan, Z.; Lei, J.; Yan, N. Molecular Basis for Ligand Modulation of a Mammalian Voltage-Gated Ca²⁺ Channel. *Cell* **2019**, 177, 1495-1506.e12.
- (51) Zhao, Y.; Huang, G.; Wu, Q.; Wu, K.; Li, R.; Lei, J.; Pan, X.; Yan, N. Cryo-EM structures of apo and antagonist-bound human Cav3.1. *Nature* **2019**, 576, 492-497.
- (52) Zhu, C.Z.; Vortherms, T.A.; Zhang, M.; Xu, J.; Swensen, A.M.; Niforatos, W.; Neelands, T.; Milicic, I.; Lewis, L.G.; Zhong, C.; Gauvin, D.; Mikusa, J.; Zhan, C.; Pai, M.; Roderwald, V.; Chu, K.L.; Cole, E.E.; Besspalov, A.; Searle, X.B.; McGaraughty, S.; Bitner, R.S.; Jarvis, M.F.; Bannon, A.W.; Joshi, S.K.; Scott, V.E.; Lee, C.H. Mechanistic insights into the analgesic efficacy of A-1264087, a novel neuronal Ca(2+) channel blocker that reduces nociception in rat preclinical pain models. *J Pain* **2014**, 15, 387.e1-14.

FIGURE LEGENDS

Figure 1. Synthesis of quinoline-based compounds. (A) Schematic diagram of the various quinoline-based compounds synthesized and tested for their effects on voltage-gated calcium channels. (B) Chemical characteristics of synthesized compounds.

Figure 2. Screening of quinoline-based compounds on recombinant $Ca_v3.2$ channels. (A) Mean percentage of current inhibition produced by acute application of 30 μ M quinoline-based compounds ($n = 4-6$ per compound). T-type currents were elicited by a step depolarization to -20 mV from a holding potential of -100 mV. (B) Summary of the structure-activity relationship (SAR). The structure of surfen (**S4**) is shown as reference compound.

Figure 3. In vitro cytotoxicity of quinoline-based compounds. (A) Structures of the four most potent compounds (**S5**, **S6**, **S12**, and **S13**) for their blocking activity on recombinant $Ca_v3.2$ channels. The structure of **S4** (surfen, reference compound) is shown for comparison. (B) Corresponding mean half-maximal cytotoxic concentration (IC_{50}) on several human cancer cells and primary fibroblasts ($n = 3$ per compound). CCRF-CEM, human lymphoblastic leukemia; HeLa, human cervical carcinoma; HepG2, human liver cancer; HL-60, human promyelocytic leukemia.

Figure 4. Pharmacological evaluation of **S13** across recombinant voltage-gated calcium channels. (A) Representative time course of current inhibition along with whole-cell current traces recorded from cells expressing LVA ($Ca_v3.1$, $Ca_v3.2$, and $Ca_v3.3$) and HVA ($Ca_v1.2$, $Ca_v2.1$, and $Ca_v2.2$) channels in response to a step depolarization to -20 mV (LVA channels) and +10 mV (LVA channels) from a holding potential of -100 mV, before (black traces) and after (blue traces) acute application of **S13** (30 μ M). (B) Corresponding mean percentage of maximal current inhibition ($n = 4-6$ per channel). (C-D) Corresponding dose-response curves of **S13** for $Ca_v3.2$ and $Ca_v2.2$ channels ($n = 16-25$ for each concentration).

Figure 5. Effects of **S13** on the gating properties of recombinant $\text{Ca}_v3.2$ and $\text{Ca}_v2.2$ channels. (A) Mean current-voltage (I/V) relationships of recombinant $\text{Ca}_v3.2$ channels recorded by automated patch-clamp in cells pre-treated for 2 min with vehicle (DMSO) and 30 μM **S13** (blue symbols). The continuous lines represent the fit of the I/V curves with the modified Boltzmann Eq. (1). (B) Corresponding mean maximal macroscopic conductance values (G_{max}) obtained from the fit of the I/V curves. (C) Corresponding mean normalized voltage dependence of activation of $\text{Ca}_v3.2$ channels fitted (continuous lines) with the modified Boltzmann Eq. (2). The inset shows the mean half-activation potential values obtained from the fit of the conductance curves. (D) Mean normalized voltage dependence of steady-state inactivation of $\text{Ca}_v3.2$ channels fitted (continuous lines) with the two-state Boltzmann Eq. (3). The inset shows the mean half-inactivation potential values obtained from the fit of the inactivation curves. (E-H) Legend same as (A-D) but for recombinant $\text{Ca}_v2.2$ channels. Statistical significance was evaluated by one-way ANOVA in comparison to vehicle-treated cells.

Figure 6. Molecular docking of **S13** on $\text{Ca}_v2.2$ and $\text{Ca}_v3.2$ channels. (A-B) $\text{Ca}_v2.2$ structure (PDB ID: 7mix)¹² and $\text{Ca}_v3.2$ homology model⁹ with top docking poses from Glide enhanced sampling (black lines) and from induced-fit (black sticks). The docking scores are given in kcal/mol, bold for induced-fit results. (C-D) Close-up views of best induced-fit poses for each structure (view rotated by 90° from top panels), with potential contacts within 4 Å shown as dashed lines. Domains colored as indicated, key helices labeled for domain I in lower panels. (E) Close-up view from the extracellular side showing best induced-fit pose for $\text{Ca}_v2.2$ overlaid with structures of $\text{Ca}_v2.2$ with bound PD173212 (PDB ID: 7vfv) and “blocker 1” (PDB ID: 7vfw)⁸. (F) Close-up view as in (E) showing best induced-fit pose for $\text{Ca}_v3.2$ overlaid with structures of $\text{Ca}_v3.1$ with bound Z944 (PDB ID: 6kzp)⁵¹ and $\text{Ca}_v3.3$ with bound mibefradil, otilonium bromide, or pimozide (PDB IDs: 7wlj, 7wlk, 7wli, respectively)¹⁵.

Figure 7. Effects of **S13** on native voltage-gated calcium (Ca_v), sodium (Na_v), and potassium (K_v) channels in DRG neurons. (A) Representative calcium current traces recorded in medium-sized DRG neurons in response to a step depolarization to -40 mV

(LVA) channels, left panel) and +10 mV (HVA channels, right panel) from a holding potential of -100 mV, before (black traces) and after (blue traces) acute application of **S13** (30 μ M). (B) Legend same as (A) but for sodium (left panel) and potassium (right panel) currents elicited by a step depolarization to -10 mV and +50 mV, respectively. (C) Corresponding mean percentage of current inhibitions.

Figure 8. Analgesic effect of **S13** on nerve injury-induced mechanical hyperalgesia. (A) Mean paw withdrawal threshold (PWT) in adult male rats before (BL, base line), and after 10 days following spinal nerve ligation (Pre-drug). A single intrathecal injection of **S13** (10 μ g/5 μ L, blue circles) produced a significant reduction of mechanical allodynia, which was not observed in control animals injected with saline (open circles). (B) Corresponding mean integral of the PWT measured over 6h following drug treatment. (C-D) Legend same as (A-B) but for female rats. Statistical significance was evaluated by two-way ANOVA followed by Turkey's post hoc test in comparison to vehicle-treated animals (panels A and C), and by Mann-Whitney test (panels B and D).